Discontinuous Galerkin timestepping for nonlinear parabolic problems

Thesis submitted for the degree of

Doctor of Philosophy

at the

University of Leicester

by

Mohammad Sabawi

Department of Mathematics

University of Leicester

February 2018

"Imagination is more important than knowledge. For knowledge is limited to all we now know and understand, while imagination embraces the entire world, and all there ever will be to know and understand."

Albert Einstein

Discontinuous Galerkin timestepping for nonlinear parabolic problems

by

Mohammad Sabawi

Abstract

We study space–time finite element methods for semilinear parabolic problems in $(1 + d)$–dimensions for $d = 2, 3$. The discretisation in time is based on the discontinuous Galerkin timestepping method with implicit treatment of the linear terms and either implicit or explicit multistep discretisation of the zeroth order nonlinear reaction terms. Conforming finite element methods are used for the space discretisation. For this implicit-explicit IMEX–dG family of methods, we derive a *posteriori* and *a priori* energy-type error bounds and we perform extended numerical experiments. We derive a novel *hp*–version *a posteriori* error bounds in the $L_\infty(L_2)$ and $L_2(H^1)$ norms assuming an only locally Lipschitz growth condition for the nonlinear reactions and *no* monotonicity of the nonlinear terms. The analysis builds upon the recent work in [60], for the respective linear problem, which is in turn based on combining the elliptic and dG reconstructions in [83, 84] and continuation argument. The *a posteriori* error bounds appear to be of optimal order and efficient in a series of numerical experiments.

Secondly, we prove a novel *hp*–version *a priori* error bounds for the fully–discrete IMEX–dG timestepping schemes in the same setting in $L_\infty(L_2)$ and $L_2(H^1)$ norms. These error bounds are explicit with respect to both the temporal and spatial meshsizes k_n and h, respectively, and, where possible, with respect to the possibly varying temporal polynomial degree r. The *a priori* error estimates are derived using the elliptic projection technique with an inf-sup argument in time. Standard tools such as Grönwall inequality and discrete stability estimates for fully discrete semilinear parabolic problems with merely locally-Lipschitz continuous nonlinear reaction terms are used. The *a priori* analysis extends the applicability of the results from [52] to this setting with low regularity. The results are tested by an extensive set of numerical experiments.

Acknowledgements

Studying the PhD is a time-consuming and involving project and during this busy time, we certainly need help and support of many people. I am glad and happy to acknowledge the support and help of many people for me during my PhD study time at the University of Leicester. I would like to take this opportunity to express my thanks and gratitude for all the people who helped me in my research, and I will just name a few.

Firstly, I would like to express my indebtedness and gratitude to my supervisors, Emmanuil Georgoulis and Andrea Cangiani, for their help, patience, support and guidance during this long time. Their advice, encouragement and hints were valuable and crucial in finishing my research.

Special thanks to my PhD colleagues and friends, Oliver, Sam, Zhaonan, Younis and Stephen for their helpful discussions about the theory and implementation of the finite element method and in particular in the finite element coding. Many thanks to my friends in Michael Atiyah Building, Ali, Hassan, Mohammad, Omar, Saeed, Mudher, Ahmed and Hoger for their help and encouragement. Also, I would like to thank all the staff of the mathematics department for their help and support. Lastly, all thanks and gratitude to all my darling family, my beloved wife (Ehab), my kind parents, my dear sisters and my darling children (Ibraheem, Yousif, and Mustafa), who without their support and encouragement I could not finish my study. I thank them for their patience for the short time I spent with them during this period.

Contents

List of Figures

To my dear wife Ehab, my loved parents, my beloved sisters, and my lovely children, Ibraheem, Yousif and Mustafa.

Chapter 1

Introduction

1.1 Background

The finite element method (FEM) is one of the most powerful, efficient, and general techniques for solving partial differential equations, modelling a wide range of problems in different areas such as biology, chemistry, physics, and engineering. The FEM applies to a wide range of problems which can be written in variational (weak) form and allows for high order approximations; its popularity and success is especially due to its flexibility and accuracy in dealing with complicated problems and geometries. The finite element method dates back to the 1940s in the works of Hrennikoff and Courant, and builds their ideas and techniques on the works of Galerkin, Rayleigh and Ritz. The method was then re–discovered in the 1950s by engineers to solve common engineering problems, and after that has been studied rigorously by mathematicians in the 1960s and 1970s. During long decades of development, many engineers, scientists, and mathematicians have contributed to the popularity of finite element methods, we refer to the following monographs for more details [109, 95, 41].

In its earlier stages the finite element method started with standard continuous finite element discretisations of the space variable following the Galerkin paradigm. Typically, for the discretisation of the time variable, the conventional time stepping methods are used such as Runge–Kutta or multistep methods. The finite element

in space and time is studied for the first time at the end of the 60s in the work of Argyris and Scharpf [12]. The continuous Galerkin (cG) finite element method for the time variable is first studied and analysed by Hulme [66, 65] in 1972 for ordinary differential equations. Also, its relation to other collocation methods is considered. Lesaint and Raviart [80] investigated the cG method for first order hyperbolic neutron transport equations. The first detailed analysis for discontinuous Galerkin (dG) time stepping schemes are carried out by Eriksson, Johnson and Thomée [47]. The directly–related discontinuous Galerkin finite element method for first order hyperbolic problems is traced back to the work of Reed and Hill [93] in 1973.

Variational time–stepping methods nowadays are more popular, and they are gaining increasing interest. Variational time–stepping methods of Galerkin–type are based on weak formulations of the initial–value problems. They are known in the literature by different names such as variational time discretisation methods, variational time–marching schemes, variational time–advancing schemes and dG or continuous Galerkin (cG) time–stepping schemes. For dG and cG schemes the test spaces are discontinuous, i.e., they consist of discontinuous polynomials in time, which naturally decouples the discrete Galerkin variational formulations into local problems on each time step. In this work, we study discontinuous Galerkin timestepping schemes; this is a family of arbitrary order timestepping methods resulting in discontinuous, in general, approximations in the time variable. Discontinuous Galerkin timestepping methods can be also recast as certain families of dissipative implicit Runge-Kutta methods upon suitable choices of quadrature rules [80, 8]. In particular, dG timestepping schemes with quadrature at Gauss–Radau points are equivalent to the implicit Runge–Kutta Radau method with r intermediate stages (IRK–R(r)), where both are collocation methods. These methods have attractive convergence properties in the discretisation of first order derivatives mentioned above such as higher order convergence rates of order $r+1$ for polynomial of order r and superconvergence of order $2r+1$ at the time nodes. dG methods are convenient to use within adaptive algorithms whereby the time and/or space meshes are adapted to the solution in an automatic fashion, typically driven by *a posteriori* error estimators; this is due to the lack of necessity of any continuity requirements between timesteps which can allow for locally variable

order approximations and local timestepping. Also, dG timestepping schemes of order r are equivalent at the nodal points with the standard difference subdiagonal Padé schemes of order $(r, r-1)$ [109].

Moreover, classical time-stepping methods are not appropriate for problems with time-dependent domains (variable domains) or time-dependent free boundary problems. For the treatment of such problems, the use of variational space-time methods is essential [24]. Recent works [25, 23, 22, 24] have examined higher order time discrete arbitrary Lagrangian Eulerian (ALE) formulation by the use of dG time-stepping schemes. The authors performed both the *a posteriori* and *a priori* error analysis as well as the stability analysis for higher order discontinuous Galerkin time stepping schemes for ALE problems. Also, the discontinuous Galerkin time variational schemes played an important role in the study of optimal control problems. Chrysafinos and coworkers [32, 35, 34, 33] studied the convergence of optimal control problems related to semilinear parabolic equations such as FitzHugh-Nagumo system and evolutionary Stokes equations associated with constrained optimal control problems by using discontinuous time stepping methods of arbitrary orders using the continuous finite element method in space. Sudirham and coworkers [108] examined space–time Galerkin discretisation for the advection–diffusion problems in the context of the ALE formulation.

The increasing popularity of *a posteriori* error estimates in deriving efficient and accurate adaptive methods that reduce the cost and time of computations has put forth the need to develop such estimates for numerical methods for more complex/nonlinear problems. Indeed, in recent years, adaptive finite element methods have become important tools in solving complicated problems such as problems with local singularities such as singularities arising from sharp shock–like fronts, interior or boundary layers, and re-entrant corners, and they are the subject of intensive research and study. *A posteriori* error analysis for stationary/elliptic problems has been studied widely, and important developments have been achieved. On the other hand, the study of nonlinear stationary problems and time–dependent problems is still not yet mature [111, 3]. In particular, the study of time *hp*–adaptivity, space-time–*hp*–adaptivity (fully *hp*–adaptivity), and *a posteriori* error

analysis for the Galerkin variational time–stepping methods, used in the context of numerical solution of nonlinear evolution partial differential equations, has not been addressed before in the literature.

1.2 Literature review

Space-time variational methods for the discretisation of evolutionary PDEs are becoming more popular as evidenced by the recent and ongoing research in this field [107, 105, 26]. Error analysis and aspects of implementation of these methods have been studied by many authors [68, 37, 80, 13, 63, 64, 47, 52, 82, 79, 2, 85, 67, 74, 94, 99, 103, 100, 101, 6, 5, 21, 97, 73, 17, 114, 106, 25, 23, 22, 24, 62, 118]. In [37], the authors investigated the application of dG timestepping schemes for linear non–stiff ordinary differential equations. The first error analysis for linear parabolic problems is done in [68] by Jamet. In [97] Schieweck studied the stability properties of cG timestepping schemes. The authors in [62, 118] presented a novel unified framework of discontinuous Galerkin method for deriving different time stepping schemes, via different boundary conditions for the time variable, numerical quadrature and test functions. Aziz and Monk [13] investigated the cG method and they showed that the cG(1), i.e., continuous Galerkin methods with linear elements is equivalent to the Crank–Nicolson method with time averaged data. Also, they derived error estimates for this method. These methods have received considerable interest in the context of space–time adaptivity throughout the years, as they offer a variational, arbitrary order timestepping framework and, crucially, allow for locally variable timestep sizes in different spatial regions of the computational domain. On the other hand, one of the most challenging aspects of implementation of variational time stepping schemes "such as discontinuous Galerkin timestepping methods" is the high computational cost (memory size and implementation time) for solving the block algebraic linear systems arising from using these methods for discretising time-dependent PDEs or ODEs. The reduction of the computational cost of the implementation of variational discontinuous or continuous time marching schemes is one of the challenging issues in using these

methods. Many researchers have considered these issues from different numerical view points such as [99, 114, 94, 106]. Also, in [114] Basting and Weller proposed and analysed efficient preconditioners for block algebraic linear systems resulting from solving linear parabolic equations by variational time stepping methods. Richter, Springer and Vexler [94] analysed the solution of the nonlinear systems arising from solving nonlinear parabolic equations by using discontinuous Galerkin methods of order r in time. They avoided the inevitable complex coefficients arising from direct decoupling of the nonlinear systems by a judicious use of the Newton method. Also, in the recent article [106], Smears derived a fully robust and efficient preconditioning scheme for the block algebraic linear systems arising from the solution of parabolic problems by dG variational time discretisation schemes.

All these works employed the h–version dG timestepping schemes where the approximation order r is fixed and usually low order, while decreasing the time steps. This approach leads to algebraic rates of convergence of order $r + 1$ for smooth solutions in time. The p– and hp–versions of the FEM were initiated in the 1980s by Babŭska, Szabö and their co-workers [14, 15**?**]

The p– and hp–versions Galerkin timestepping methods can solve the transient problems which have smooth solutions with local singularities with high algebraic and even exponential convergence rates, and their analysis have been subject of great interest, see e.g. [99, 100, 101, 103, 102, 115, 60, 76, 90, 98, 117]. In particular, Schötzau and Schwab initiated and introduced the hp–version Galerkin time-stepping methods in a series of papers [103, 100, 101, 102], where they studied, analysed and examined hp–dG–time stepping methods for the initial value ODE problem to the fully discrete canonical parabolic problem, proving new explicit *a priori* error estimates for the approximations orders and time steps and showing that dG time stepping methods have exponential/spectral accuracy for smooth time–dependent problems. Mustapha [90] examined the numerical solution of the fractional subdiffusion problems by the use of hp–time stepping discontinuous Galerkin methods. The solution of nonlinear PDEs by hp–dG time–advancing schemes have attracted more research and interest recently. In [105] and [107] the

authors studied the numerical solution of the nonlinear Hamilton–Jacobi–Bellman equation by using fully discrete hp– and $hp-\tau q$– versions of discontinuous Galerkin time stepping methods respectively. Janssen and Wihler in [69] investigated hp–Galerkin time stepping methods for nonlinear initial value problems. They proved the existence results for the continuous and discontinuous Galerkin methods for problems with Lipschitz–type nonlinearities and blow–up in finite time. We also note the recent work [76] on adaptive hp-version dG-timestepping methods for finite time blow–up detection in semilinear parabolic problems.

Rigorous *a posteriori* error bounds for numerical methods for evolution problems are now a mature yet significantly expanding subject. The *a posteriori* error analysis of standard numerical methods for linear parabolic problems has been studied by many researchers. The classical works for the *a posteriori* error analysis for the dG timestepping schemes started with the seminal works of Erkisson, Johnson et al. [42, 43, 44, 45], in which they were studied and analysed space–time finite element methods involving dG–timestepping via duality techniques; see also [51, 53]. Picasso [91] showed *a posteriori* bounds of residual type for backward Euler timestepping methods. The idea of reconstruction was introduced in 2003 by Makridakis and Nochetto [83] for deriving optimal order *a posteriori* error estimates for semi-discrete linear parabolic problems through the energy method, and was further developed for the case of fully–discrete linear parabolic problems in [77]. A significant body of literature following in this vein is [7, 8, 83, 38, 59, 78, 50, 18, 74, 87, 92, 88]; we also refer to the survey [81] in which a general overview and treatment for the reconstruction technique is given. We note that the dG–timestepping reconstruction from [84] utilises the Gauss-Radau nodes, which are known to be points of superconvergence for the dG method in one dimension; see also [96] for a review of superconvergence in dG methods and the related question of postprocessing. *A posteriori* error analysis for linear parabolic problems for space-time methods has also received renewed attention during the 10 years or so: there has been a renewed interest in the derivation of rigorous *a posteriori* error bounds for dG timestepping schemes [84, 98, 76, 48, 49, 60, 55].

In spite of the progress made in the *a posteriori* error analysis of linear parabolic

problems discretised by traditional and classical time-marching schemes, semilinear and, generally, nonlinear evolution equations pose a number of additional challenges. These include the treatment of nonlinear reactions, the proof of lower bounds, etc. An interesting approach for semilinear parabolic problems is the use of so-called *continuation arguments* for the proof of *a posteriori* bounds. This idea appeared in [72] and further developed in [19, 20] for the Allen-Cahn and the Ginzburg-Landau equations and related phase–field models; see also [61, 54]. Related to this, in [75], the authors studied and derived the error estimates for blow-up solutions for semilinear parabolic equations which was further developed in the fully-discrete setting in [30]. All these developments in using continuation arguments for the proof of *a posteriori* bounds assumed standard low order timestepping schemes and, in particular, the backward Euler method.

Therefore, the proof of *a posteriori* error bounds for arbitrary order space–time methods involving dG-timestepping for nonlinear parabolic problems with strong nonlinearities (e.g., non globally Lipschitz) remains an interesting challenge which we aim to address in this thesis. At the same time, the proof of standard *a priori* error bounds for the same family of methods under such weak assumptions on the nonlinear growth is also elusive.

The *a priori* error analysis for classical timestepping schemes is now understood at large, see e.g. [116, 110, 28, 20, 29] and the references therein. In [28, 29], the authors examined the a priori error analysis for semilinear interface parabolic problems. The variational time–marching schemes are considered by many authors in different contexts [47, 52, 82, 101, 113, 117, 109, 23, 26]. Schötazu and Schwab [101] analysed and derived the *a priori* error estimates for the *hp*-version dG timestepping methods for initial value problems. Wihler [117] investigated the *a priori* error bounds for the *hp*–version cG timestepping schemes for nonlinear initial value problems.

1.3 Contributions of this work and outline

In this work, we consider the numerical solution of semilinear parabolic problems by using discontinuous Galerkin timestepping schemes in conjunction with conforming finite elements in space. To avoid the necessity of solving a nonlinear system for each time step, an implicit–explicit dG timestepping scheme is employed. This approach was first introduced in [52]. For this method we prove *a posteriori* and *a priori* error bounds for the case of merely locally Lipschitz nonlinear reactions that are *not* assumed to satisfy any monotonicity properties, thereby there is no coercivity in a stronger norm than the standard $L_\infty(L_2) + L_2(H^1)$–norm.

We are firstly concerned with the derivation of *hp*–version *a posteriori* error bounds in the $L_\infty(L_2)$– and $L_2(H^1)$–norms for fully discrete implicit–explicit (IMEX) methods of variable order for semilinear parabolic problems of reaction-diffusion type. The nonlinear reaction term is assumed to be locally Lipschitz and satisfying a growth condition in the spirit of [110]. The time discretisation consists of a *hp*–version discontinuous Galerkin method treating implicitly the diffusion spatial operator, and using an explicit multistep method for the nonlinear reaction term. This is combined with the standard conforming finite element method used for the spatial discretisation. The multistep IMEX–dG time discretisation we consider in this work was introduced in [52], whereby *a priori* error bounds were proven for the case of globally Lipschitz nonlinear reactions. To reduce the computational overhead, the nonlinear reactions are treated explicitly via sufficiently high–order interpolation of solution values from previous timesteps [52]. Therefore, the solution of one *linear* system per timestep is required. The proof combines the recent space–time reconstruction proposed in [60], along with a suitable implicit perturbation of the explicitly discretised nonlinear reaction part in the spirit of [58, 57]. The treatment of the non-Lipschitz nonlinearity involves a continuation argument in the spirit of [19, 28, 30] along with suitable Sobolev imbeddings. To the best of our knowledge, this is the first time such *a posteriori* error bounds for the fully–discrete methods involving dG–timestepping for nonlinear evolution PDEs appeared in the literature. Crucially, *no a priori* Courant-Friedrichs-Lewy (CFL) type conditions (with the respective often obscure constants involved) will

be required for the validity of our *a posteriori* error bounds for explicit timestepping methods (cf., also [58, 57]). Indeed, for unstable combinations of local spatial and temporal meshsizes, the *a posteriori* estimator remains reliable. In fact, this remarkable property motivates the study of *a posteriori* estimation of CFL constants as a non-standard potential use of rigorous *a posteriori* error upper bounds for (implicit–)explicit methods; this will be discussed elsewhere, as it is beyond the scope of this work.

On the other hand, the *a priori* error analysis for dG–timestepping schemes is both classical [47, 52, 109] and modern [36, 25, 113, 69, 70] in that a number of issues regarding regularity assumptions of the exact solution and the treatment of challenging nonlinearities have received considerable interest lately. In this work, we derive *hp*–version *a priori* error bounds for the fully–discrete IMEX–dG timestepping scheme discussed above in $L_\infty(L_2)$ and $L_2(H^1)$ norms. These error bounds are also explicit with respect to the local, possibly varying, order in the time discretisation (*hp*-version *a priori* error estimates). They are derived via a combination of classical ideas, such as the use of an elliptic projection technique and the discrete Grönwall inequality. Also, we employed enhanced discrete stability estimates in the $H^1(L_2)$–seminorm. We applied ideas from the recent works [27, 26] and extending them to the IMEX-dG discretisation of semilinear parabolic problems with merely locally-Lipschitz continuous nonlinear reaction term, thereby generalising the applicability of the results from [52] with lowest possible regularity. Also, we derived these error bounds with significantly less restrictive assumptions on the nonlinear reaction growth. Moreover, to the best of our knowledge, there are no previous results on *a priori* error bounds for fully–discrete methods involving dG–timestepping for nonlinear evolution PDEs, with locally-Lipschitz continuous nonlinearities.

The remainder of this thesis is organised as follows. Chapter 2 is introductory: we introduce some notation, and define the space–time scheme and space–time reconstruction operators, and derive the fully discrete implicit–explicit (IMEX) method of variable order for semilinear parabolic problems. Furthermore, a series of numerical examples investigating the performance of the numerical method

for solving semilinear parabolic systems from biology and ecology are given. In Chapter 3, we consider the derivation of *a posteriori* error bounds for the fully discrete semilinear parabolic problems in $L_\infty(L_2)$ and $L_2(H^1)$ norms. Also, a set of numerical examples for linear and nonlinear parabolic equation highlighting the performance of the *a posteriori* error estimates are presented. *A priori* error bounds for the fully–discrete semilinear parabolic problems in $L_\infty(L_2)$ and $L_2(H^1)$ norms with as set of numerical experiments testing the validity of these error bounds are presented in Chapter 4. Some conclusions are given in Chapter 5.

Chapter 2

hp-Version discontinuous Galerkin timestepping methods for parabolic problems

2.1 Introduction

Discontinuous Galerkin timestepping methods are arbitrary order single step implicit dissipative methods. Due to this, they are suitable for dissipative evolution equations and, in particular, for various classes of parabolic problems. The order of convergence of dG(r) time–marching methods of polynomial degree r is $r+1$ for sufficiently smooth exact solutions. Also, these methods are A–stable and sometimes strongly A–stable, for more details see [97]. Another appealing feature of the discontinuous Galerkin timestepping methods, is that they require lower regularity of solutions compared to other timestepping schemes, and they naturally allow for locally variable time steps (i.e., different timestep sizes at different parts of the spatial domain) and variable polynomials orders making them more convenient for h–, p–, and hp–versions time-stepping schemes. Consequently, they are more relevant to use for h–, p–, hp–adaptivity.

Here we study a fully–discrete implicit time–discontinuous and spatially conforming Galerkin scheme for evolutionary semilinear parabolic problems. For convenience in this chapter, we will follow Rothe's approach by firstly discretising in time, and then discretising the resulting scheme in space to obtain at the end the fully discrete space–time scheme for parabolic problems. Finally, we will present a series of numerical applications of dG–timestepping schemes of various orders in mathematical biology and mathematical ecology.

Remark 2.1. Throughout the thesis, the constant C is used to denote an arbitrary real constant, and it is not necessarily the same each time it occurs.

2.2 Useful inequalities

In this section, we recall from [95] some inequalities which will be used frequently in the remaining of this thesis.

Definition 2.2 (Hölder's inequality)**.** Let $1 \leq p, q \leq \infty$ such that $\frac{1}{p} + \frac{1}{q}$, then for any $u \in L_p(\Omega)$ and $v \in L_q(\Omega)$, the product $uv \in L_1(\Omega)$, and we have

$$|(u, v)_\Omega| \leq \|u\|_{L_p(\Omega)} \|v\|_{L_q(\Omega)}. \tag{2.1}$$

"Note that" the Cauchy–Schwarz's inequality is a special case of the Hölder's inequality when $p = q = 2$.

Definition 2.3 (Young's inequality)**.** For every $a, b \in R$, and for every $\varepsilon > 0$, we have

$$ab \leq \frac{\varepsilon}{2} a^2 + \frac{1}{2\varepsilon} b^2. \tag{2.2}$$

Definition 2.4 (Continuous Gronwall's inequality)**.** Let u, v, w be piecewise continuous nonnegative functions defined on the interval (a, b). Assume that v is nondecreasing function and that there is a positive constant C independent of t

such that, for all $t \in (a, b)$,

$$u(t) + w(t) \leq v(t) + C \int_a^t u(\tau)\, \mathrm{d}\tau. \tag{2.3}$$

Then, for all $t \in (a, b)$,

$$u(t) + w(t) \leq e^{C(t-a)} v(t). \tag{2.4}$$

Definition 2.5 (Discrete Gronwall's inequality)**.** Let $(a_n)_n, (b_n)_n$, and $(c_n)_n$ be sequences of nonnegative numbers satisfying, for all $n \geq 0$,

$$a_n \leq b_n + \sum_{i=0}^{n} c_i a_i. \tag{2.5}$$

Then, for all $n \geq 0$,

$$a_n \leq b_n + \sum_{i=0}^{n} b_i c_i \, exp\Big(\sum_{j=i}^{n} c_j\Big). \tag{2.6}$$

Definition 2.6 (Poincaré–Friedrichs inequality)**.** There is a positive constant C such that for every $v \in H^1(\Omega)$,

$$\|v\|_{L_2(\Omega)} \leq C\Big(\|\nabla v\|_{L_2(\Omega)} + |\int_{\partial\Omega} v|\Big). \tag{2.7}$$

As special case, we have, for every $v \in H_0^1(\Omega)$,

$$\|v\|_{L_2(\Omega)} \leq C\|\nabla v\|_{L_2(\Omega)}. \tag{2.8}$$

Definition 2.7 (Sobolev imbedding inequality)**.** For $1 \leq q < \infty$, and if $\Omega \subset \mathbb{R}^2$, the space $H_0^1(\Omega)$ is imbedded into the space $L_q(\Omega)$, i.e., for every $v \in H_0^1(\Omega)$,

$$\|v\|_{L_q(\Omega)} \leq C\|\nabla v\|_{L_2(\Omega)}. \tag{2.9}$$

2.3 Problem setup and the numerical method

2.3.1 Preliminaries and the abstract setting

For $\mathcal{H}$ a real Hilbert space and $\mathcal{I} = [a, b] \subset \mathbb{R}$, the Bochner space $L_p(\mathcal{I}; \mathcal{H})$ is defined by $L_p(\mathcal{I}; \mathcal{H}) := \{v : \mathcal{I} \to \mathcal{H} \text{ such that } \|v\|_{L_p(\mathcal{I};\mathcal{H})} < \infty\}$, with the respective norm given by

$$\|v\|_{L_p(\mathcal{I};\mathcal{H})} := \begin{cases} \Big(\int_{\mathcal{I}} \|v(t)\|_{\mathcal{H}}^p \, \mathrm{d}t \Big)^{1/p}, & \text{for } 1 \le p < \infty, \\ \operatorname{ess\,sup}_{t \in \mathcal{I}} \|v(t)\|_{\mathcal{H}}, & \text{for } p = \infty. \end{cases}$$

Upon denoting by v' the (weak) derivative of v with respect to the "time"-variable $t \in \mathcal{I}$, we can also define the Sobolev-Bochner spaces of order k (with respect to the time derivatives), where k is a positive integer, as

$$W_p^k(\mathcal{I}; \mathcal{H}) := \{v, v', v'', \cdots, v^k : \mathcal{I} \to \mathcal{H} \text{ such that } \|v\|_{W_p^k(\mathcal{I};\mathcal{H})} < \infty\}.$$

As special case, we define

$$W_p^1(\mathcal{I}; \mathcal{H}) := \{v, v' : \mathcal{I} \to \mathcal{H} \text{ such that } \|v\|_{W_p^1(\mathcal{I};\mathcal{H})} < \infty\},$$

and $\|v\|_{W_p^1(\mathcal{I};\mathcal{H})} := \Big(\|v\|^p_{L_p(\mathcal{I};\mathcal{H})} + \|v'\|^p_{L_p(\mathcal{I};\mathcal{H})} \Big)^{1/p}$. When $\Big(\mathcal{H}, (\cdot, \cdot)_{\mathcal{H}}\Big)$ is a Hilbert space with respective inner product, $L_2(\mathcal{I}; \mathcal{H})$ and $H^1(\mathcal{I}; \mathcal{H}) \equiv W_2^1(\mathcal{I}; \mathcal{H})$ are also Hilbert spaces endowed with the inner products $\int_{\mathcal{I}} (v(t), w(t))_{\mathcal{H}} \, \mathrm{d}t$ and $\int_{\mathcal{I}} (v(t), w(t))_{\mathcal{H}} + (v'(t), w'(t))_{\mathcal{H}} \, \mathrm{d}t$, respectively. We may also write $Z(a, b; \mathcal{H})$ instead of $Z(\mathcal{I}; \mathcal{H})$ for $Z \in \{L_p, W_p^1\}$, see [109, 95].

We also denote by $C(\mathcal{I}; \mathcal{V}) := \{v : \mathcal{I} \longrightarrow \mathcal{V} : v \text{ is continuous}\}$ the space of continuous in time functions equipped with the norm

$$\|v\|_{C(\mathcal{I};\mathcal{V})} := \sup_{t \in \mathcal{I}} \|v(t)\|_{\mathcal{V}}.$$

Let $\mathcal{V} \subset \mathcal{H}$ be another Hilbert space with norm $\|\cdot\|_{\mathcal{V}}$ and let $\mathcal{V}^*$ denote its dual space defined on the space of all functions z for which the norm

$$\|z\|_{\mathcal{V}^*} := \sup_{0 \neq v \in \mathcal{V}} \frac{(z, v)_{\mathcal{H}}}{\|v\|_{\mathcal{V}}},$$

is finite. The spaces $\mathcal{V}$, $\mathcal{H}$ and $\mathcal{V}^*$ form a, so-called, Gelfand triple

$$\mathcal{V} \hookrightarrow \mathcal{H} \hookrightarrow \mathcal{V}^*,$$

with the duality pairing $\langle \cdot, \cdot \rangle_{\mathcal{V}^* \times \mathcal{V}}$ extending the inner product $(\cdot, \cdot)_{\mathcal{H}}$, in the sense that, for all $u \in \mathcal{H}$ and $v \in \mathcal{V}$ holds $\langle u, v \rangle_{\mathcal{V}^* \times \mathcal{V}} = (u, v)_{\mathcal{H}}$. The subscript $\mathcal{V}^* \times \mathcal{V}$ in the duality pairing will be omitted whenever no confusion is likely to occur. Although we shall work within the above abstract setting, a typical case is when $\mathcal{H} = L_2(\Omega)$, $\mathcal{V} = H_0^1(\Omega)$, $\mathcal{V}^* = H^{-1}(\Omega)$.

We consider the semilinear parabolic initial value problem:
find $u \in H^1(0, T; \mathcal{V}^*) \cap L_2(0, T; \mathcal{V})$ such that

$$u' + \mathcal{A}u = f(\cdot, u) \quad \text{for all } t \in \mathcal{I}, \qquad u(0) = u_0, \tag{2.10}$$

for some known function $u_0 \in \mathcal{H}$, $u = u(t, x), x \in \mathbb{R}^d$, where d is a positive constant, and $\mathcal{A} : \mathcal{V} \longrightarrow \mathcal{V}^*$ is a linear elliptic operator, which is continuous and coercive(elliptic) with respect to the norm of $\mathcal{V}$. We also define the bilinear form $a : \mathcal{V} \times \mathcal{V} \longrightarrow \mathbb{R}$ associated with $\mathcal{A}$ by

$$\langle \mathcal{A}v, w \rangle_{\mathcal{V}^* \times \mathcal{V}} = a(v, w) \quad \text{for all } v, w \in \mathcal{V}, \tag{2.11}$$

which inherits the continuity and coercivity properties of $\mathcal{A}$, viz.,

$$|a(v, w)| \leq C_{\text{cont}} \|v\|_{\mathcal{V}} \|w\|_{\mathcal{V}} \quad \text{for all } v, w \in \mathcal{V}, \tag{2.12}$$

$$a(v, v) \geq C_{\text{coer}} \|v\|_{\mathcal{V}}^2 \quad \text{for all } v \in \mathcal{V}, \tag{2.13}$$

with C_{cont}, C_{coer} positive constants independent of v, w. Of course, the analysis presented below can be generalised to the case where a satisfies a Gärding-type

inequality instead; we prefer to keep the presentation simple by assuming just he coercivity of a instead throughout.

The function $f : \mathcal{I} \times \mathbb{R}^d \times \mathbb{R} \to \mathbb{R}$ is smooth and locally Lipschitz–continuous, bounded in the first two arguments and satisfies the growth condition for the third argument [110]:

$$|f(t,x,z_1) - f(t,x,z_2)| \leq C|z_1 - z_2|(1 + |z_1| + |z_2|)^{\mathbf{r}}, \quad \text{for } \mathbf{r} \geq 0, \tag{2.14}$$

for all $z_1, z_2 \in \mathbb{R}$ with $|\cdot|$ denoting the Euclidean distance. Here, C is a positive constant, uniform with respect to the first two arguments. The range of $\mathbf{r}$ will be further constrained from above in what follows, depending on the dimension of the spatial computational domain $\Omega \subset \mathbb{R}^d$. In what follows, we shall often suppress for brevity the dependence of f on its first two arguments writing, therefore, $f(t,x,w) = f(w)$. Generalisations of the above assumptions in the first two arguments are possible in the context of certain Caratheodory-type conditions, but we refrain from discussing these in the interest of simplicity of the presentation. Crucially, however, we do *not* assume any monotonicity of the nonlinear reaction terms. As a result, we do not have any extra control in norms other than the respective linear problem.

2.3.2 Space–time Galerkin spaces

Let $\mathcal{I} = [0,T]$ be the time interval with final time $T > 0$ and, for $0 = t_0 < t_1 < ... < t_N = T$, consider the partition $\{\mathcal{I}_n, n = 0, ..., N\}$ of I into subintervals $\mathcal{I}_n := (t_{n-1}, t_n]$ for $n = 1, ..., N$, and $I_0 := \{0\}$, with corresponding timesteps $k_n := t_n - t_{n-1}$, $n = 1, 2, ..., N$. We also consider a finite sequence $\{\mathcal{V}_n\}_{n=0}^N$ with $\mathcal{V}_n \subset \mathcal{V}$, $n = 0, ..., N$ of conforming finite element subspaces of $\mathcal{V}$, associated with the time subintervals $\mathcal{I}_n$.

Let $\mathcal{H}$ be a Hilbert space. We define

$$\mathcal{P}^r(\mathbb{R};\mathcal{H}) := \{p : \mathbb{R} \to \mathcal{H} : p(t) = \sum_{i=0}^{r} \psi_i t^i, \psi_i \in \mathcal{H}, i = 0, 1 \ldots, r\},$$

as the space of $\mathcal{H}$–valued polynomials of degree at most r. More generally, we define $\mathcal{P}^r(\mathcal{I};\mathcal{H}) := \{p|_{\mathcal{I}} : p \in \mathcal{P}^r(\mathbb{R};\mathcal{H})\}$. We also consider the time-discrete and the space-time finite element subspaces

$$\mathcal{Y}_n(S) := \mathcal{P}^{r_n}(\mathcal{I}_n;S),\ S \in \{\mathcal{H},\mathcal{V}\}, \quad \text{and} \quad \mathcal{X}_n(\tilde{S}) := \mathcal{P}^{r_n}(\mathcal{I}_n;\tilde{S}),\ \tilde{S} \in \{\mathcal{V}_n,\mathcal{V}_h\},$$

respectively, for all $n = 0, 1, \ldots, N$ with r_n denoting the local temporal polynomial degree, which may vary from one timestep to another, and $\mathcal{V}_h \subset \mathcal{V}$ is a (conforming) finite element space.

We can then define the time–discrete and the space–time Galerkin spaces

$$\mathcal{Y}(S) \equiv \mathcal{Y}_{\mathbf{r}}(S) := \{v : [0,T] \to S : v|_{\mathcal{I}_n} \in \mathcal{Y}_n(S),\ n = 0, 1, \ldots, N\},$$

and

$$\mathcal{X}(\tilde{S}) \equiv \mathcal{X}_{\mathbf{r}}(\tilde{S}) := \{v : [0,T] \to \tilde{S} : v|_{\mathcal{I}_n} \in \mathcal{X}_n(\tilde{S}),\ n = 0, 1, \ldots, N\},$$

respectively, often suppressing the dependence on the polynomial degree vector $\mathsf{r} := (r_1, r_2, \ldots, r_N)$ for brevity.

Moreover, for a piecewise continuous function $v : I \subset \mathbb{R} \to \mathcal{H}$, with the time nodes t_n as possible points of discontinuity, we define the *time–jump*

$$[v]_n := v_n^+ - v_n^-,$$

where $v_n^{\pm} := \lim_{\delta \to 0^+} v(t_n \pm \delta)$, the respective one–sided (right and left) limits for $n = 0, 1, \ldots, N$. For more details, see [99, 73].

2.3.3 The fully discrete IMEX space–time finite element schemes

In this section, we drive the fully–discrete *implicit* time discontinuous and spatially continuous Galerkin discretisation of the problem (2.10). Writing the model

problem (2.10) in weak form by testing it with a smooth function χ and integrating over the spatial domain Ω, and also integrating in time over the time domain $\mathcal{I} = [0, T]$, we have

$$\int_0^T \Big((u', \chi)_{\mathcal{H}} + a(u, \chi) \Big) \, \mathrm{d}t = \int_0^T (f(u), \chi)_{\mathcal{H}} \, \mathrm{d}t, \ \forall \chi \in \mathcal{X}. \tag{2.15}$$

Now, integrating by parts the first term in (2.15) and letting $\chi(T) = 0$, we obtain

$$\int_0^T \Big(-(u, \chi')_{\mathcal{H}} + a(u, \chi) \Big) \, \mathrm{d}t = (u_0, \chi(0))_{\mathcal{H}} + \int_0^T (f(u), \chi)_{\mathcal{H}} \, \mathrm{d}t \ \forall \chi \in \mathcal{X}. \tag{2.16}$$

Now, approximating the exact solution u by a function $U \in \mathcal{X}_n$, yields

$$\int_0^T \Big(-(U, v')_{\mathcal{H}} + a(U, v) \Big) \, \mathrm{d}t = (U_0^-, v_0^+)_{\mathcal{H}} + \int_0^T (f(u), v)_{\mathcal{H}} \, \mathrm{d}t \ \forall v \in \mathcal{X}_n. \tag{2.17}$$

Integrating by parts the first term in (2.17) in each time interval $\mathcal{I}_n$, and noting that $v_T^+ = 0$, implies

$$\begin{aligned} -\int_0^T (U, v')_{\mathcal{H}} \, \mathrm{d}t &= -\sum_{n=1}^N \left(\Big((U, v)_{\mathcal{H}} |_{t_{n-1}}^{t_n} - \int_{t_{n-1}}^{t_n} (U', v) \Big) \, \mathrm{d}t \right) \forall v \in \mathcal{X}_n \\ &= \int_0^T (U', v)_{\mathcal{H}} \, \mathrm{d}t + \sum_{n=2}^N ([U]_{n-1}, v_{n-1}^+)_{\mathcal{H}} + (U_0^+, v_0^+)_{\mathcal{H}}. \end{aligned} \tag{2.18}$$

Substituting (2.18) in (2.17), we arrive at

$$\begin{aligned} \int_0^T \Big((U', v)_{\mathcal{H}} + a(U, v) \Big) \, \mathrm{d}t + \sum_{n=2}^N ([U]_{n-1}, v_{n-1}^+)_{\mathcal{H}} + (U_0^+, v_0^+)_{\mathcal{H}} \\ = (U_0^-, v_0^+)_{\mathcal{H}} + \int_0^T (f(u), v)_{\mathcal{H}} \, \mathrm{d}t \ \forall v \in \mathcal{X}_n. \end{aligned} \tag{2.19}$$

Due to the discontinuity of $v \in \mathcal{X}_n$, choosing $v = 0$ outside the time interval $\mathcal{I}_n$ decouples the problem (2.19) into one problem on each time interval $\mathcal{I}_n$ for $n \leq N$. Finally, we arrive at the fully–discrete *implicit* time discontinuous and spatially conforming Galerkin approximation of (2.10) which reads: set $U_0^- := \tilde{P}_0 u_0$ and find $U \in \mathcal{X}$ such that

$$\int_{\mathcal{I}_n} \left((U', v)_{\mathcal{H}} + a(U, v) \right) \, \mathrm{d}t + ([U]_{n-1}, v_{n-1}^+)_{\mathcal{H}} = \int_{\mathcal{I}_n} (f(U), v)_{\mathcal{H}} \, \mathrm{d}t \tag{2.20}$$

for all $v \in \mathcal{X}_n$ and for $n = 1, ..., N$, Here $\tilde{P}_0$ denotes the elliptic projection operator and will be defined later, and $[U]_n = U_n^+ - U_n^-$, see [109]. The space-time method (2.20) is fully implicit in the sense that a nonlinear system of equations for the numerical degrees of freedom has to be solved at each time interval.

Aiming for a linearly implicit method, we follow [52] and we replace $f(U)$ in (2.20) by its linear interpolant in time $\Pi f(U)$, defined so that $\Pi f(U)|_{\mathcal{I}_n} \in \mathcal{P}^\mu(\mathcal{I}_n; \mathcal{V}_n)$, for all $n = 1, \ldots, N$, where $\mu = 2r_n$, using values of U from previous time intervals $\mathcal{I}_m, m < n$ only and extrapolating the resulting interpolant into $\mathcal{I}_n$. In this case, the solution process will result in a linear system for U per time-step, giving rise to an implicit–explicit (IMEX) method. Of course, one can also interpolate on the previous and the current time intervals $\mathcal{I}_m, m \leq n$. This case will lead to a nonlinear system of equations for U, although it can potentially be easier to implement for certain nonlinearities f. In both cases, the time interpolant $\Pi f(U)$ can be represented on each $\mathcal{I}_n$ as

$$\Pi f(U)(t)|_{\mathcal{I}_n} := \Pi^\mu_{n-\jmath} f(U)(t) := \sum_{\eta=n-\jmath-\mu}^{n-\jmath} \xi_\eta(t) f(t_\eta, \cdot, U_\eta^-), \tag{2.21}$$

where $\Pi^\mu_{n-\jmath}$, $\jmath = 0, 1$, is the interpolation operator for polynomials of degree μ at the nodes $t_{n-\jmath-\mu}, \ldots, t_{n-\jmath}$ and ξ_η are the respective Lagrange basis functions defined as follows:

$$\xi_\eta = \mathbf{\Pi}_{i=n-\jmath-\mu}^{n-\jmath} \frac{(t - t_i)}{(t_\eta - t_i)}, i \neq \eta, \ \jmath = 0, 1, \tag{2.22}$$

for $\eta = n - \jmath - \mu, \cdots, n - \jmath$. The corresponding IMEX space–time scheme reads: set $U_0^- := \tilde{P}_0 u_0$ and find $U \in \mathcal{X}$ such that

$$\int_{\mathcal{I}_n} ((U', v)_{\mathcal{H}} + a(U, v)) \, \mathrm{d}t + ([U]_{n-1}, v_{n-1}^+)_{\mathcal{H}} = \int_{\mathcal{I}_n} (\Pi f(U), v)_{\mathcal{H}} \, \mathrm{d}t \tag{2.23}$$

for all $v \in \mathcal{X}_n$, for $n = \mu + \jmath, ..., N$. Of course, as this is a multistep method, we can only use it after a certain number of time-steps, depending on the order of the method. Without loss of convergence rate, however, we can consider a few (very small in size) timesteps with the zeroth order method, i.e., the implicit Euler method with explicit treatment of the nonlinear reaction, before using (2.23) with

higher order than zero. The interpolant degree $\mu = 2r_n$ is required to represent the integrand $(\Pi f(U), v)_{\mathcal{H}}$ without loss of convergence rates. Finally, for $\jmath = 1$, we arrive at the IMEX method, while, for $\jmath = 0$, we retrieve the fully implicit scheme; for further details we refer to [52]. Note that the values U_η^- are known to be points of superconvergence for the respective time-discrete problem, where the method has superconvergence rates $2r + 1$ at these points [71, 6]; see also [96].

2.4 Numerical implementation

In this section, we derive the numerical implementation of (2.23) by introducing appropriate basis for the space–time trial and test spaces, to arrive at a formulation where the numerical scheme can be computed by iterating through the time steps (time slabs) and solving a linear system at every time step. Firstly, we discretise in time and subsequently we discretise the resulting problem in space.

2.4.1 Discretisation in time

The discrete solution U is a polynomial function of the time variable of degree r. As such, it can be written in terms of basis functions $\phi_{n,j}(t) \in \mathcal{Y}_n,\ \forall j = 0, 1, ..., r$ as

$$U(t) := \sum_{j=0}^{r} U_n^j \phi_{n,j}(t), \quad \forall t \in \mathcal{I}_n, \tag{2.24}$$

and

$$U'(t) := \sum_{j=0}^{r} U_n^j \phi'_{n,j}(t), \quad \forall t \in \mathcal{I}_n, \tag{2.25}$$

where: U_n^j are the coefficients in the ansatzes (2.24) and (2.25) are elements of the space $\mathcal{V}_n$ and the basis functions $\phi_{n,j}$ are Lagrange polynomials of degree r defined for $r + 1$ nodal (support) points $t_{n,j} \in \mathcal{I}_n,\ j = 0, 1, ..., r$, to satisfy the conditions

$$\phi_{n,j}(t_i) = \delta_{i,j}, \forall i, j = 0, 1, ..., r, \tag{2.26}$$

where $\delta_{i,j}$ is the Kronecker delta

$$\delta_{i,j} = \begin{cases} 1 & \text{if } i = j, \\ 0 & \text{if } i \neq j. \end{cases} \tag{2.27}$$

The test functions in (2.23) can be chosen as products of two functions $\mathbf{v} = v\phi_{n,i}, i = 0, 1, ..., r$ where $v \in \mathcal{V}_n$ (space function) and $\phi_{n,i} \in \mathcal{X}_n$ (time function).

Now, setting $\mathbf{v} = v\phi_{n,i}$ and using (2.21), we can rewrite (2.23) as an $\mathcal{I}_n$–problem: set $U_0^- := \tilde{P}_0 u_0$ and find $U \in \mathcal{X}$ such that for all $v \in \mathcal{V}_n$ it holds

$$\begin{aligned} &\int_{\mathcal{I}_n} \Big((U', v)_{\mathcal{H}} + a(U, v) \Big) \phi_{n,i} \, \mathrm{d}t + ([U]_{n-1}, v)_{\mathcal{H}} \phi_{n,i}(t_{n-1}) \\ &= \int_{\mathcal{I}_n} \sum_{\eta=n-\jmath-\mu}^{n-\jmath} \xi_\eta (f(U_\eta^-), v)_{\mathcal{H}} \phi_{n,i} \, \mathrm{d}t \end{aligned} \tag{2.28}$$

for $i = 0, 1, ..., r$. We note this interpolant can be applied from the $(\mu+1)th$ interval i.e on $\mathcal{I}_{\mu+1}, \cdots, \mathcal{I}_N$, but can not be used on the first (μ) intervals i.e. on $\mathcal{I}_1, \cdots, \mathcal{I}_\mu$. For this reason we need to construct special interpolants for the first μ intervals. In the particular case when the solution is a constant polynomial, i.e. when $r_n = 0$, then the interpolant also is a constant polynomial, and, obviously, the constant interpolant can be applied for all the intervals $\mathcal{I}_1, \cdots, \mathcal{I}_n$.

By inserting the representations (2.24) and (2.25) in (2.28) we have the following linear algebraic system for the $r+1$ unknown coefficients $U_n^j \in \mathcal{V}_n, j = 0, 1, ..., r$:

$$\begin{aligned} &\sum_{j=0}^{r} (U_n^j, v)_{\mathcal{H}} \int_{\mathcal{I}_n} \phi'_{n,j} \phi_{n,i} \, \mathrm{d}t + \sum_{j=0}^{r} a(U_n^j, v) \int_{\mathcal{I}_n} \phi_{n,j} \phi_{n,i} \, \mathrm{d}t \\ &+ \sum_{j=0}^{r} (U_n^j, v)_{\mathcal{H}} \phi_{n,j}(t_{n-1}) \phi_{n,i}(t_{n-1}) \\ &= (U_{n-1}^{(0)}, v)_{\mathcal{H}} \phi_{n,i}(t_{n-1}) + \sum_{\eta=n-\jmath-\mu}^{n-\jmath} (f(U_\eta^-), v)_{\mathcal{H}} \int_{\mathcal{I}_n} \xi_\eta \phi_{n,i} \, \mathrm{d}t, \end{aligned} \tag{2.29}$$

where $U_{n-1}^{(0)} = U_{n-1}^-$ is the initial condition on the time interval $\mathcal{I}_n$ and, hence, it is obtained from the solution on the previous time interval $\mathcal{I}_{n-1}$.

The time integrals over $\mathcal{I}_n$ in (2.29) with the basis functions, test functions and

support points are mapped into the reference interval $\hat{\mathcal{I}} = [0, 1]$ and all computations are subsequently performed on the reference interval $\hat{\mathcal{I}}$. For this reason we define the affine domain transformation $T_n : \hat{\mathcal{I}} \longrightarrow \mathcal{I}_n$, such that

$$t := T_n(\hat{t}) = k_n\hat{t} + t_{n-1},\ \forall \hat{t} \in \hat{\mathcal{I}},\ n = 1, ..., N, \tag{2.30}$$

and the inverse reference mapping $T_n^{-1} : \mathcal{I}_n \longrightarrow \hat{\mathcal{I}}$ that maps back from the reference interval $\hat{\mathcal{I}}$ to the domain interval $\mathcal{I}_n$, given by

$$\hat{t} := T_n^{-1}(t) = (t - t_{n-1})/k_n,\ \forall t \in \mathcal{I}_n,\ n = 1, ..., N. \tag{2.31}$$

We define the reference basis functions and reference test functions $\hat{\phi}_j \in P^r(\hat{I}; \mathcal{V})$, $j = 0, 1, ..., r$ on the reference interval $\hat{\mathcal{I}}$ to be Lagrange polynomials of order $r \geq 0$ with respect to $r + 1$ nodal points $\hat{t}_j \in \hat{\mathcal{I}}$, $j = 0, 1, ..., r$ such that

$$\hat{\phi}_j(\hat{t}_i) = \delta_{i,j}, \forall i, j = 0, 1, ..., r. \tag{2.32}$$

The corresponding support points in the original domain interval $\mathcal{I}_n$ are given by

$$t_{n,j} = T_n(\hat{t}_j),\ j = 0, 1, ..., N.$$

Similarly, the relation between the original basis and the reference basis is

$$\phi_{n,j}(t) := \phi_{n,j}(T_n(\hat{t})) = \phi_{n,j}(t) \circ T_n(\hat{t}) = \hat{\phi}_j(\hat{t}),\ \hat{t} \in \hat{\mathcal{I}}, \forall n = 1, ..., N. \tag{2.33}$$

Now, by mapping the time integrals in (2.29) to the reference interval $\hat{\mathcal{I}}$ we obtain

$$\begin{aligned} &\sum_{j=0}^{r}(U_n^j, v)\int_{\hat{\mathcal{I}}}\hat{\phi}_j'\hat{\phi}_i\,d\hat{t} + k_n\sum_{j=0}^{r}a(U_n^j, v)\int_{\hat{\mathcal{I}}}\hat{\phi}_j\hat{\phi}_i\,\mathrm{d}\hat{t} + \sum_{j=0}^{r}(U_n^j, v)\hat{\phi}_j(0)\hat{\phi}_i(0) \\ &= (U_{n-1}^{(0)}, v)\hat{\phi}_i(0) + k_n\sum_{\eta=n-\jmath-\mu}^{n-\jmath}(f(U_\eta^-), v)\int_{\hat{\mathcal{I}}}\hat{\xi}_\eta\hat{\phi}_i\,\mathrm{d}\hat{t}. \end{aligned} \tag{2.34}$$

For brevity, we denote the integrals and coefficients in (2.34) by

$$\alpha_{i,j} := \int_{\hat{\mathcal{I}}}\hat{\phi}_j'\hat{\phi}_i\,\mathrm{d}\hat{t},\ i, j = 0, 1, ..., r, \tag{2.35}$$

$$\beta_{i,j} := \int_{\hat{\mathcal{I}}} \hat{\phi}_j \hat{\phi}_i \, \mathrm{d}\hat{t}, \ i,j = 0,1,...,r, \tag{2.36}$$

$$\gamma_{i,j} := \hat{\phi}_j(0)\hat{\phi}_i(0), \ i,j = 0,1,...,r,$$

$$\sigma_i := \hat{\phi}_i(0), \ i = 0,1,...,r,$$

and

$$\varrho_{i,\eta} := \int_{\hat{\mathcal{I}}} \hat{\xi}_\eta \hat{\phi}_i \, \mathrm{d}\hat{t}, \ \eta = n - \jmath - \mu, \cdots, n - \jmath, \ i = 0,1,\cdots,r, \jmath = 0,1,$$

thereby arriving at

$$\begin{aligned} &\sum_{j=0}^{r} \Big(\epsilon_{i,j}(U_n^j, v) + k_n \beta_{i,j} a(U_n^j, v) \Big) \\ &= \sigma_i(U_{n-1}^{(0)}, v) + k_n \sum_{\eta=n-\jmath-\mu}^{n-\jmath} \varrho_{i,\eta}(f(U_\eta^-), v), \quad i = 0,1,...,r, \end{aligned} \tag{2.37}$$

where

$$\epsilon_{i,j} := \alpha_{i,j} + \gamma_{i,j}, \ i,j = 0,1,...,r. \tag{2.38}$$

2.4.2 Discretisation in space

In this section, we expand upon the spatial discretisation of (2.37) in view of deriving the complete space–time discrete schemes. Since the discrete functions U_n^j belong to the discrete space $\mathcal{V}_n$ they can be written as a linear combination of its basis functions. Let n_h be the dimension of $\mathcal{V}_n$, the number of the degrees of freedom (dofs) in space at each time step. Assume that a set of nodal dofs is given and let $\zeta_l(x) \in \mathcal{V}_n$ be the corresponding Lagrangian basis. Let $\underline{\mathbf{U}}_n^j \in R^{n_h}$ be the vector of nodal values associated to the functions $U_n^j \in \mathcal{V}_n$. Then, the approximate finite element solution $U_h(t,x)$ is written as

$$U_n^j(t,x) := \sum_{l=1}^{n_h} (\underline{\mathbf{U}}_n^j)_l \, \zeta_l(x) \quad \forall t \in \mathcal{I}_n, \ x \in \Omega. \tag{2.39}$$

The approximate time discrete solution $U(t) \in \mathcal{V}$ in (2.24) is approximated now by space–time fully discrete finite element solution $U_h(t,x) \in \mathcal{V}_n$ and is represented

on the reference time interval $\hat{\mathcal{I}}$ by

$$U_h(\hat{t},x) := \sum_{l=1}^{n_h}\sum_{j=0}^{r}(\underline{\mathbf{U}}_n^j)_l\,\zeta_l(x)\hat{\phi}_j(\hat{t}) \quad \forall \hat{t}\in\hat{\mathcal{I}},\ x\in\Omega. \tag{2.40}$$

The nonlinear function $f(U)$, and, consequently, the nonlinear term $(f(U_\eta^-),v)$ reads

$$f(U_\eta^-) := \sum_{l=1}^{n_h} f(\underline{\mathbf{U}}_\eta^-)_l\,\zeta_l(x) \quad \forall x\in\Omega, \tag{2.41}$$

$$(f(U_\eta^-),v)_{\mathcal{H}} = (\sum_{l=1}^{n_h} f(\underline{\mathbf{U}}_\eta^-)_l\,\zeta_l,\zeta_s)_{\mathcal{H}} = \sum_{l=1}^{n_h} f(\underline{\mathbf{U}}_\eta^-)_l(\zeta_l,\zeta_s)_{\mathcal{H}}, \tag{2.42}$$

where the subscript l represents the values of the interpolant and the basis functions at the nodal points.

Hence, after inserting all these terms into (2.37), we get

$$\begin{aligned}&\sum_{j=0}^{r}\epsilon_{i,j}\sum_{l=1}^{n_h}(\underline{\mathbf{U}}_n^j)_l(\zeta_l,\zeta_s)_{\mathcal{H}} + k_n\sum_{j=0}^{r}\beta_{i,j}(\underline{\mathbf{U}}_n^j)_l\sum_{l=1}^{n_h}a(\zeta_l,\zeta_s)\\ &= \sigma_i\sum_{l=1}^{n_h}\underline{\mathbf{U}}_{n-1}^{(0)}(\zeta_l,\zeta_s)_{\mathcal{H}} + k_n\sum_{\eta=n-\jmath-\mu\mu}^{n-\jmath}\varrho_{i,\eta}\sum_{l=1}^{n_h}f(\underline{\mathbf{U}}_\eta^-)_l(\zeta_l,\zeta_s)_{\mathcal{H}},\end{aligned} \tag{2.43}$$

for $s=1,...,n_h$.

We denote the mass matrix $M\in R^{n_h}\times R^{n_h}$ by

$$M_{l,s} := (\zeta_l,\zeta_s)_{\mathcal{H}}; \tag{2.44}$$

also, the stiffness matrix $S\in R^{n_h}\times R^{n_h}$ is defined by

$$S_{l,s} := a(\zeta_l,\zeta_s), \tag{2.45}$$

which leads to

$$\sum_{j=0}^{r}\epsilon_{i,j}M\underline{\mathbf{U}}_n^j + k_n\sum_{j=0}^{r}\beta_{i,j}S\underline{\mathbf{U}}_n^j = \sigma_i M\underline{\mathbf{U}}_{n-1}^{(0)} + k_n\sum_{\eta=n-\jmath-\mu}^{n-\jmath}\varrho_{i,\eta}Mf(\underline{\mathbf{U}}_\eta^-) \tag{2.46}$$

for $i = 0, 1, ..., r$. This system is used to find the solution on the time interval $\mathcal{I}_n$ where $n \geq \mu + \jmath$. That is, $n \geq \mu$ in the fully implicit nonlinear case and $n \geq \mu + 1$ in the implicit–explicit (IMEX) case. The matrix form of the general case of the system in (2.46) and the matrix forms for the fully-implicit and implicit–explicit cases can be found in Appendix A.

The integrals in (2.34) are evaluated by using appropriate quadrature rules. Different choices of quadrature formulas can be used depending on the specific application. Also, the integrands in (2.35) and (2.36) are polynomials of degree $2r - 1$ and $2r$, respectively, and can be integrated exactly by using appropriate numerical quadrature rules.

2.5 hp–dG–timestepping for parabolic systems

We now study the variational discretisation of a semilinear system of evolutionary parabolic equations in the form: find $u, v : \mathcal{I} \times \Omega \longrightarrow R$ such that

$$\begin{aligned}
&\frac{\partial u}{\partial t} - l_1 \Delta u = f(u, v), \quad \text{in } \mathcal{I} \times \Omega, \\
&\frac{\partial v}{\partial t} - l_2 \Delta v = g(u, v), \quad \text{in } \mathcal{I} \times \Omega, \\
&u(t, \mathbf{x}) = 0, \ v(t, \mathbf{x}) = 0, \qquad \text{for } t \in \mathcal{I} \text{ and } \mathbf{x} \in \partial\Omega, \\
&u(0, \mathbf{x}) = u_0, \ v(0, \mathbf{x}) = v_0, \qquad \text{for } \mathbf{x} \in \Omega,
\end{aligned} \tag{2.47}$$

where l_1, l_2 are the diffusion coefficients, $\Omega \subset \mathbb{R}^d,\ d = 1, 2, 3$ is a polygonal domain (polyhedral domain in $\mathbb{R}^3$), $\mathbb{R}$ is the field of real numbers and $\mathcal{I} = [0, T]$ is a finite time interval with $T > 0$ being the final time. The unknowns $u = u(t, \mathbf{x}), v = v(t, \mathbf{x})$ represent the solution at the point (position) $\mathbf{x}$ at time $t \in \mathcal{I}$. $f(u, v), g(u, v)$ are smooth functions and u_0, v_0 are the initial conditions at time $t = 0$. We will consider here for simplicity in treatment and exposure the homogeneous Dirichlet boundary conditions (zero boundary conditions) on the boundary of the domain Ω. The case of non-essential (Neumann) boundary conditions also follows without any technical challenge, although it is omitted here for brevity. With respect to

the notation used in previous sections, this problem corresponds to $\mathcal{A} = -\Delta$, $\mathcal{V} = H_0^1(\Omega)$ and $\mathcal{H} = L_2(\Omega)$.

The process of finding a solution of a system of equations is the same for each unknown variable in the system. The same techniques used in the derivation of the dG time-marching schemes for a single semilinear equation can be extended easily to the system of two (or more) semilinear equations with just some simple modifications. Indeed, by following the same steps we used in the previous sections for obtaining (2.20) for (2.10) we arrive at the following linear system of equations for the system in (2.47):

$$\begin{aligned}
\sum_{j=0}^{r} \epsilon_{i,j} M \underline{\mathbf{U}}_n^j + l_1 k_n \sum_{j=0}^{r} \beta_{i,j} S \underline{\mathbf{U}}_n^j &= \sigma_i M \underline{\mathbf{U}}_{n-1}^{(0)} + k_n \sum_{\eta=n-\jmath-\mu}^{n-\jmath} \varrho_{i,\eta} M f(\underline{\mathbf{U}}_\eta^-, \underline{\mathbf{V}}_\eta^-), \\
\sum_{j=0}^{r} \epsilon_{i,j} M \underline{\mathbf{V}}_n^j + l_2 k_n \sum_{j=0}^{r} \beta_{i,j} S \underline{\mathbf{V}}_n^j &= \sigma_i M \underline{\mathbf{V}}_{n-1}^{(0)} + k_n \sum_{\eta=n-\jmath-\mu}^{n-\jmath} \varrho_{i,\eta} M g(\underline{\mathbf{U}}_\eta^-, \underline{\mathbf{V}}_\eta^-),
\end{aligned} \tag{2.48}$$

for $i = 0, 1, ..., r$. The matrix form of the general case of the system in (2.48) and the matrix forms for the fully-implicit and implicit–explicit cases can be found in Appendix A.

Remark 2.8. The process of finding the approximate solutions to single linear parabolic equations or systems of linear parabolic equations is similar to the case of single semilinear parabolic equations or systems of semilinear parabolic equations. The only difference is that the nonlinear source term $f(U)$ is replaced by the linear source term $f(t, \mathbf{x})$ and by using appropriate quadrature rules the integrals involved the source function f can be computed easily.

2.6 Numerical examples and applications

Reaction-diffusion systems are very popular as mathematical models in a wide range of applications in mathematical biology and mathematical ecology, such as population dynamics and modelling of biological processes. Typically, these models are nonlinear and, in particular, semilinear parabolic PDE problems. The

solutions to such problems are usually impossible or very difficult to find analytically. Hence, the alternative is to compute these solutions approximately by using numerical methods such as the finite element methods. In this section, we will consider the numerical solution to special cases of these problems modelling cyclic competition between different species by using the time–discontinuous and space–continuous Galerkin finite element methods presented above. The numerical implementation is based on the `deal.II` finite element library [16] and the tests run in the high performance computing facility ALICE at the University of Leicester.

2.6.1 Example 1: Fisher system

We consider the solution of the following semilinear reaction-diffusion system

$$\begin{aligned} &\frac{\partial u}{\partial t} - \Delta u = f(u,v), \text{ in } \mathcal{I}\times\Omega, \\ &\frac{\partial v}{\partial t} - \Delta v = g(u,v), \text{ in } \mathcal{I}\times\Omega, \\ &u = v = 0, \quad \text{for } t\in\mathcal{I} \text{ and } \mathbf{x}\in\partial\Omega, \\ &u(0,\mathbf{x}) = u_0,\ v(0,\mathbf{x}) = v_0,\ \mathbf{x}\in\Omega, \end{aligned} \tag{2.49}$$

where $\mathbf{x} = (x, y)$, for $\mathcal{I}\times\Omega = [0,1]\times[0,1]^2$, and the nonlinearities are given by

$$f(u,v) = u(1-v) + f_1(t,x,y),$$

$$g(u,v) = v(1-u) + g_1(t,x,y),$$

and f_1, g_1 are independent of the solution components u and v. The initial conditions and boundary conditions are chosen such that the exact solution is:

$$u = e^{-t}x(1-x)y(1-y),$$

$$v = e^{-2t}x(1-x)y(1-y).$$

We use a rectangular mesh consisting of 1024 uniform biquadratic elements in space ($p = 2$) and uniform linear elements in time $r = 1$, which we denote for

brevity as dG(1)–cG(2) scheme. Given that the solution components are quadratic polynomials in space, this ensures that the space error is negligible and consequently the time error dominates. This allows for assessing the order of convergence of the dG timestepping method by varying the timestep size k_n while the mesh size is kept fixed at $h = 1/32$. In particular, we study the asymptotic behaviour of the error $e = u - U$ in the $L_\infty(L_\infty)$–, $L_2(L_2)$–, and $L_\infty(L_2)$– error norms by monitoring the evolution of the experimental order of convergence (EOC) over time on a sequence of uniformly refined meshes in time. We also examine the superconvergence of the L_2–error at the endpoints of the time intervals, denoted by $\ell_\infty(L_2)$–error. The resulting errors are plotted against the corresponding time step size k_n. The EOC of a given sequence of positive quantities a_i defined on a sequence of meshes of step sizes b_i is defined by

$$\mathrm{EOC}(a, i) = \frac{\log(a_i/a_{i-1})}{\log(b_i/b_{i-1})}. \tag{2.50}$$

We report the EOC relative to the last computed quantities in the figure as an indication of the asymptotic rate of convergence. In this example, a_i represent the error norms and b_i are the time step sizes k_n.

In Figure 2.1 (a), (b) and (c) we report the $L_\infty(L_\infty)$– $L_2(L_2)$– and $L_\infty(L_2)$–norm errors, respectively, all of which are of optimal order of convergence with $EOC \approx 2$. Also, Figure 2.1 (d) shows that the superconvergence of the $\ell_\infty(L_2)$– error norm at the endpoints of the time intervals with $EOC \approx 3$. The results are in agreement with theoretical results in Chapter 4.

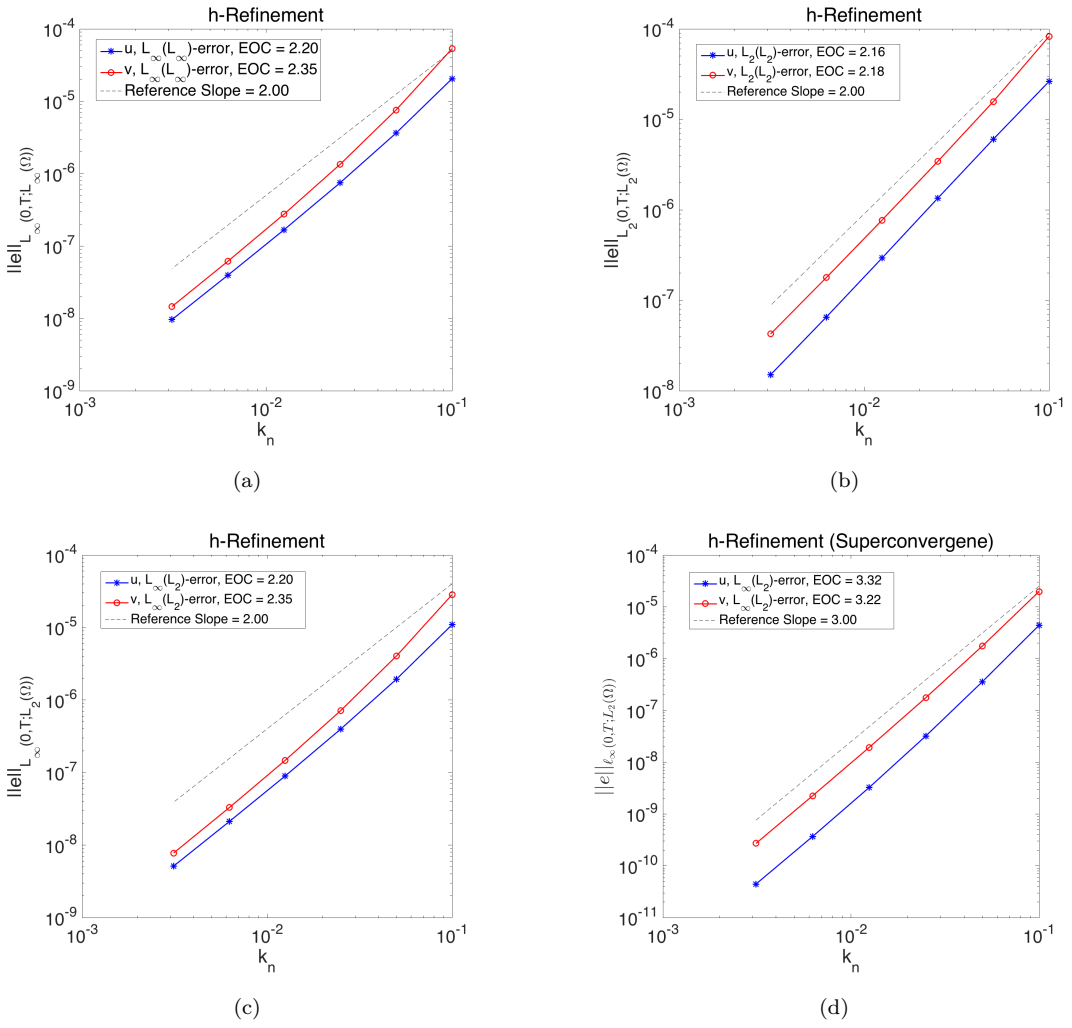

FIGURE 2.1: Example 1: Convergence history for dG(1)–cG(2) scheme for solving Fisher System.

2.6.2 Example 2: Cycling Lotka–Volterra competition system

We solve the semilinear system of three–species competition consisting of three semilinear parabolic equations with homogeneous Neumann boundary conditions

$$\begin{aligned}
\frac{\partial u_1}{\partial t} - D_1\Delta u_1 &= \alpha_1 u_1(1 - a_{1,1}u_1 - a_{1,2}u_2 - a_{1,3}u_3),\\
\frac{\partial u_2}{\partial t} - D_2\Delta u_2 &= \alpha_2 u_2(1 - a_{2,1}u_1 - a_{2,2}u_2 - a_{2,3}u_3),\\
\frac{\partial u_3}{\partial t} - D_3\Delta u_3 &= \alpha_3 u_3(1 - a_{3,1}u_1 - a_{3,2}u_2 - a_{3,3}u_3),
\end{aligned} \tag{2.51}$$

with the initial conditions

$$\begin{aligned} u_1^0 &= \frac{1}{1+e^{(-\gamma(x'+\sqrt{3}\min(y',0)))}}, \\ u_2^0 &= \frac{1}{1+e^{(\gamma(x'-\sqrt{3}\min(y',0)))}}, \\ u_3^0 &= 1-\frac{1}{1+e^{(-\gamma(y'+1/\sqrt{3}|x'|))}}, \end{aligned} \tag{2.52}$$

where u_1, u_2, u_3 are the densities (concentrations) of the three species at time t and position (x, y), D_1, D_2, D_3 are the constant diffusion coefficients of these three species, respectively, and $\alpha_1, \alpha_2, \alpha_3$ represent the intrinsic growth rates of the three species, respectively. The coefficients $a_{i,j},\ i, j = 1, 2, 3$, model the limiting effect that the presence of species $u_j,\ j = 1, 2, 3$ has on species $u_i,\ i = 1, 2, 3$. In particular $\frac{1}{a_{i,i}}$ is the carrying capacity of species $i,\ i = 1, 2, 3$. The parameter γ is called the marginal factor and $x',\ y'$ are the shifted coordinates of $x,\ y$ where $x' = x - 0.7L,\ y' = y - 0.7L$, where L is the length of the space domain.

We consider the time domain $\mathcal{I} = [0, 100]$ and the spatial domain $\Omega = [0, 150]^2$. The coefficients and parameters have the following values:

$$\begin{aligned} &D_1 = D_2 = D_3 = 1, \\ &\alpha_1 = \alpha_2 = \alpha_3 = 1, \\ &a_{1,1} = a_{1,2} = a_{2,3} = a_{3,1} = 1, \\ &a_{1,3} = a_{2,1} = a_{3,2} = 2, \\ &L = 150, \gamma = 0.5. \end{aligned}$$

We solve the problem by using a dG time stepping method with conforming continuous finite element in space dG(r)-cG(p) with $r = 1$ and $p = 1, 2$, on a rectangular mesh consisting of 4096 uniform biquadratic elements with 4225 and 16641 degrees of freedom in space, respectively. The time step size is $k_n = 0.01$ resulting in 10000 time steps and 49923 degrees of freedom in time. The numerical solution is shown in Figure 2.2. For more details see [86, 1, 31]. The solution's fine scales need high order numerical schemes for solving such problems with high accuracy.

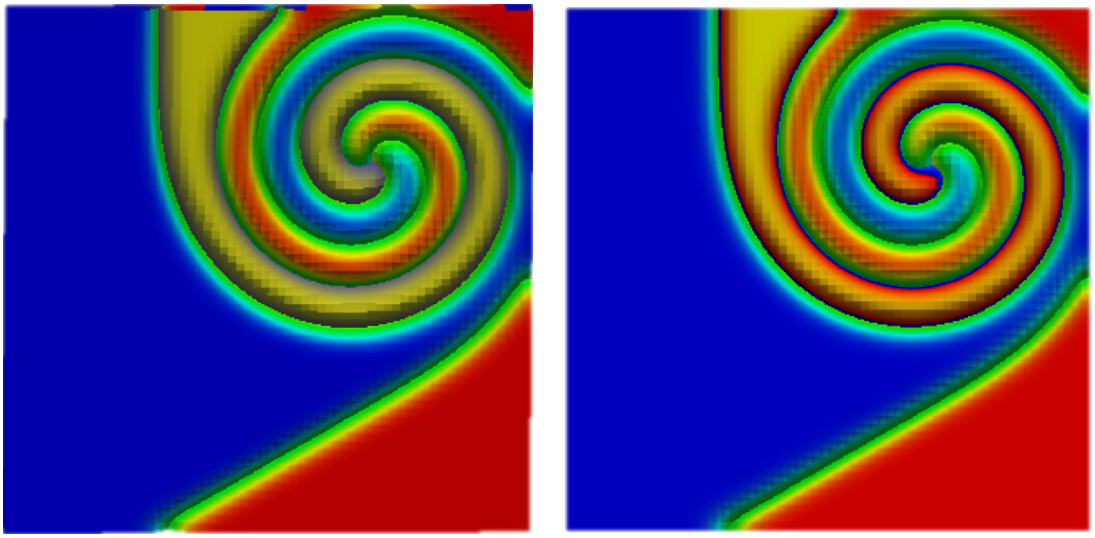

(a) (b)

FIGURE 2.2: Example 2: The solution at the final time $T = 100$: u_1 in yellow, u_2 in blue, and u_3 in red: (a) dG(1)–cG(1), (b) dG(1)–cG(2).

2.6.3 Example 3: Predator–prey system

In this example, we consider the solution for the predator–prey system consisting of two semilinear parabolic equations with homogeneous Neumann boundary conditions

$$\begin{aligned} \frac{\partial u}{\partial t} - \Delta u &= \gamma u(u-\beta)(1-u) - \frac{uv}{1+\alpha u}, \\ \frac{\partial v}{\partial t} - \epsilon \Delta v &= \frac{uv}{1+\alpha u} - \delta v, \end{aligned} \tag{2.53}$$

with the initial conditions

$$u_0 = \begin{cases} p, \text{ if } |x - L/2| \leq \triangle_{11} \text{ and } |y - L/2| \leq \triangle_{12}, \\ 0, \text{ otherwise,} \end{cases}$$

$$v_0 = \begin{cases} q, \text{ if } |x - L/2 - a| \leq \triangle_{21} \text{ and } |y - L/2 - b| \leq \triangle_{22}, \\ 0, \text{ otherwise.} \end{cases}$$

Here, u and v are the dimensionless densities (concentrations) of the prey and predator at time t and position (x, y), $\epsilon = \frac{D_2}{D_1}$ is the ratio of the diffusion coefficients, where D_1 is the diffusion coefficient of the prey and D_2 is the diffusion

coefficient of the predator, $\alpha,\ \beta, \gamma,\ \delta$ are ecological parameters and L is the length of the space domain.

We consider the time domain $\mathcal{I} = [0, 163.46]$ and the spatial domain $\Omega = [0, 200]^2$. The coefficients and parameters have the following values:

$$\epsilon = 1,\ \alpha = 0.2,\ \beta = 0.1,\ \gamma = 3, \delta = 0.37, p = 1, q = 0.5,$$
$$L = 200, a = 5, b = 30,\ \triangle_{11}{=}\triangle_{12}{=}\triangle_{21}{=}\triangle_{22}{=}\ 20.$$

The mesh in space is rectangular and consists of 4096 uniform biquadratic elements with 16641 degrees of freedom, and for the time discretisation, we use first degree polynomials (linear elements) with time step size $k_n = 0.01$ and 16346 time steps resulting in 49923 degrees of freedom in time. Figure 2.3 shows the generation

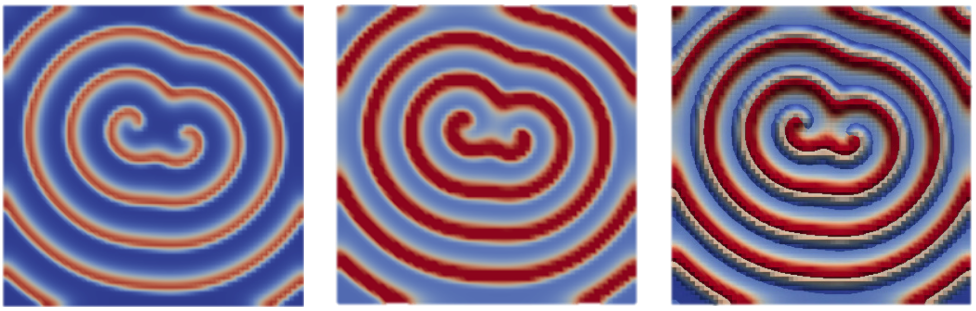

(a) (b) (c)

FIGURE 2.3: Example 3: The solution at the final time $T = 163.46$: (a) The Prey, (b) The Predator, (c) The Prey and the Predator superimposed on the same plot.

of periodical concentric rings for the interactions of the spiral ends. The existing results of this example are typically obtained by using low order time stepping schemes and, in particular explicit time stepping schemes. The advantages of using dG timestepping in solving these problems is the combination of high order of accuracy and the possibility of using large time steps due to the method being implicit in the elliptic operator so that we can solve the problem without any restrictions on the time step size. We refer to [89] for more details on this particular model.

Chapter 3

A posteriori error analysis

3.1 Introduction

A posteriori error analysis plays an important role in developing and devising efficient adaptive algorithms which can lead to significant reduction in the computational costs of approximating the solutions by the numerical methods and this is a crucial property of any reliable numerical scheme. In a posteriori error analysis we are interested in finding bounds in the form

$$||e|| = ||u - U|| \leq \mathbb{E}[U, f, h, k_n],$$

for some function $\mathbb{E}$ depending on the approximate solution U and the right hand side f of the underlying problem, in the relevant norm $\|.\|$, but it does not depend on the exact solution u of the the underlying problem. The estimator $\mathbb{E}$ is an approximation of the error in the relevant norm if $||e|| \approx \mathbb{E}$. Also, it depends on the data of the problem, mesh step size h and the time step size k_n (discretisation parameters).

The main used techniques for obtaining *a posteriori* and *a priori* error bounds are the *energy*, *duality*, and *reconstruction*. In the energy technique, the error representation formula is tested with the error or any quantity of interest related to the error such as temporal or spatial derivatives or integrals of it. The duality

approach depends upon estimating the stability factor analytically or computationally by solving and using the stability properties of the linear backward dual problem. For linear PDEs this approach is sharp and for nonlinear PDEs as in our case (semilinear problems) the analysis relies on stability properties of the linearised dual problem, and in this case, special care is needed to deal with the strong stability of the linearised problem. Optimal orders can be obtained in the $L_\infty(0,T;L_2(\Omega))$ norm by using the duality approach but some tight restrictions on the spatial mesh have to be imposed. The other disadvantage to this approach is that no error estimates can be obtained for the gradients. This technique was introduced by Johnson in 1991, see [43]. For more details about this approach see [43, 43, 40, 46].

It is a well known fact that the energy technique for parabolic problems results in optimal rates in $L_2(0,T;H^1(\Omega))$ norm and suboptimal rates in $L_\infty(0,T;L_2(\Omega))$ and $L_2(\Omega)$ norms, but by combining it with construction technique we can retrieve the optimality in these error norms. The other advantage of the energy technique is that it enables us to treat nonlinearities with ease. In our analysis we will use the energy and reconstruction approaches with a continuation argument for energy estimates in deriving our a posteriori error bounds. For more details about these issues, see [83, 78].

The reconstruction technique allows us to derive optimal error bounds for higher order methods for both linear and nonlinear problems with reasonable and practical assumptions. Also, this technique is flexible and can be used with both the energy and duality approaches. In the reconstruction technique the estimator $\mathbb{E}$ has four appealing features: (i) $\mathbb{E}$ is a computable quantity and depends only on the approximate solution U and the data of the problem; (ii) If $\mathbb{E}$ is not computable then it can be bounded by a bounded quantity; (iii) $\mathbb{E}$ is of optimal order and requires lowest possible regularity; (IV) $\mathbb{E}$ contains computable and explicit stability constants specially for linear problems. For more details see [81].

An error estimator is reliable in the relevant norm if there exists $\kappa_1 > 0$, independent of the exact solution u, satisfying $||e|| \leq \kappa_1 \mathbb{E}$. $\mathbb{E}$ is efficient if there exists $\kappa_2 > 0$, independent of the exact solution u, such that $\kappa_2 \mathbb{E} \leq ||e||$. Since these

constants can not be computed explicitly, this motivates the notion of an effectivity index EI and inverse effectivity index IEI. The effectivity index is defined as the ratio of the estimator $\mathbb{E}$ to $||e||$ i.e.

$$EI := \frac{\mathbb{E}}{||e||},$$

and

$$IEI := \frac{||e||}{\mathbb{E}}.$$

Furthermore, the estimator $\mathbb{E}$ is robust if the constants κ_1 and κ_2 do not depend on the discrete finite element solution U, data of the problem and discretisation parameters, and it is asymptotically robust if it is robust when the discretisation parameters are sufficiently small [3, 112].

We will derive a posteriori error estimates in $L_\infty(L_2)$ and $L_2(H^1)$ norms for fully discrete IMEX space–time finite element methods. We use an implicit–explicit (hp–version) dG timestepping scheme with conforming finite elements in space. We will derive these a posteriori bounds for the semilinear initial value problem defined in (2.10) in Chapter 2.

We recall from Section 2.3.3 in Chapter 2 that the fully–discrete IMEX space–time scheme reads: find $U \in \mathcal{X}$ such that

$$\int_{\mathcal{I}_n} \left((U', v)_{\mathcal{H}} + a(U, v)\right) \,\mathrm{d}t + ([U]_{n-1}, v_{n-1}^+)_{\mathcal{H}} = \int_{\mathcal{I}_n} (\Pi f(U), v)_{\mathcal{H}} \,\mathrm{d}t \tag{3.1}$$

for all $v \in \mathcal{X}_n$, for $n = \mu + \jmath, ..., N$. Depending on the choice of the interpolant $\Pi f(U)$ defined in (2.21) we have two cases: the fully implicit scheme and the implicit–explicit (IMEX) scheme. Despite the specific choices discussed earlier, in what follows, we shall endeavour to be general with respect to the particular approximation of the nonlinear term. To that end, we shall refrain from using specific properties of any particular interpolant/extrapolant used in the proof of the a posteriori error bounds below, in an effort to be versatile in the choice of linearisation. Indeed, the a posteriori error bounds given below will involve the computable quantity $\Pi f(U) - f(U)$.

3.2 Reconstructions

We now discuss the space-time reconstruction technique proposed in [60] for linear parabolic problems, which is a combination of the concepts of elliptic reconstruction for the spatial discretisation [83, 77] and of the dG-timestepping reconstruction presented first in [84], and further analysed in the *hp*-setting in [98].

3.2.1 Elliptic reconstruction

For each conforming finite element space $\mathcal{V}_n \subset \mathcal{V}$, we define the respective discrete elliptic operator $\mathbf{A}_n : \mathcal{V}_n \to \mathcal{V}_n$ to be the unique linear operator such that $(\mathbf{A}_n w, \mathbf{v})_{\mathcal{H}} = a(w, \mathbf{v})$, for all $\mathbf{v}, w \in \mathcal{V}_n$.

Given $U(t) \in \mathcal{X}_n$, $n = 0, ..., N$, for $t \in \mathcal{I}_n$, the *elliptic reconstruction* $\tilde{U}(t) = \tilde{R}U(t) \in \mathcal{Y}_n$ of U is defined as

$$a(\tilde{U}(t), v) = (\mathbf{A}_n U(t), v)_{\mathcal{H}}, \quad \text{for all } v \in \mathcal{V}, \text{ and } t \in \mathcal{I}_n. \tag{3.2}$$

The relation (3.2) can be written in pointwise form as $\mathcal{A}\tilde{U}(\cdot, t) = \mathbf{A}_n U(\cdot, t)$, for all $t \in I_n$. The *reconstruction operator* $\tilde{R} : \mathcal{X} \to \mathcal{Y}$ can be represented as $\tilde{R}|_{\mathcal{I}_n} = \mathcal{A}^{-1}\mathbf{A}_n : \mathcal{V}_n \to \mathcal{V}$ for all $n = 0, 1, \ldots, N$; we refer to [83, 77, 60] for details.

From the definition of $\mathbf{A}_n$ and from (3.2), we have

$$a(\tilde{U}(t), w) = (\mathbf{A}_n U(t), w)_{\mathcal{H}} = a(U(t), w), \quad \text{for all } w \in \mathcal{V}_n, \tag{3.3}$$

and, hence, we have

$$U = \tilde{P}_n \tilde{U}, \tag{3.4}$$

at each $t \in \mathcal{I}_n$. That is, U is the elliptic projection of the elliptic reconstruction $\tilde{U}$. In other words, U is the approximate solution of the elliptic problem whose exact solution is the elliptic reconstruction function $\tilde{U}$. Therefore, a crucial consequence of this construction is the ability to estimate the difference $\tilde{U} - U$ by *a posteriori* error estimators for elliptic problems in various norms available in the literature.

As we prefer to keep the exposition independent of specific choices of *a posteriori* error bounds for elliptic problems, we opt for merely postulating their existence.

To account for mesh–change effects, we also define the smallest common superspace $\mathcal{V}_n^{\oplus} := \mathcal{V}_{n-1} + \mathcal{V}_n$, and the largest common subspace $\mathcal{V}_n^{\ominus} := \mathcal{V}_{n-1} \cap \mathcal{V}_n$, for all $n = 1, \ldots, N$.

We introduce the $\mathcal{H}$–projection operator $P : \mathcal{V}^* \to \mathcal{V}$ defined by

$$(Pv, \chi)_{\mathcal{H}} = \langle v, \chi \rangle \quad \text{for all } \chi \in \mathcal{V}; \tag{3.5}$$

if we replace $\mathcal{V}$ by one of $\mathcal{V}_n, \mathcal{V}_n^{\oplus}$ or $\mathcal{V}_n^{\ominus}$ in the above definition, the corresponding $\mathcal{H}$–projection operators are denoted by $P_n, P_n^{\oplus}$ or $P_n^{\ominus}$, respectively. Also, we define the *elliptic projection* operator $\tilde{P}_n : \mathcal{V} \to \mathcal{V}_n$ by

$$a(\tilde{P}_n v, w) = a(v, w) \quad \text{for all } w \in \mathcal{V}_n, \tag{3.6}$$

with $\tilde{P}_n^{\ominus}$ the respective elliptic projection onto $\mathcal{V}_n^{\ominus}$.

For $w \in \mathcal{H}$, we define the *time lifting operator* $L_n : \mathcal{H} \to \mathcal{P}^{r_n}(\mathcal{I}_n; \mathcal{H})$, by

$$\int_{\mathcal{I}_n} (L_n(w), v)_{\mathcal{H}} \, \mathrm{d}t = (w, v_{n-1}^+)_{\mathcal{H}} \quad \text{for all } v \in \mathcal{P}^{r_n}(\mathcal{I}_n; \mathcal{H}). \tag{3.7}$$

If $\mathcal{W} \subset \mathcal{H}$ is a linear subspace of $\mathcal{H}$, we have the property

$$w \in \mathcal{W} \quad \text{implies} \quad L_n(w) \in \mathcal{P}^{r_n}(\mathcal{I}_n; \mathcal{W}); \tag{3.8}$$

for more details, we refer to [98].

Assumption 3.1 (Elliptic *a posteriori* error bounds). Let $w \in \mathcal{V}$ be the exact solution of the elliptic problem $\mathcal{A}w = g$ with respective boundary conditions and let $W \in \mathcal{V}_h \subset \mathcal{V}$ be the finite element solution of this problem in the finite element space $\mathcal{V}_h$. We assume that there exist *a posteriori* error bounds

$$\|w - W\|_S \leq \mathbb{E}_S[W, g], \tag{3.9}$$

for $S \in \{\mathcal{H}, \mathcal{V}, \mathcal{V}^*\}$.

The literature for such elliptic *a posteriori* error bounds is vast; see, e.g., [3, 9, 112, 11, 10] and the references therein.

Proposition 3.2 (Dual norm estimate)**.** *Let $\mathcal{V}_h \subset \mathcal{V}$ be a (conforming) finite element space and let $\mathbf{A}_h$ the respective discrete elliptic operator defined by $\mathbf{A}_h : \mathcal{V}_h \to \mathcal{V}_h$ such that $(\mathbf{A}_h W, V)_{\mathcal{H}} = a(W, V)$, for all $V, W \in \mathcal{V}_h$. For any $v \in \mathcal{V}^*$, defining the function ξ as $\xi := \mathbf{A}_h^{-1} P v$, we have the bound*

$$\|v\|_{\mathcal{V}^*}^2 \leq \tilde{\alpha}^2 \mathbb{E}_{\mathcal{V}}[\xi, v] + \tilde{\alpha}(Pv, \xi)_{\mathcal{H}}. \tag{3.10}$$

where $\tilde{\alpha} > 0$ is such that $\|v\|_{\mathcal{V}^*} \leq \tilde{\alpha}\|v\|_{\mathcal{H}}$.

Proof. For the proof, we refer to [60]. □

In particular, Assumption 3.1 will imply the validity of the estimates

$$\|\tilde{U} - U\|_S \leq \mathbb{E}_S[U, \mathbf{A}_n U], \quad S \in \{\mathcal{H}, \mathcal{V}, \mathcal{V}^*\}, \tag{3.11}$$

among other things; which are presented in Proposition 3.8 below for details.

By replacing $\mathcal{V}_n$ with $\mathcal{V}_n^{\oplus}$ or by $\mathcal{V}_n^{\ominus}$, we signify the corresponding discrete operators $\mathbf{A}_n^{\oplus}$ or $\mathbf{A}_n^{\ominus}$, and we denote by $\tilde{R}_n^{\oplus}$ or by $\tilde{R}_n^{\ominus}$ the respective elliptic reconstructions.

Using (3.3), the IMEX method (3.1) can be re-written as

$$\int_{\mathcal{I}_n} \Big((U', v)_{\mathcal{H}} + a(\tilde{U}, v) \Big) \,\mathrm{d}t + ([U]_{n-1}, v_{n-1}^+)_{\mathcal{H}} = \int_{\mathcal{I}_n} (\Pi f(U), v)_{\mathcal{H}} \,\mathrm{d}t \tag{3.12}$$

for all $v \in \mathcal{X}_n$, for $n = 1, \ldots, N$.

3.2.2 Time reconstruction of $\tilde{U}$

We define the time reconstruction function $\hat{U} \in H^1(0, T; \mathcal{H})$ of the elliptic reconstruction $\tilde{U} \in \mathcal{Y}$ (of the approximate solution U,) as follows: for each $\mathcal{I}_n$,

$n = 1, \ldots, N$,

$$\hat{U}|_{\mathcal{I}_n} \in \mathcal{P}^{r_n+1}(\mathcal{I}_n; \mathcal{V}), \quad n = 1, \ldots, N, \tag{3.13}$$

satisfies

$$\int_{\mathcal{I}_n} (\hat{U}', v)_{\mathcal{H}} \, \mathrm{d}t = \int_{\mathcal{I}_n} (\tilde{U}', v)_{\mathcal{H}} \, \mathrm{d}t + ([\tilde{U}]_{n-1}, v_{n-1}^+)_{\mathcal{H}} \quad \text{for all } v \in \mathcal{Y}_n, \tag{3.14}$$

and

$$\hat{U}_{n-1}^+ = \begin{cases} u_0, & n = 0; \\ \tilde{U}_{n-1}^-, & n = 1, \ldots, N. \end{cases} \tag{3.15}$$

The time reconstruction $\hat{U}$ is well-defined: we have $r_n + 2$ unknowns per time interval $\mathcal{I}_n$ and $r_n + 1$ conditions from (3.14) and one more condition from (3.15). The time reconstruction is also *unique* and *globally continuous* with respect to the time variable as shown in the following lemma. This property is useful in deriving a pointwise perturbed differential equation for the error (the error representation formula), or a part thereof. Also, it allows us to use the continuation argument in the *a posteriori* error analysis. We note that, the time reconstruction $\hat{U}$ is a higher order reconstruction (polynomial in time on the time interval $\mathcal{I}_n$), and it is one degree higher than the elliptic reconstruction $\tilde{U}$. We finally note from (3.14) and (3.15) that the time reconstruction is constructed (elementwise) locally.

Equivalently, using the lifting operator (3.7), we can define $\hat{U}|_{\mathcal{I}_n} \in \mathcal{P}^{r_{n+1}}(\mathcal{I}_n; \mathcal{V})$ on each time interval $\mathcal{I}_n$, $n = 1, \ldots, N$, by

$$\hat{U}|_{I_n}(t) := \int_{t_{n-1}}^{t} \left(\tilde{U}' + L_n([\tilde{U}]_{n-1}) \right) \mathrm{d}\tau + \tilde{U}_{n-1}^-, \tag{3.16}$$

where we recall that $\tilde{U}_0^- := u_0$. For convenience, we also encode the time reconstruction process as an operator $\hat{R}|_{\mathcal{I}_n} : \mathcal{P}^{r_n}(\mathcal{I}_n; \mathcal{V}) \to \mathcal{P}^{r_n+1}(\mathcal{I}_n; \mathcal{V})$, $n = 1, \ldots, N$. Hence, we have $\hat{U} = \hat{R}\tilde{U}$.

Lemma 3.3 (Continuity of the time reconstruction)**.** *The time reconstruction, which is uniquely defined in* (3.14) *and* (3.15)*, is globally continuous.*

Proof. By integrating by parts the left–hand side of (3.14), we see

$$\int_{\mathcal{I}_n} (\hat{U}', v)_{\mathcal{H}} \, \mathrm{d}t = -\int_{\mathcal{I}_n} (\hat{U}, v')_{\mathcal{H}} \, \mathrm{d}t + (\hat{U}_n^-, v_n^-)_{\mathcal{H}} - (\hat{U}_{n-1}^+, v_{n-1}^+)_{\mathcal{H}}, \ \forall v \in \mathcal{Y}_n. \quad (3.17)$$

Now, integrating by parts the right–hand side of (3.14), we find

$$\begin{aligned} \int_{\mathcal{I}_n} (\tilde{U}', v)_{\mathcal{H}} \, \mathrm{d}t + ([\tilde{U}]_{n-1}, v_{n-1}^+)_{\mathcal{H}} = \ & - \int_{\mathcal{I}_n} (\tilde{U}, v')_{\mathcal{H}} \, \mathrm{d}t + (\tilde{U}_n^-, v_n^-)_{\mathcal{H}} \\ & - (\tilde{U}_{n-1}^-, v_{n-1}^+)_{\mathcal{H}}, \ \forall v \in \mathcal{Y}_n. \end{aligned} \quad (3.18)$$

From (3.17) and (3.18) we have

$$\begin{aligned} & - \int_{\mathcal{I}_n} (\hat{U}, v')_{\mathcal{H}} \, \mathrm{d}t + (\hat{U}_n^-, v_n^-)_{\mathcal{H}} - (\hat{U}_{n-1}^+, v_{n-1}^+)_{\mathcal{H}} = \\ & - \int_{\mathcal{I}_n} (\tilde{U}, v')_{\mathcal{H}} \, \mathrm{d}t + (\tilde{U}_n^-, v_n^-)_{\mathcal{H}} - (\tilde{U}_{n-1}^-, v_{n-1}^+)_{\mathcal{H}}, \ \forall v \in \mathcal{Y}_n. \end{aligned} \quad (3.19)$$

Hence,

$$-\int_{\mathcal{I}_n} (\hat{U}, v')_{\mathcal{H}} \, \mathrm{d}t + (\hat{U}_n^-, v_n^-)_{\mathcal{H}} = -\int_{\mathcal{I}_n} (\tilde{U}, v')_{\mathcal{H}} \, \mathrm{d}t + (\tilde{U}_n^-, v_n^-)_{\mathcal{H}}, \ \forall v \in \mathcal{Y}_n, \quad (3.20)$$

since $\hat{U}_{n-1}^+ = \tilde{U}_{n-1}^-$. By choosing v constant in time we obtain

$$(\hat{U}_n^-, v)_{\mathcal{H}} = (\tilde{U}_n^-, v)_{\mathcal{H}}, \ \forall v \in \mathcal{Y}_n. \quad (3.21)$$

Consequently we get

$$\hat{U}_n^- = \tilde{U}_n^-. \quad (3.22)$$

Hence, $\hat{U}$ is a globally continuous function. □

Proposition 3.4 (Time reconstruction error bounds)**.** *Let $S \subseteq \mathcal{H}$ and $\Psi \in P^{r_n}(\mathcal{I}_n; S)$, for $n = 1, ..., N$. Then, we have the identities:*

$$\|\hat{\Psi} - \Psi\|_{L_2(\mathcal{I}_n;S)} = C_n \|[\Psi]_{n-1}\|_S, \ S \in \{\mathcal{H}, \mathcal{V}, \mathcal{V}^*\}, \quad (3.23)$$

with

$$C_n := \left(\frac{k_n(r_n+1)}{(2r_n+1)(2r_n+3)} \right)^{1/2},$$

and

$$\|\hat{\Psi} - \Psi\|_{L_\infty(\mathcal{I}_n;S)} = \|[\Psi]_{n-1}\|_S, \tag{3.24}$$

where $\hat{\Psi}$ *is defined by*

$$\int_{\mathcal{I}_n} (\hat{\Psi}', v)_{\mathcal{H}} \,\mathrm{d}t = \int_{\mathcal{I}_n} (\Psi', v)_{\mathcal{H}} \,\mathrm{d}t + ([\Psi]_{n-1}, v_{n-1}^+)_{\mathcal{H}} \quad \textit{for all } v \in \mathcal{Y}_n,$$

and $\hat{\Psi}_{n-1}^+ = \Psi_{n-1}^-$, $n = 1, ..., N$ *and* Ψ_0^- *given.*

Proof. The proof of (3.23) first appeared in [84, Lemma 2.2]; the formula for C_n was further refined to be explicit in the dependence on r_n in [98, Theorem 2]. □

3.3 *A posteriori* error bounds

We begin by decomposing the error as

$$e := u - U = (u - \hat{U}) + (\hat{U} - \tilde{U}) + (\tilde{U} - U) = \rho + \sigma + \epsilon.$$

Note that σ is the time reconstruction error which can be estimated using Proposition 3.4. Similarly, ϵ is the elliptic reconstruction error and, therefore, can be estimated using Assumption 3.1. Thus, it remains to estimate ρ by quantities involving the problem data and/or σ and ϵ. To do so, we shall work with energy estimates, in conjunction with a continuation argument to treat the non-Lipschitzian nonlinear reactions.

From (3.12) and the definition of the time reconstruction (3.14), (3.15), we deduce

$$\begin{aligned} &\int_{\mathcal{I}_n} \Big((\hat{U}', v)_{\mathcal{H}} + a(\tilde{U}, v) \Big) \,\mathrm{d}t \\ &= \int_{\mathcal{I}_n} \Big((\Pi f(U), v)_{\mathcal{H}} + (\epsilon', v)_{\mathcal{H}} \Big) \,\mathrm{d}t + ([\epsilon]_{n-1}, v_{n-1}^+)_{\mathcal{H}}, \text{ for all } v \in \mathcal{X}_n, \end{aligned} \tag{3.25}$$

which can be written in pointwise form as

$$P_n \hat{U}' + \mathcal{A}\hat{U} = P_n \Pi f(U) + P_n \Big(\epsilon' + L_n([\epsilon]_{n-1}) \Big) + \mathcal{A}\sigma, \tag{3.26}$$

$n = 1, \ldots, N$. Subtracting (3.26) from (2.10), we obtain

$$\rho' + \mathcal{A}\rho = f(u) - P_n \Pi f(U) + P_n \hat{U}' - \hat{U}' - P_n\Big(\epsilon' + L_n([\epsilon]_{n-1})\Big) - \mathcal{A}\sigma, \quad (3.27)$$

for $n = 1, \ldots, N$. From (3.16), we deduce that $\hat{U}' = \tilde{U}' + L_n([\tilde{U}]_{n-1})$ and, therefore, we can arrive at

$$P_n \hat{U}' - \hat{U}' - P_n\Big(\epsilon' + L_n([\epsilon]_{n-1})\Big) = -\epsilon' - L_n([\epsilon]_{n-1}) + L_n(U_{n-1}^- - P_n U_{n-1}^-),$$

upon observing that $P_n U' = U'$ in $\mathcal{I}_n$. Using this identity in (3.27) we arrive at an error equation for ρ:

$$\rho' + \mathcal{A}\rho = f(u) - P_n \Pi f(U) - \epsilon' - L_n([\epsilon]_{n-1}) + L_n(U_{n-1}^- - P_n U_{n-1}^-) - \mathcal{A}\sigma, \quad (3.28)$$

on which we can now apply energy–type arguments.

For brevity, we set $\mathrm{P} : [0, T] \to \mathcal{V}$, defined as $\mathrm{P}|_{\mathcal{I}_n} = P_n$, $n = 0, \ldots, N$; we shall use the corresponding notation $\mathrm{L}(v)$ to denote collectively the liftings on each time interval, and so, $\mathrm{L}(v)|_{\mathcal{I}_n} = L_n(v_{n-1})$, $n = 1, \ldots, N$. Also, we denote by $\mathrm{e_{mc}} : [0, T] \to \mathcal{V}$ the *error due to the mesh change* between the finite element spaces $\mathcal{V}_{n-1}$ and $\mathcal{V}_n$ given by $\mathrm{e_{mc}}|_{\mathcal{I}_n} := L_n(U_{n-1}^- - P_n U_{n-1}^-)$, $n = 1, \ldots, N$.

We test (3.28) with ρ, integrate in space and in time between 0 to $t \in \mathcal{I}$, we deduce

$$\begin{aligned} \frac{1}{2}\|\rho(t)\|_{\mathcal{H}}^2 + \int_0^t a(\rho, \rho)\,\mathrm{d}\tau = & \int_0^t (f(u) - \mathrm{P}\Pi f(U), \rho)_{\mathcal{H}}\,\mathrm{d}\tau + \int_0^t (\mathrm{e_{mc}}, \rho)_{\mathcal{H}}\,\mathrm{d}\tau \\ & - \int_0^t (\epsilon' + \mathrm{L}([\epsilon]), \rho)_{\mathcal{H}}\,\mathrm{d}\tau - \int_0^t a(\sigma, \rho)\,\mathrm{d}\tau, \end{aligned} \quad (3.29)$$

noticing that $\rho(0) = 0$ by construction. Employing the coercivity (2.13) and continuity (2.12) of a, the last estimate implies

$$\begin{aligned} & \frac{1}{2}\|\rho(t)\|_{\mathcal{H}}^2 + C_{\mathrm{coer}} \int_0^t \|\rho\|_{\mathcal{V}}^2\,\mathrm{d}\tau \le \int_0^t (f(u) - \mathrm{P}\Pi f(U), \rho)_{\mathcal{H}}\,\mathrm{d}\tau \\ & + \int_0^t (\mathrm{e_{mc}}, \rho)_{\mathcal{H}}\,\mathrm{d}\tau - \int_0^t (D\epsilon, \rho)_{\mathcal{H}}\,\mathrm{d}\tau - C_{\mathrm{cont}} \int_0^t \|\sigma\|_{\mathcal{V}} \|\rho\|_{\mathcal{V}}\,\mathrm{d}\tau, \end{aligned} \quad (3.30)$$

upon introducing the notation $D\epsilon := \epsilon' + \mathrm{L}([\epsilon])$. Using Young inequality for the third and fourth terms on the right hand side of (3.30), implies that

$$\begin{aligned}\frac{1}{2}\|\rho(t)\|_{\mathcal{H}}^2 + \big(1-\gamma\big)C_{\mathrm{coer}}\int_0^t \|\rho\|_{\mathcal{V}}^2\,\mathrm{d}\tau \le \int_0^t (f(u)-\mathrm{P}\Pi f(U),\rho)_{\mathcal{H}}\,\mathrm{d}\tau \\ + \int_0^t (\mathrm{e}_{\mathrm{mc}},\rho)_{\mathcal{H}}\,\mathrm{d}\tau + \frac{1}{2\gamma C_{\mathrm{coer}}}\int_0^t \Big(\|D\epsilon\|_{\mathcal{V}^*}^2 + C_{\mathrm{cont}}^2\|\sigma\|_{\mathcal{V}}^2\Big)\,\mathrm{d}\tau,\end{aligned} \tag{3.31}$$

for any $\gamma > 0$. The second term on the right-hand side of (3.30) can be further estimated by

$$\begin{aligned}\int_0^t (\mathrm{e}_{\mathrm{mc}},\rho)_{\mathcal{H}}\,\mathrm{d}\tau &\le \lambda\|\rho\|_{L_\infty(0,t;\mathcal{H})}\int_0^t \|\mathrm{e}_{\mathrm{mc}}\|_{\mathcal{H}}\,\mathrm{d}\tau + (1-\lambda)\int_0^t \|\mathrm{e}_{\mathrm{mc}}\|_{\mathcal{V}^*}\|\rho\|_{\mathcal{V}}\,\mathrm{d}\tau \\ &\le \frac{\operatorname{sign}\lambda}{4}\|\rho\|_{L_\infty(0,t;\mathcal{H})}^2 + \lambda^2\Big(\int_0^t \|\mathrm{e}_{\mathrm{mc}}\|_{\mathcal{H}}\,\mathrm{d}t\Big)^2 \\ &\quad + \frac{(1-\lambda)^2}{C_{\mathrm{coer}}}\int_0^t \|\mathrm{e}_{\mathrm{mc}}\|_{\mathcal{V}^*}^2\,\mathrm{d}\tau + \operatorname{sign}(1-\lambda)\frac{C_{\mathrm{coer}}}{4}\int_0^t \|\rho\|_{\mathcal{V}}^2\,\mathrm{d}\tau,\end{aligned} \tag{3.32}$$

for any $0 \le \lambda \le 1$, with the sign denoting a sign function where, in particular, $\operatorname{sign}\nu = 0$ if $\nu = 0$. An interesting choice is $\lambda := \min\{1, t^{-1/2}\}$, in that it can counteract the imbalance caused by the L^1-accumulation of the error on the second term on the right-hand side of (3.32):

$$\lambda^2\Big(\int_0^t \|\mathrm{e}_{\mathrm{mc}}\|_{\mathcal{H}}\,\mathrm{d}\tau\Big)^2 \le \lambda^2 t\int_0^t \|\mathrm{e}_{\mathrm{mc}}\|_{\mathcal{H}}^2\,\mathrm{d}\tau \le \int_0^t \|\mathrm{e}_{\mathrm{mc}}\|_{\mathcal{H}}^2\,\mathrm{d}\tau,$$

thereby retaining a dimensional balance in the context of long–time simulations; we refer to [60, Remark 4.10] for a related discussion. The accumulation of the mesh change error can be of importance in practical simulations [39], as it accounts for the loss of information caused by the mesh modification.

Selecting now $\gamma = \gamma_\lambda := 1/2 - \operatorname{sign}(1-\lambda)/4$ in (3.30) and using (3.32), we arrive at

$$\begin{aligned}\|\rho(t)\|_{\mathcal{H}}^2 + C_{\mathrm{coer}}\int_0^t \|\rho\|_{\mathcal{V}}^2\,\mathrm{d}\tau \le 2\int_0^t (f(u)-\mathrm{P}\Pi f(U),\rho)_{\mathcal{H}}\,\mathrm{d}\tau \\ + 2\lambda^2\|\mathrm{e}_{\mathrm{mc}}\|_{L_1(0,t;\mathcal{H})}^2 + \frac{2(1-\lambda)^2}{C_{\mathrm{coer}}}\|\mathrm{e}_{\mathrm{mc}}\|_{L_2(0,t;\mathcal{V}^*)}^2 \\ + \frac{1}{\gamma_\lambda C_{\mathrm{coer}}}\Big(\|D\epsilon\|_{L_2(0,t;\mathcal{V}^*)}^2 + C_{\mathrm{cont}}^2\|\sigma\|_{L_2(0,t;\mathcal{V})}^2\Big) \\ + \frac{\operatorname{sign}\lambda}{2}\|\rho\|_{L_\infty(0,t;\mathcal{H})}^2.\end{aligned} \tag{3.33}$$

To estimate the last term on the right-hand side of (3.33), we return to (3.30) setting $\gamma = 2\gamma_\lambda$ to deduce

$$\begin{aligned}\frac{1}{2}\|\rho(t)\|_{\mathcal{H}}^2 \leq \Big(\int_0^t (f(u) - \mathrm{P}\Pi f(U), \rho)_{\mathcal{H}}\,\mathrm{d}\tau \\ + \frac{1}{4\gamma_\lambda C_{\mathrm{coer}}}\Big(\|D\epsilon\|_{L_2(0,t;\mathcal{V}^*)}^2 + C_{\mathrm{cont}}^2\|\sigma\|_{L_2(0,t;\mathcal{V})}^2\Big) \\ + \lambda^2\|\mathrm{e_{mc}}\|_{L_1(0,t;\mathcal{H})}^2 + \frac{(1-\lambda)^2}{C_{\mathrm{coer}}}\|\mathrm{e_{mc}}\|_{L_2(0,t;\mathcal{V}^*)}^2\Big) \\ + \frac{\operatorname{sign}\lambda}{4}\|\rho\|_{L_\infty(0,t;\mathcal{H})}^2 := (I) + \frac{\operatorname{sign}\lambda}{4}\|\rho\|_{L_\infty(0,t;\mathcal{H})}^2.\end{aligned} \tag{3.34}$$

Now setting $t = t^*$ such that $\|\rho(t^*)\|_{\mathcal{H}} = \|\rho\|_{L_\infty(0,t;\mathcal{H})}$ in (3.34), we deduce

$$\frac{2-\operatorname{sign}\lambda}{4}\|\rho\|_{L_\infty(0,t;\mathcal{H})}^2 \leq (I), \quad \text{or} \quad \frac{\operatorname{sign}\lambda}{2}\|\rho\|_{L_\infty(0,t;\mathcal{H})}^2 \leq \frac{2\operatorname{sign}\lambda}{2-\operatorname{sign}\lambda}(I), \tag{3.35}$$

which we use to bound the last term on the right-hand side of (3.34) further and, by adding $\|\rho\|_{L_\infty(0,t;\mathcal{H})}^2 \leq 4/(2-\operatorname{sign}\lambda)(I)$ to the resulting estimate, we arrive finally at

$$\begin{aligned}\|\rho\|_{L_\infty(0,t;\mathcal{H})}^2 + C_{\mathrm{coer}}\|\rho\|_{L_2(0,t;\mathcal{V})}^2 \leq \frac{c_{2,\lambda}}{C_{\mathrm{coer}}}\Big(\|D\epsilon\|_{L_2(0,t;\mathcal{V}^*)}^2 + C_{\mathrm{cont}}^2\|\sigma\|_{L_2(0,t;\mathcal{V})}^2\Big) \\ + c_{1,\lambda}\Big(\int_0^t |(f(u) - \mathrm{P}\Pi f(U), \rho)_{\mathcal{H}}|\,\mathrm{d}\tau \\ + \lambda^2\|\mathrm{e_{mc}}\|_{L_1(0,t;\mathcal{H})}^2 + \frac{(1-\lambda)^2}{C_{\mathrm{coer}}}\|\mathrm{e_{mc}}\|_{L_2(0,t;\mathcal{V}^*)}^2\Big)\end{aligned} \tag{3.36}$$

with $c_{1,\lambda} = 4$ for $\lambda = 0$ and $c_{1,\lambda} = 8$ for $0 < \lambda \leq 1$, and $c_{2,\lambda} = 4$ if $\lambda = 0$, $c_{2,\lambda} = 16/3$ if $0 < \lambda < 1$, and $c_{2,\lambda} = 8/3$ if $\lambda = 1$.

We shall now estimate each term on the right–hand side of (3.36) separately.

3.3.1 Estimating the nonlinear term

We decompose the integrand in the nonlinear term in (3.36) as

$$(f(u) - \mathrm{P}\Pi f(U), \rho)_{\mathcal{H}} \leq (f(u) - f(U), \rho)_{\mathcal{H}} + \|f(U) - \mathrm{P}\Pi f(U)\|_{\mathcal{V}^*}\|\rho\|_{\mathcal{V}}, \tag{3.37}$$

with $\|f(U) - \mathrm{P}\Pi f(U)\|_{\mathcal{V}^*}$ measuring how well $\mathrm{P}\Pi f(U)$ approximates $f(U)$.

As we shall make use of the Sobolev Imbedding Theorem, the discussion in this section comes under the specific choice $\mathcal{H} = L_2(\Omega)$ and $\mathcal{V} = H_0^1(\Omega)$; the case of non-essential boundary conditions also follows without any technical challenge, although it is omitted here for brevity.

Lemma 3.5 (Estimation of the nonlinear term)**.** *If the nonlinear reaction f is as in Section 3.1, satisfying the growth condition* (2.14) *with $0 \leq \mathbf{r} < 2$ for $d = 2$, and with $0 \leq \mathbf{r} \leq 4/3$ for $d = 3$, we have the bound*

$$\begin{aligned}\int_\Omega |f(u) - f(U)||\rho| \,\mathrm{d}x \leq{}& C\|\rho\|_{L_2(\Omega)}^{\mathbf{r}}\|\nabla\rho\|_{L_2(\Omega)}^2 + CG(U)\|\rho\|_{L_2(\Omega)}^2 \\ &+ C\Big(\|\sigma\|_{L_2(\Omega)}^{\mathbf{r}}\|\nabla\sigma\|_{L_2(\Omega)}^2 + \|\epsilon\|_{L_2(\Omega)}^{\mathbf{r}}\|\nabla\epsilon\|_{L_2(\Omega)}^2\Big) \\ &+ CG(U)\Big(\|\sigma\|_{L_2(\Omega)}^2 + \|\epsilon\|_{L_2(\Omega)}^2\Big),\end{aligned} \tag{3.38}$$

where $G(U) := 1 + \|U\|_{L_\infty(\Omega)}^{\mathbf{r}}$.

Proof. Using the growth condition (2.14), along with the elementary inequality $|a+b|^{\mathbf{r}} \leq C(|a|^{\mathbf{r}} + |b|^{\mathbf{r}})$, we have, respectively,

$$\begin{aligned}\int_\Omega |f(u) - f(U)||\rho| \,\mathrm{d}x &\leq C\int_\Omega |u-U|(1 + |u|^{\mathbf{r}} + |U|^{\mathbf{r}})|\rho| \,\mathrm{d}x \\ &\leq C\int_\Omega |u-U|(1 + |u-U|^{\mathbf{r}} + |U|^{\mathbf{r}})|\rho| \,\mathrm{d}x \\ &\leq C\int_\Omega |u-U|^{\mathbf{r}+1}|\rho| \,\mathrm{d}x \\ &\quad + C\int_\Omega (1 + |U|^{\mathbf{r}})|u-U||\rho| \,\mathrm{d}x.\end{aligned} \tag{3.39}$$

For the first term on the right–hand side of (3.39) we use the inequality

$$\int_\Omega |v|^{\mathbf{r}+1}|w| \,\mathrm{d}x = \frac{\mathbf{r}+1}{\mathbf{r}+2}\|v\|_{L_{\mathbf{r}+2}(\Omega)}^{\mathbf{r}+2} + \frac{1}{\mathbf{r}+2}\|w\|_{L_{\mathbf{r}+2}(\Omega)}^{\mathbf{r}+2}, \tag{3.40}$$

thereby, deducing

$$\int_\Omega |u-U|^{\mathbf{r}+1}|\rho| \,\mathrm{d}x \leq C(\|\rho\|_{L_{\mathbf{r}+2}(\Omega)}^{\mathbf{r}+2} + \|\sigma\|_{L_{\mathbf{r}+2}(\Omega)}^{\mathbf{r}+2} + \|\epsilon\|_{L_{\mathbf{r}+2}(\Omega)}^{\mathbf{r}+2}). \tag{3.41}$$

Recalling the assumption $0 \leq \mathbf{r} < 2$, Hölder's inequality with exponent $p = 2/\mathbf{r}$, (and, thus, $q = 2/(2-\mathbf{r})$,) we have

$$\|\rho\|^{\mathbf{r}+2}_{L_{\mathbf{r}+2}(\Omega)} = \int_\Omega |\rho|^{\mathbf{r}}|\rho|^2 \,\mathrm{d}x \leq \|\rho\|^{\mathbf{r}}_{L_2(\Omega)}\|\rho\|^2_{L^{4/(2-\mathbf{r})}(\Omega)} \leq C\|\rho\|^{\mathbf{r}}_{L_2(\Omega)}\|\nabla\rho\|^2_{L_2(\Omega)}, \tag{3.42}$$

using the Sobolev Imbedding Theorem $\|\rho\|_{L^{4/(2-\mathbf{r})}(\Omega)} \leq C_S\|\nabla\rho\|_{L_2(\Omega)}$, with $0 \leq \mathbf{r} < 2$ for $d = 2$ and $0 \leq \mathbf{r} \leq 4/3$ for $d = 3$. Similarly, we have the same estimate (3.42), with ρ replaced by σ and ϵ.

Now, the second term of (3.39) can be dealt with as follows

$$\begin{aligned}\int_\Omega (1+|U|^{\mathbf{r}})|u-U||\rho|\,\mathrm{d}x &\leq \int_\Omega (1+|U|^{\mathbf{r}})\left(|\rho|^2 + |\sigma||\rho| + |\epsilon||\rho|\right)\,\mathrm{d}x \\ &\leq \int_\Omega (1+|U|^{\mathbf{r}})\Big(2|\rho|^2 + \frac{1}{2}|\sigma|^2 + \frac{1}{2}|\epsilon|^2\Big)\,\mathrm{d}x \\ &\leq (1+\|U\|^{\mathbf{r}}_{L_\infty(\Omega)})\Big(2\|\rho\|^2_{L_2(\Omega)} + \frac{1}{2}\|\sigma\|^2_{L_2(\Omega)} + \frac{1}{2}\|\epsilon\|^2_{L_2(\Omega)}\Big).\end{aligned} \tag{3.43}$$

Combining the above estimates, we arrive at the required bound.

□

To retain the abstract and more compact notation from the previous section, we write (3.38) as follows

$$\begin{aligned}(f(u)-f(U),\rho)_{\mathcal{H}} \leq C\Big(&\|\rho\|^{\mathbf{r}}_{\mathcal{H}}\|\rho\|^2_{\mathcal{V}} + G(U)\|\rho\|^2_{\mathcal{H}} \\ &+ \left(\|\sigma\|^{\mathbf{r}}_{\mathcal{H}}\|\sigma\|^2_{\mathcal{V}} + \|\epsilon\|^{\mathbf{r}}_{\mathcal{H}}\|\epsilon\|^2_{\mathcal{V}}\right) \\ &+ G(U)\Big(\|\sigma\|^2_{\mathcal{H}} + \|\epsilon\|^2_{\mathcal{H}}\Big)\Big),\end{aligned} \tag{3.44}$$

and we assume its validity henceforth for any $\mathcal{H}$ and $\mathcal{V}$.

3.3.2 Completing the estimate

The bound of the nonlinear term (3.44) still contains norms of ρ on the right-hand side. To eliminate these, we shall employ a continuation argument in the spirit of [19, 28, 30].

To this end, using Lemma (3.5) to bound the respective term on the right–hand side of (3.36), we arrive at

$$\begin{aligned}\|\rho\|^2_{L_\infty(0,t;\mathcal{H})} + \frac{C_{\rm coer}}{2}\int_0^t \|\rho\|^2_{\mathcal{V}}\,\mathrm{d}\tau \leq E_1(t,U,\sigma,\epsilon) + C\int_0^t \|\rho\|^{\mathbf{r}}_{\mathcal{H}}\|\rho\|^2_{\mathcal{V}}\,\mathrm{d}\tau \\ + C\int_0^t G(U)\|\rho\|^2_{\mathcal{H}}\,\mathrm{d}\tau,\end{aligned} \tag{3.45}$$

where

$$\begin{aligned}E_1(t,U,\sigma,\epsilon) := \frac{c_{2,\lambda}}{C_{\rm coer}}\Big(\|D\epsilon\|^2_{L_2(0,t;\mathcal{V}^*)} + C^2_{\rm cont}\|\sigma\|^2_{L_2(0,t;\mathcal{V})}\Big) \\ + \frac{2c_{1,\lambda}}{C_{\rm coer}}\|f(U) - \mathrm{P}\Pi f(U)\|^2_{L_2(0,t;\mathcal{V}^*)} \\ + c_{1,\lambda}\Big(\lambda^2\|\mathrm{e}_{\rm mc}\|^2_{L_1(0,t;\mathcal{H})} + \frac{(1-\lambda)^2}{C_{\rm coer}}\|\mathrm{e}_{\rm mc}\|^2_{L_2(0,t;\mathcal{V}^*)}\Big) \\ + C\int_0^t \Big(\|\sigma\|^{\mathbf{r}}_{\mathcal{H}}\|\sigma\|^2_{\mathcal{V}} + \|\epsilon\|^{\mathbf{r}}_{\mathcal{H}}\|\epsilon\|^2_{\mathcal{V}} + G(U)\Big(\|\sigma\|^2_{\mathcal{H}} + \|\epsilon\|^2_{\mathcal{H}}\Big)\Big)\,\mathrm{d}\tau.\end{aligned} \tag{3.46}$$

Upon observing that

$$\begin{aligned}\int_0^t \|\rho\|^r_{\mathcal{H}}\|\rho\|^2_{\mathcal{V}}\,\mathrm{d}\tau &\leq \|\rho\|^{\mathbf{r}}_{L_\infty(0,t;\mathcal{H})}\int_0^t \|\rho\|^2_{\mathcal{V}}\,\mathrm{d}\tau \\ &\leq \Big(\|\rho\|^2_{L_\infty(0,t;\mathcal{H})} + \int_0^t \|\rho\|^2_{\mathcal{V}}\,\mathrm{d}\tau\Big)^{1+\frac{r}{2}} \\ &\leq C\Big(\|\rho\|^2_{L_\infty(0,t;\mathcal{H})} + \frac{C_{\rm coer}}{2}\int_0^t \|\rho\|^2_{\mathcal{V}}\,\mathrm{d}\tau\Big)^{1+\frac{r}{2}},\end{aligned} \tag{3.47}$$

we deduce

$$\begin{aligned}\|\rho\|^2_{L_\infty(0,t;\mathcal{H})} + \frac{C_{\rm coer}}{2}\int_0^t \|\rho\|^2_{\mathcal{V}}\,\mathrm{d}\tau \leq E_1(t,U,\sigma,\epsilon) + C_1\int_0^t G(U)\|\rho\|^2_{\mathcal{H}}\,\mathrm{d}\tau \\ + C_2\Big(\|\rho\|^2_{L_\infty(0,t;\mathcal{H})} + \frac{C_{\rm coer}}{2}\int_0^t \|\rho\|^2_{\mathcal{V}}\,\mathrm{d}\tau\Big)^{1+\frac{\mathbf{r}}{2}},\end{aligned} \tag{3.48}$$

for known constants $C_1, C_2 > 0$. For each $n = 1, \ldots, N$, we let $\delta_n := E_1(t_n, U, \sigma, \epsilon)$. and consider the interval

$$J_n := \Big\{t \in [0,t_n] : \|\rho\|^2_{L_\infty(0,t;\mathcal{H})} + \frac{C_{\rm coer}}{2}\int_0^t \|\rho\|^2_{\mathcal{V}}\,\mathrm{d}t \leq 4\delta_n F(t_n,U)\Big\},$$

where we set $F(t_n,U) := \exp\Big(C_1\int_0^{t_n} G(U)\,\mathrm{d}\tau\Big)$, for brevity. We observe that $J_n \neq \emptyset$ as $\|\rho\|^2_{L_\infty(0,t;\mathcal{H})} + \frac{C_{\rm coer}}{2}\int_0^t \|\rho\|^2_{\mathcal{V}}\,\mathrm{d}\tau$ is continuous with respect to t and that it is equal to zero for $t = 0$, owing to the property $\rho(0) = 0$; also, J_n is closed.

Assuming, without loss of generality, that $r > 0$, (for, otherwise, f in (2.10) is globally Lipschitz continuous and, thus, the a posteriori bounds follow by combining the results from [60] along with a standard Grönwall inequality,) we set $t^\sharp := \max J_n > 0$.

Suppose that $t_n > t^\sharp$, i.e., $t_n \notin J_n$. Hence, $\delta_n = E_1(t_n, U, \sigma, \epsilon) \geq E_1(t^\sharp, U, \sigma, \epsilon)$. Therefore, (3.48) with $t = t^\sharp$ yields

$$\begin{aligned} \|\rho\|^2_{L_\infty(0,t^\sharp;\mathcal{H})} + \frac{C_{\rm coer}}{2}\int_0^{t^\sharp} \|\rho\|^2_{\mathcal{V}}\,\mathrm{d}\tau \leq \delta_n + C_2\Big(4\delta_n F(t_n,U)\Big)^{1+\frac{r}{2}} \\ + C_1\int_0^{t^\sharp} G(U)\|\rho\|^2_{\mathcal{H}}\,\mathrm{d}\tau, \end{aligned} \tag{3.49}$$

and Grönwall inequality, thus, implies

$$\|\rho\|^2_{L_\infty(0,t^\sharp;\mathcal{H})} + \frac{C_{\rm coer}}{2}\int_0^{t^\sharp} \|\rho\|^2_{\mathcal{V}}\,\mathrm{d}\tau \leq F(t_n,U)\Big(C_2\Big(4\delta_n F(t_n,U)\Big)^{1+\frac{\mathrm{r}}{2}} + \delta_n\Big), \tag{3.50}$$

since $F(t_n, U) \geq F(t^\sharp, U)$. Upon assuming that δ_n is such that

$$C_2\Big(4\delta_n F(t_n,U)\Big)^{1+\frac{\mathrm{r}}{2}} \leq \delta_n, \quad \text{or} \quad \delta_n \leq C_2^{-2/\mathrm{r}}\Big(4F(t_n,U)\Big)^{-\frac{2+\mathrm{r}}{\mathrm{r}}},$$

the estimate (3.50) becomes

$$\|\rho\|^2_{L_\infty(0,t^\sharp;\mathcal{H})} + \frac{C_{\rm coer}}{2}\int_0^{t^\sharp} \|\rho\|^2_{\mathcal{V}}\,\mathrm{d}\tau \leq 2\delta_n F(t_n,U); \tag{3.51}$$

this is a contradiction, as $t^\sharp$ was assumed to be the maximum element of J_n. Hence, $t_n = t^\sharp$ and, thus, we have already proven the following result.

Lemma 3.6. *Assuming the validity of estimate* (3.44)*, (or, in the special case of* $\mathcal{H} = L_2(\Omega)$ *and* $\mathcal{V} = H^1_0(\Omega)$*, assuming the hypotheses of Lemma 3.5,) the following conditional estimate holds: provided that*

$$E_1(t_n, U, \sigma, \epsilon) \leq C_2^{-2/\mathrm{r}}\Big(4F(t_n,U)\Big)^{-\frac{2+\mathrm{r}}{\mathrm{r}}}, \tag{3.52}$$

we have the bound

$$\|\rho\|^2_{L_\infty(0,t_n;\mathcal{H})} + \frac{C_{\rm coer}}{2}\|\rho\|^2_{L_2(0,t_n;\mathcal{V})} \leq 4F(t_n,U)E_1(t_n,U,\sigma,\epsilon). \tag{3.53}$$

We observe that the condition (3.52) in the estimate above is computable, provided that $E_1(t_n, U, \sigma, \epsilon)$ is computable. With this in mind, we shall bound the norms of σ and ϵ in E_1 by computable quantities below. Crucially, if δ_n is computable, then (3.53) becomes an *a posteriori* bound for ρ. The triangle inequality, would then already yield an *a posteriori* bound for the error e. Of course, we expect that δ_n decreases arbitrarily as the maximum timestep and spatial meshsize decay and/or the order of the dG-timestepping increases. We note, finally, that such conditional estimates are the "*a posteriori* equivalents" to the standard smallness assumptions on timestep and meshsize appearing in *a priori* error bounds for finite element methods for nonlinear evolution problems.

Remark 3.7. Crucially, there is no explicit CFL-type restriction in the statement of Lemma 3.6, despite this being concerned with an IMEX discretisation. Indeed, for unstable combinations of timesteps and spatial meshsizes, the bound (3.53) remains valid, provided the condition (3.52) is satisfied. It is, therefore, conceivable that (3.52) holds for CFL-unstable scenarios also; in such cases, (3.53) will remain valid, resulting to arbitrarily large right–hand sides, c.f., also [58].

3.3.3 Estimating the norms of σ and of ϵ

Proposition 3.8 (Bounds on norms of ϵ)**.** *Given Assumption 3.1, if* $\tilde{U} = RU$*, then for* $t \in \mathcal{I}_n$*,* $n = 0, 1 \ldots, N$*, we have, for* $\epsilon = \tilde{U} - U$ *and* $D\epsilon = \epsilon' + \mathrm{L}([\epsilon])$*, respectively, the bound*

$$\|\epsilon\|_S \leq \eta_{S,n} := \mathbb{E}_S[U, \mathbf{A}_n U], \tag{3.54}$$

and

$$\|D\epsilon\|_{\mathcal{V}^*} \leq \zeta_{\mathcal{V}^*,n} \tag{3.55}$$

with

$$\zeta_{\mathcal{V}^*,n} := \mathbb{E}_{\mathcal{V}^*}[\tilde{P}_n^{\ominus}(U' + L_n([U]_{n-1})), \mathbf{A}_n U' + \mathbf{A}_n L_n(U_{n-1}^+) - \mathbf{A}_{n-1} L_n(U_{n-1}^-)].$$

Proof. Noting that the elliptic reconstruction $\tilde{U}$ is time–independent and therefore commutes with time differentiation, (3.54) follows immediately by (3.2) along with Assumption 3.1.

Now, observing the identity,

$$a(\tilde{U}' + L_n([\tilde{U}]_{n-1}), v) = (\mathbf{A}_n U' + \mathbf{A}_n L_n(U^+_{n-1}) - \mathbf{A}_{n-1} L_n(U^-_{n-1}), v)_{\mathcal{H}}, \qquad (3.56)$$

which is valid for all $v \in \mathcal{V}$, we have the Galerkin orthogonality property

$$a(\tilde{U}' + L_n([\tilde{U}]_{n-1}), \mathrm{v}) = a(U' + L_n([U]_{n-1}), \mathrm{v}) \quad \text{for all } \mathrm{v} \in \mathcal{V}^{\ominus}_n. \qquad (3.57)$$

The above means that the elliptic problem (3.56) has the finite element solution $\tilde{P}^{\ominus}_n(U' + L_n([U]_{n-1}))$ on $\mathcal{V}^{\ominus}_n$. In view of Assumption 3.1, (3.55) follows. □

It is possible to prove an alternative bound to (3.55) by assuming a Poincaré-Friedrichs/spectral gap type inequality $\|v\|_{\mathcal{H}} \leq C_{\mathrm{PF}} \|v\|_{\mathcal{V}}$ and an *a posteriori* error bound in the $\mathcal{H}$–norm. Indeed, if we seek $z \in \mathcal{V}$, such that $a(v, z) = (D\epsilon, v)_{\mathcal{H}}$, and we assume that z is smooth enough, we have

$$\|D\epsilon\|^2_{\mathcal{H}} = a(D\epsilon, z) = a(D\epsilon, z - Z),$$

for any $Z \in \mathcal{V}^{\ominus}_n$ from the Galerkin orthogonality (3.57). From this point, one can work in a standard fashion to arrive at a residual–type (or other) *a posteriori* error bound $\mathbb{E}^{\ominus}_{\mathcal{H}}$ utilising the approximation properties of $\mathcal{V}^{\ominus}_n$ and (any) additional regularity $z \in V' \subset \mathcal{V}$, say, such that $\|z\|_{\mathcal{V}'} \leq C\|D\epsilon\|_{\mathcal{H}}$, resulting to a bound of the form

$$\|D\epsilon\|_{\mathcal{H}} \leq \zeta_{\mathcal{H},n}$$

where

$$\zeta_{\mathcal{H},n} := \mathbb{E}^{\ominus}_{\mathcal{H}}(U' + L_n([U]_{n-1}), \mathbf{A}_n U' + \mathbf{A}_n L_n(U^+_{n-1}) - \mathbf{A}_{n-1} L_n(U^-_{n-1})).$$

Now,

$$\|D\epsilon\|_{\mathcal{V}^*} = \sup_{0\neq w\in\mathcal{V}} \frac{(D\epsilon, w)_{\mathcal{H}}}{\|w\|_{\mathcal{V}}} \leq \sup_{0\neq w\in\mathcal{V}} \frac{\|D\epsilon\|_{\mathcal{H}}\|w\|_{\mathcal{H}}}{\|w\|_{\mathcal{V}}} \leq C_{\mathrm{PF}}\|D\epsilon\|_{\mathcal{H}},$$

resulting in the alternative estimate $\|D\epsilon\|_{\mathcal{V}^*} \leq C_{\mathrm{PF}}\zeta_{\mathcal{H},n}$; cf., also [77] for a related result in the lowest order case using backward Euler timestepping. This estimate has the advantage of not requiring the elliptic projection onto $\mathcal{V}_n^{\ominus}$ be evaluated. In practice, one can take the minimum of the two estimates

$$\|D\epsilon\|_{\mathcal{V}^*} \leq \min\left\{\zeta_{\mathcal{V}^*,n}, C_{\mathrm{PF}}\zeta_{\mathcal{H},n}\right\} =: \zeta_{\min,n}, \tag{3.58}$$

on $\mathcal{I}_n$, $n = 1,\ldots,N$, provided they are available. For instance, when $\mathcal{H} = L_2(\Omega)$ and $\mathcal{V} = H_0^1(\Omega)$, both estimates in (3.58) are valid.

Proposition 3.9 (Bounds on norms of σ)**.** *Given Assumption* (3.1)*, for each* $\mathcal{I}_n$*,* $n = 0, 1\ldots, N$*, we have, for* $\sigma = \hat{U} - \tilde{U}$*, the bounds*

$$\|\sigma\|_{L_2(\mathcal{I}_n;S)} \leq C_n\left(\theta_{S,n} + \|[U]_{n-1}\|_S\right),$$

where

$$\theta_{S,n} := \mathbb{E}_S[\tilde{P}_n^{\ominus}[U]_{n-1}, \mathbf{A}_n U_{n-1}^+ - \mathbf{A}_{n-1}U_{n-1}^-],$$

for $S \in \{\mathcal{H}, \mathcal{V}\}$*, and*

$$\|\sigma\|_{L_\infty(\mathcal{I}_n;\mathcal{H})} \leq \theta_{\mathcal{H},n} + \|[U]_{n-1}\|_{\mathcal{H}}.$$

Proof. From Proposition 3.4, we have

$$\|\sigma\|^2_{L_2(\mathcal{I}_n;\mathcal{V})} = \|\hat{U} - \tilde{U}\|^2_{L_2(\mathcal{I}_n;\mathcal{V})} = C_n^2\|[\tilde{U}]_{n-1}\|^2_{\mathcal{V}}. \tag{3.59}$$

The triangle inequality implies $\|[\tilde{U}]_{n-1}\|_{\mathcal{V}} \leq \|[\epsilon]_{n-1}\|_{\mathcal{V}} + \|[U]_{n-1}\|_{\mathcal{V}}$. To estimate $\|[\epsilon]_{n-1}\|_{\mathcal{V}}$, we work completely analogously to the proof of Proposition 3.8: we observe the Galerkin orthogonality

$$a([\tilde{U}]_{n-1}, \mathrm{v}) = a([U]_{n-1}, \mathrm{v}) \quad \text{for all } V \in \mathcal{V}_n^{\ominus},$$

which, together with Assumption 3.1 give rise to the estimate

$$\|[\epsilon]_{n-1}\|_{\mathcal{V}} \leq \mathbb{E}_{\mathcal{V}}[\tilde{P}_n^{\ominus}[U]_{n-1}, \mathbf{A}_n U_{n-1}^{+} - \mathbf{A}_{n-1} U_{n-1}^{-}].$$

From (3.24) in Proposition 3.4, we also have

$$\|\sigma\|_{L_\infty(\mathcal{I}_n;\mathcal{H})} = \|[\tilde{U}]_{n-1}\|_{\mathcal{H}} \leq \|[\epsilon]_{n-1}\|_{\mathcal{H}} + \|[U]_{n-1}\|_{\mathcal{H}},$$

which, working as above, gives the second estimate. □

For an alternative bound, we refer to [60, Lemma 4.4].

Remark 3.10. If no mesh modification takes place, i.e., when $\mathcal{V}_{n-1} = \mathcal{V}_n$, the above estimates simplify considerably, since we then have

$$\theta_{S,n} = \mathbb{E}_S[[U]_{n-1}, \mathbf{A}_n[U]_{n-1}].$$

Using Propositions 3.8 and 3.9 we can bound the term $E_1(t_n, U, \sigma, \epsilon)$ given in (3.46) by $\mathbb{E}_1(t_n, U)$ defined as

$$\begin{aligned}
\mathbb{E}_1(t_n, U) := \frac{c_{2,\lambda}}{C_{\text{coer}}} \sum_{n=1}^{N} \Big(\zeta_{\min,n}^2 + C_{\text{cont}}^2 \Big(C_n (\theta_{\mathcal{V},n} + \|[U]_{n-1}\|_{\mathcal{V}}) \Big)^2 \Big) \\
+ \frac{2c_{1,\lambda}}{C_{\text{coer}}} \|f(U) - \mathrm{P}\Pi f(U)\|_{L_2(0,t_n;\mathcal{V}^*)}^2 \\
+ c_{1,\lambda} \Big(\lambda^2 \|\mathrm{e}_{\text{mc}}\|_{L_1(0,t_n;\mathcal{H})}^2 + \frac{(1-\lambda)^2}{C_{\text{coer}}} \|\mathrm{e}_{\text{mc}}\|_{L_2(0,t_n;\mathcal{V}^*)}^2 \Big) \\
+ C \sum_{n=1}^{N} \Bigg(\Big(\theta_{\mathcal{H},n} + \|[U]_{n-1}\|_{\mathcal{H}} \Big)^r \Big(C_n \left(\theta_{\mathcal{V},n} + \|[U]_{n-1}\|_{\mathcal{V}} \right) \Big) \\
+ \Big(\max_{t \in \mathcal{I}_n} \eta_{\mathcal{H},n}(t) \Big)^r \int_{\mathcal{I}_n} \eta_{\mathcal{V},n}^2(t) \, \mathrm{d}t \\
+ \max_{t \in \mathcal{I}_n} G(U(t)) \Big(\Big(C_n \theta_{\mathcal{H},n} + C_n \|[U]_{n-1}\|_{\mathcal{H}} \Big)^2 + \int_{\mathcal{I}_n} \eta_{\mathcal{H},n}^2(t) \, \mathrm{d}t \Big) \Bigg),
\end{aligned}$$

using which, we are now in a position to finalise the a posteriori error analysis.

3.3.4 The final *a posteriori* error bounds

Using the bounds of ρ, σ and ϵ, we are now ready to complete the a posteriori error analysis.

Theorem 3.11 ($L_\infty(\mathcal{I};\mathcal{H})$–norm estimate)**.** *Assuming the validity of estimate* (3.44)*, (or, in the special case of* $\mathcal{H} = L_2(\Omega)$ *and* $\mathcal{V} = H_0^1(\Omega)$*, assuming the hypotheses of Lemma 3.5,) the following conditional estimate holds: provided that*

$$\mathbb{E}_1(t_n, U) \leq C_2^{-2/r}\Big(4F(t_n, U)\Big)^{-\frac{2+r}{r}}, \tag{3.60}$$

for $n = 1, ..., N$*, we have the* a posteriori *error bound*

$$\begin{aligned}\|u - U\|^2_{L_\infty(0,t_n;\mathcal{H})} \leq\ & 4F(t_n, U)\mathbb{E}_1(t_n, U) \\ & + \max_{i=1,\dots,n}\Big(\theta_{\mathcal{H},i} + \|[U]_{i-1}\|_{\mathcal{H}}\Big)^2 + \max_{t\in[0,t_n]}\eta^2_{\mathcal{H},n}.\end{aligned} \tag{3.61}$$

Proof. We begin by using triangle inequality which implies

$$\|u - U\|^2_{L_\infty(0,t_n;\mathcal{H})} \leq \|\rho\|^2_{L_\infty(0,t_n;\mathcal{H})} + \|\sigma\|^2_{L_\infty(0,t_n;\mathcal{H})} + \|\epsilon\|^2_{L_\infty(0,t_n;\mathcal{H})}. \tag{3.62}$$

Then by observing that the proof and the statement of Lemma 3.6 holds with $E_1(t_n, U, \sigma, \epsilon)$ replaced by $\mathbb{E}_1(t_n, U)$, we have

$$\|\rho\|^2_{L_\infty(0,t_n;\mathcal{H})} \leq 4F(t_n, U)\mathbb{E}_1(t_n, U). \tag{3.63}$$

Noting that σ represents the time reconstruction error, then from Proposition 3.4 we obtain

$$\|\sigma\|^2_{L_\infty(0,t_n;\mathcal{H})} = \|\hat{U} - \tilde{U}\|^2_{L_\infty(0,t_n;\mathcal{H})} := \max_{n=1,\dots,N}\|[\tilde{U}]_{n-1}\|^2_{\mathcal{H}}. \tag{3.64}$$

Proposition 3.9 implies that

$$\|\sigma\|^2_{L_\infty(0,t_n;\mathcal{H})} \leq \max_{i=1,\dots,n}\Big(\theta_{\mathcal{H},i} + \|[U]_{i-1}\|_{\mathcal{H}}\Big)^2. \tag{3.65}$$

Now, it remains to bound $\epsilon = \tilde{U} - U$ which is the elliptic error and by the aid of Proposition 3.8 we obtain

$$\|\epsilon\|^2_{L_\infty(0,t_n;\mathcal{H})} \leq \max_{t\in[0,t_n]} \eta^2_{\mathcal{H},n}. \tag{3.66}$$

Finally, by substituting (3.63), (3.65), and (3.66) in (3.62) we obtain the result. □

Similarly, we have an *a posteriori* bound in the $L_2(\mathcal{I};\mathcal{V})$–norm.

Theorem 3.12 ($L_2(\mathcal{I};\mathcal{V})$–norm estimate)**.** *Assuming the validity of estimate* (3.44)*, (or, in the special case of* $\mathcal{H} = L_2(\Omega)$ *and* $\mathcal{V} = H^1_0(\Omega)$*, assuming the hypotheses of Lemma 3.5,) the following conditional estimate holds: provided that* (3.52) *holds for* $n = 1, ..., N$*, we have the* a posteriori *error bound*

$$\begin{aligned}\|u - U\|^2_{L_2(0,t_n;\mathcal{V})} \leq \frac{6}{C_{\text{coer}}}\Big(&4F(t_n,U)\mathbb{E}_1(t_n,U)\\ &+\sum_{n=1}^{N}\Big(C_n^2\Big(\theta_{\mathcal{V},n} + \|[U]_{n-1}\|_{\mathcal{V}}\Big)^2 + \int_{\mathcal{I}_n}\eta^2_{\mathcal{V},n}\,\mathrm{d}t\Big).\end{aligned} \tag{3.67}$$

Proof. By the use of the triangle inequality we obtain

$$\|u - U\|^2_{L_2(0,t_n;\mathcal{V})} \leq \|\rho\|^2_{L_2(0,t_n;\mathcal{V})} + \|\sigma\|^2_{L_2(0,t_n;\mathcal{V})} + \|\epsilon\|^2_{L_2(0,t_n;\mathcal{V})}. \tag{3.68}$$

Noting that the proof and the statement of Lemma 3.6 holds with $E_1(t_n, U, \sigma, \epsilon)$ replaced by $\mathbb{E}_1(t_n, U)$, and then we have

$$\|\rho\|^2_{L_2(0,t_n;\mathcal{V})} \leq \frac{8}{C_{\text{coer}}}F(t_n,U)\mathbb{E}_1(t_n,U). \tag{3.69}$$

Also, observe that σ is the time reconstruction error, hence from Propositions 3.4 and 3.9 we obtain

$$\|\sigma\|^2_{L_2(0,t_n;\mathcal{V})} \leq \sum_{n=1}^{N} C_n^2\Big(\theta_{\mathcal{V},n} + \|[U]_{n-1}\|_{\mathcal{V}}\Big)^2. \tag{3.70}$$

Using Proposition 3.8 to bound the elliptic error ϵ we have

$$\|\epsilon\|^2_{L_2(0,t_n;\mathcal{V})} \leq \sum_{n=1}^{N}\int_{\mathcal{I}_n}\eta^2_{\mathcal{V},n}\,\mathrm{d}t. \tag{3.71}$$

Now, substituting (3.69), (3.70), (3.71) in (3.68) leading to the required result. □

3.4 Numerical experiments

We present a series of numerical experiments aimed at testing the reliability and efficiency of the *a posteriori* error bounds derived above. The numerical implementation is based on the `deal.II` finite element library [16] and the tests run in the high performance computing facility ALICE at the University of Leicester.

We study the asymptotic behaviour in the $L_\infty(L_2)$– and $L_2(H^1)$–norms of the error and of the respective estimators by monitoring the evolution of the experimental order of convergence (EOC) defined in (2.50) over time on a sequence of uniformly refined space meshes indexed by the mesh size h. In each instance, we fix a constant time step k_n as some power of h and we also use fixed polynomial degrees in both space and time. The resulting errors and estimators are plotted against the corresponding space mesh size h.

We report the EOC relative to the last computed quantities in all figures as an indication of the asymptotic rate of convergence. We also report the respective *effectivity indices*, i.e., the ratio between estimator and error for each instance. The estimator is deemed reliable if the effectivity is greater than or equal to one and it is most efficient when the effectivity is close to one.

In the examples below we consider both linear and semilinear parabolic problems. In all cases, $\mathcal{A} = \Delta$, i.e., the Dirichlet Laplacian, yielding the heat equation with either linear or nonlinear source terms and $\mathcal{H} = L_2(\Omega)$, $\mathcal{V} = H_0^1(\Omega)$, giving $\mathcal{H}^* = H^{-1}(\Omega)$.

3.4.1 Example 1: a linear problem

We test the IMEX fully discrete scheme analysed in this work on (2.10) with $\mathcal{I} \times \Omega := [0,1] \times [0,1]^2$, f is independent of the exact solution u and the initial

and boundary conditions such that the exact solution is given by

$$u(t, x, y) = \sin(\pi t) \sin(\pi x) \sin(\pi y). \tag{3.72}$$

The respective *a posteriori* error bounds when the PDE is linear can be trivially recovered from Theorems 3.11 and 3.12 by setting $r = 0$ and removing the conditionality estimate (3.52) as it is void in the linear case; this can be seen by observing that the second term on the right–hand side of (3.49) disappears when the forcing f is a function of t and x only. Alternatively, we refer to [60] for a thorough treatment of the linear case.

We report the results of two tests using different combinations of polynomial orders r and p in time and space, respectively, denoted as dG(r)–cG(p) scheme.

3.4.1.1 Example 1A: dG(1)–cG(2) scheme

Here, we employ uniform biquadratic elements in space ($p = 2$) and uniform linear elements in time ($r = 1$), i.e., the dG(1)–cG(2) scheme. Figure 3.1 shows the convergence history with $k_n = h$ (left plot) and with $k_n = h^{3/2}$ (right plot) for both the $L_\infty(L_2)$– and $L_2(H^1)$–norms. In the case $k_n = h$, we observe that the $L_2(H^1)$ estimator provides the required order of convergence as EOC ≈ 2, in close agreement with the corresponding error; the effectivity is in between 2.90 and 8.93. Also the $L_\infty(L_2)$ estimator yields the correct rate as EOC ≈ 3, with effectivity between 47.41 and 63.41.

For the case $k_n = h^{3/2}$, we again observe the expected order of convergence of the $L_2(H^1)$–norm error and estimator, while for the $L_\infty(L_2)$–norm we have an EOC of 4.64 and 4.72, respectively, corresponding to the convergence rate expected in time, thus indicating that the time discretisation error dominates in this case. The effectivity is approximately 5.28 and 7.16 for the $L_2(H^1)$– and $L_\infty(L_2)$–norm estimators, respectively. In both cases the results are in agreement with Theorems 3.11 and 3.12.

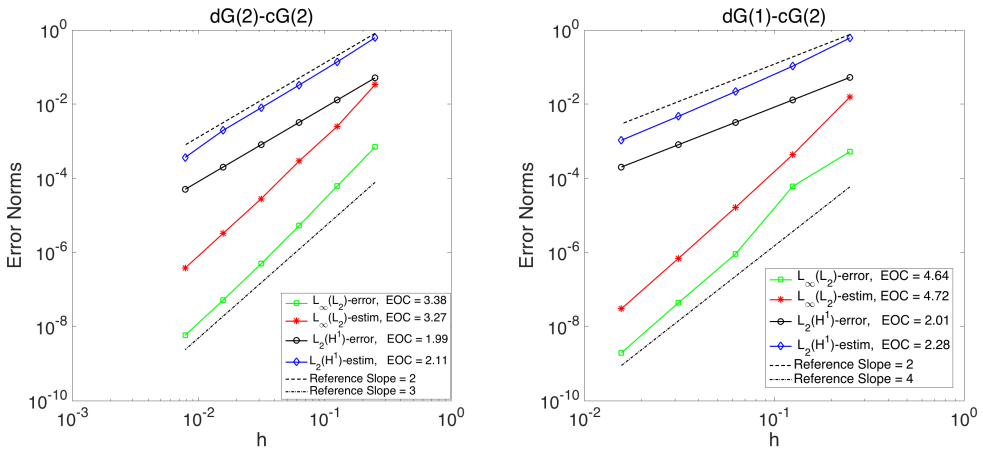

FIGURE 3.1: Example 1*A*. Convergence history for the dG(1)–cG(2) scheme with $k_n = h$ (left) and $k_n = h^{3/2}$ (right).

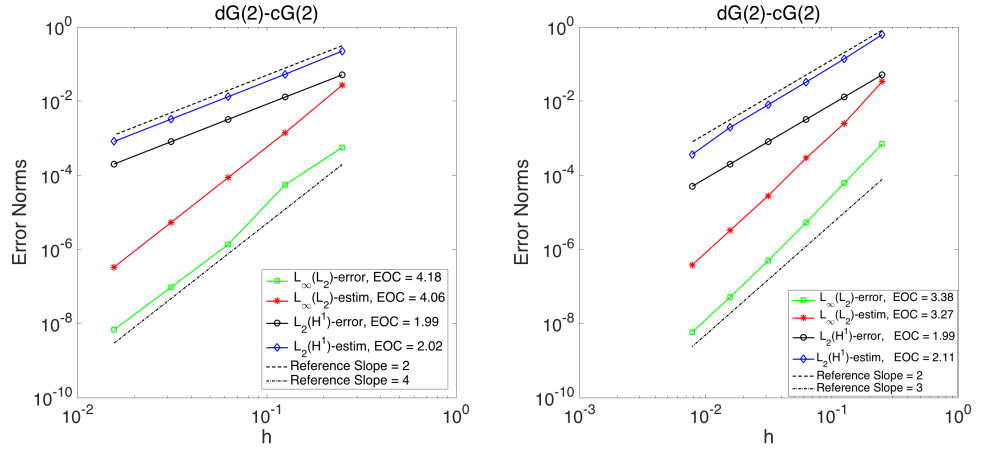

FIGURE 3.2: Example 1*B*. Convergence history for the dG(2)–cG(2) scheme with $k_n = h$ (left) and $k_n = h^{4/3}$ (right).

3.4.1.2 Example 1B: dG(2)–cG(2) scheme

Here, we consider two different relations for the timestep and space meshsize. That is, $k_n = h$ and $k_n = h^{4/3}$, respectively.

The numerical results corresponding to $k_n = h$ are shown in the left plot of Figure 3.2. We observe that our error estimators provide the expected order of convergence in both the $L_2(H^1)$– and $L_\infty(L_2)$–norms.

The results obtained with the choice $k_n = h^{4/3}$ are reported on the right plot of Figure 3.2. Again we observe an optimal experimental order of convergence as EOC $\approx$ 2 for both the $L_2(H^1)$–norm estimator and error. The respective

experimental order of convergence of the $L_\infty(L_2)$–norm estimator and error are EOC ≈ 4, corresponding to the optimal convergence rate with respect to the timestep size. In both cases, the estimators' effectivities show little differences with the corresponding values obtained in Example 1 and are, therefore omitted for brevity. Also, the results are in agreement with theoretical results in Theorems 3.11 and 3.12.

3.4.2 Example 2: a nonlinear problem

On $\mathcal{I} \times \Omega := [0,1] \times [0,1]^2$ we consider the semilinear problem (2.10) with $f = -u^2 + \tilde{f}(x,y,t)$, with $\tilde{f}$ such that the exact solution is given by

$$u(t,x,y) = \sin(\pi t)\sin(\pi x)\sin(\pi y); \tag{3.73}$$

note that we have $r = 1$ and $p = 2$ in this case. We test the respective *a posteriori* error bounds from Theorems 3.11 and 3.12. We test the dG(1)–cG(2) scheme, by considering the two choices $k_n = h$ and $k_n = h^{3/2}$ with corresponding numerical results in the left and right plots of Figure 3.3, respectively.

The results are in line with those of the linear example. In particular, for $k_n = h$ we again observe good agreement between the estimators and the corresponding errors, with EOC ≈ 2 and EOC ≈ 3 for the $L_2(H^1)$– and $L_\infty(L_2)$– quantities, respectively.

The results corresponding to $k_n = h^{3/2}$ are also confirming the theoretical asymptotic rate of convergence. For the $L_2(H^1)$–norm estimator and error we have EOC ≈ 2 and, similarly to the linear problem considered earlier, for the $L_\infty(L_2)$–norm estimator and error we have EOC ≈ 4.5. Note also that the effectivity is, in all cases, in between 1.07 and 12.18. We notice that the results coincide with the results of Theorems 3.11 and 3.12.

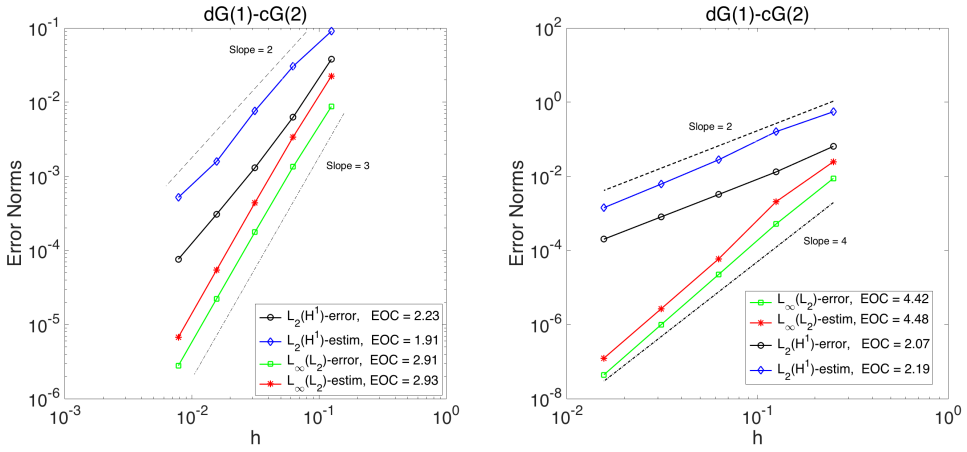

FIGURE 3.3: Example 2. Convergence history for the dG(1)–cG(2) scheme with $k_n = h$ (left) and $k_n = h^{3/2}$ (right).

Chapter 4

A priori error analysis

4.1 Introduction

Determining the quality of the approximate solutions is another interesting area of research in the study of finite element methods. *A priori* error bounds are very helpful and useful tools in this regard. They can be used to judge whether the numerical solution is close to the exact solution of the problem. In the *a priori* error analysis we are interested in bounding the actual error as follows

$$\|e\| = \|u - U\| \leq \mathsf{E}[u, f, h, k_n],$$

where the function E depends on the exact solution u and the source term f of the problem, the mesh size h, the time step size k_n, and on the data of the problem, in the relevant norm $\|.\|$. If this function approaches zero when the mesh is fine i.e. when h is small, and also for small time steps, then this indicates that the approximate solution is getting closer and closer to the actual solution. The main idea in the *a prior* error analysis is to split up the error in the following form

$$e = u - U = (u - \tilde{P}_h u) + (\tilde{P}_h u - U),$$

where $\tilde{P}_h$ is the elliptic projection operator, also, known as Wheeler or Ritz projection, which was first proposed in 1973 by Wheeler [116]. The elliptic reconstruction

used in the previous chapter is considered as the dual *a posteriori* of the elliptic projection in the *a priori* error analysis. In this section, we will consider the *a priori* error analysis in the $L_\infty(L_2)$ and $L_2(H^1)$ norms for the fully discrete IMEX space–time finite element scheme (2.23) applied to the semilinear evolution model problem defined in (2.10).

For simplicity we assume that the spatial mesh does *not* change dynamically. Let also $h : \Omega \to \mathbb{R}$ denote the elementwise constant *meshsize* function whereby $h|_K = h_K$, for every spatial element $K \in \mathcal{T}_h$, with $\mathcal{T}_h$ denoting the spatial mesh subordinate to $\mathcal{V}_h$. Throughout this work, we shall assume that $cr_{j-1} \leq r_j \leq Cr_{j-1}$, where $c, C > 0$, for all $j = 2, \dots N$ uniformly, i.e., that the polynomial degrees in the temporal variable admit a local quasi-uniformity condition.

We begin with the following auxiliary result.

Lemma 4.1. *For $v \in C(\mathcal{I}_n; \mathcal{H})$, and for $\mathcal{H} = L_2(\Omega)$, we have the inverse estimate*

$$\|v\|^2_{L_\infty(\mathcal{I}_n;\mathcal{H})} \leq \mathcal{I}_n \|v'\|^2_g ut \, \mathrm{d}t + 2 \tag{4.1}$$

Proof. letting $v \in C(\mathcal{I}_n; \mathcal{H})$ and $t^* \in \mathcal{I}_n$, so that $\|v(t^*)\|_{\mathcal{H}} = \max_{t\in\mathcal{I}_n} \|v\|_d$, we have

$$\max_{t\in\mathcal{I}_n} \|v\|_{\mathcal{H}} = \|v(t^*)\|_{\mathcal{H}} = \; - \int_{t^*}^{t_n} \frac{\mathrm{d}}{\mathrm{d}t} \|v(t)\|_{\mathcal{H}} \, \mathrm{d}t + \|v(t_n^-)\|_/ h. \tag{4.2}$$

Now,

$$\begin{aligned}
\Big| \int_{t^*}^{t_n} \frac{\mathrm{d}}{\mathrm{d}t} \|v(t)\|_{\mathcal{H}} \, \mathrm{d}t \Big| &= \Big| \int_{t^*}^{t_n} \frac{\mathrm{d}}{\mathrm{d}t} \Big(\int_\Omega v^2(t,x) \, \mathrm{d}x \Big)^{1/2} \mathrm{d}t \Big| \\
&= \frac{1}{2} \Big| \int_{t^*}^{t_n} \frac{\mathrm{d}}{\mathrm{d}t} \Big(\int_\Omega v^2(t,x) \, \mathrm{d}x \Big) \Big(\int_\Omega v^2(t,x) \, \mathrm{d}x \Big)^{-1/2} \mathrm{d}t \Big| \\
&= \Big| \int_{t^*}^{t_n} \int_\Omega v(t,x) v'(t,x) \, \mathrm{d}x \Big(\int_\Omega v^2(t,x) \, \mathrm{d}x \Big)^{-1/2} \mathrm{d}t \Big| \\
&\leq \int_{t^*}^{t_n} \|v(t)\|_{\mathcal{H}} \|v'(t)\|_{\mathcal{H}} \|v(t)\|^{-1}_{\mathcal{H}} \, \mathrm{d}t = \int_{\mathcal{I}_n} \|v'(t)\|_{\mathcal{H}} \, \mathrm{d}t.
\end{aligned}$$

Using this in (4.2), upon squaring and using the Cauchy-Schwarz inequality, gives

$$\max_{t\in\mathcal{I}_n} \|v\|^2_{\mathcal{H}} \leq 2k_n \int_{\mathcal{I}_n} \|v'(t)\|^2_{\mathcal{H}} \, \mathrm{d}t + 2\|v(t_n^-)\|^2_{\mathcal{H}}.$$

□

When $\mathcal{H}$ is not the canonical case $\mathcal{H} = L_2(\Omega)$, we make the following assumption instead.

Assumption 4.2. For $v \in C(\mathcal{I}_n; \mathcal{H})$, and for some $C > 0$, independent of k_n and of v, we have the estimate

$$\|v\|^2_{L_\infty(\mathcal{I}_n;\mathcal{H})} \leq C\Big(k_n \int_{\mathcal{I}_n} \|v'(t)\|^2_{\mathcal{H}} \,\mathrm{d}t + \|v(t_n^-)\|^2_{\mathcal{H}}\Big). \tag{4.3}$$

We introduce the space-time projection operator $\mathrm{P} : L_2(\mathcal{I}; \mathcal{V}) \to \mathcal{X}$ by

$$\mathrm{P} := \pi^n \otimes \tilde{P}_h,$$

i.e., it is a time-interval-wise L_2-orthogonal (discontinuous) projection (π^n) with respect to the time variable tensorised with the elliptic projection ($\tilde{P}_h$) in space, for some $n \in \{1, \ldots, N\}$. Also, we shall make the (mildly) simplifying assumption

$$(w, v)_{\mathcal{V}} = (\mathcal{A}w, v)_{\mathcal{H}} = (\sqrt{\mathcal{A}}w, \sqrt{\mathcal{A}}v)_{\mathcal{H}}; \tag{4.4}$$

we stress, however, that certain generalisations are possible, although not carried through here for simplicity of the presentation.

The *a priori* error bounds given below will involve the assumption that the quantity $\Pi f(u) - f(u)$ is optimally convergent and that Π is stable in suitable norms.

4.2 *A priori* error bounds

We begin by proving an *a priori* error bound for the $L_\infty(\mathcal{I}; \mathcal{H})$– and $L_2(\mathcal{I}; \mathcal{V})$–norms of the error. The proof is based on the combination of *hp*-version approximation estimates with an inf-sup condition argument, a variant of which has been presented already in [26], see also [82], along with known arguments for linear part of the operator (see, e.g., [109, Chapter 12]). The results presented below extend the theory from [52] to the case of non-Lipschitz nonlinear reactions.

4.2.1 The stability of $\mathrm{P}u - U$

For brevity we set $\vartheta := \mathrm{P}u - U$, and we decompose the error as

$$u - U = (u - \mathrm{P}u) + (\mathrm{P}u - U) =: p + \vartheta,$$

with $p := u - \mathrm{P}u$. Note that p is a projection error and, therefore, can be estimated using best approximation results. We shall now estimate ϑ, by quantities involving the problem data and/or p, by using discrete stability estimates.

The model problem (2.10) in weak form with weakly imposed initial condition reads: find $u \in H^1(\mathcal{I};\mathcal{V})$ such that

$$\int_0^{t_n} \Big((u', \mathsf{v})_{\mathcal{H}} + a(u, \mathsf{v}) \Big) \,\mathrm{d}t + (u(0), \mathsf{v}(0))_{\mathcal{H}} = \int_0^{t_n} (f(u), \mathsf{v})_{\mathcal{H}} \,\mathrm{d}t + (u_0, \mathsf{v}(0))_{\mathcal{H}}, \quad (4.5)$$

for all $\mathsf{v} \in L_2(\mathcal{I};\mathcal{V})$, and $n = 1, \ldots, N$, which upon subtracting (2.23) summed for $j = 1, \ldots, n$, yields the identity

$$\begin{aligned} &\int_0^{t_n} \Big(((u-U)', \mathsf{v})_{\mathcal{H}} + a(u - U, \mathsf{v}) \Big) \,\mathrm{d}t - \sum_{j=2}^{n} ([U]_{j-1}, \mathsf{v}_{j-1}^+)_{\mathcal{H}} + ((u-U)_0^+, \mathsf{v}_0^+)_{\mathcal{H}} \\ &= \int_0^{t_n} (f(u) - \Pi f(U), \mathsf{v})_{\mathcal{H}} \,\mathrm{d}t + (u_0 - \tilde{P}_h u_0, \mathsf{v}_0^+)_{\mathcal{H}} \end{aligned} \quad (4.6)$$

for all $\mathsf{v} \in \mathcal{X}_{\mathbf{r}}(\mathcal{V}_h)$, $n = 1, \ldots, N$. Upon setting $\mathsf{v} = \vartheta \in \mathcal{X}_{\mathbf{r}}(\mathcal{V}_h)$ in (4.6), gives

$$\begin{aligned} &\int_0^{t_n} \Big((\vartheta', \vartheta)_{\mathcal{H}} + a(u - U, \vartheta) \Big) \,\mathrm{d}t - \sum_{j=2}^{n} ([U]_{j-1}, \vartheta_{j-1}^+)_{\mathcal{H}} + \|\vartheta_0^+\|_{\mathcal{H}}^2 \\ &= \int_0^{t_n} (f(u) - \Pi f(U), \vartheta)_{\mathcal{H}} \,\mathrm{d}t - \int_0^{t_n} (p', \vartheta)_{\mathcal{H}} \,\mathrm{d}t - (p(0), \vartheta_0^+)_{\mathcal{H}}. \end{aligned} \quad (4.7)$$

Upon observing that $-[U]_{j-1} = [\vartheta]_{j-1} - [\mathrm{P}u]_{j-1}$ for $j = 2, \ldots, n$, along with the (classical) identity

$$\begin{aligned} &\int_0^{t_n} (w', w)_{\mathcal{H}} \,\mathrm{d}t + \sum_{j=2}^{n} ([w]_{j-1}, w_{j-1}^+)_{\mathcal{H}} + \|w_0^+\|_{\mathcal{H}}^2 \\ &= \frac{1}{2}\|w_n^-\|_{\mathcal{H}}^2 + \frac{1}{2}\sum_{j=2}^{n} \|[w]_{j-1}\|_{\mathcal{H}}^2 + \frac{1}{2}\|w_0^+\|_{\mathcal{H}}^2, \end{aligned}$$

(4.7) yields

$$\begin{aligned}
&\frac{1}{2}\|\vartheta_n^-\|_{\mathcal{H}}^2+\frac{1}{2}\sum_{j=2}^{n}\|[\vartheta]_{j-1}\|_{\mathcal{H}}^2+\frac{1}{2}\|\vartheta_0^+\|_{\mathcal{H}}^2+\int_0^{t_n}a(u-U,\vartheta)\,\mathrm{d}t\\
&=\int_0^{t_n}(f(u)-\Pi f(U),\vartheta)_{\mathcal{H}}\,\mathrm{d}t-\int_0^{t_n}(p',\vartheta)_{\mathcal{H}}\,\mathrm{d}t-(p(0),\vartheta_0^+)_{\mathcal{H}}\\
&\quad+\sum_{j=2}^{n}([\mathrm{P}u]_{j-1},\vartheta_{j-1}^+)_{\mathcal{H}}\\
&=\int_0^{t_n}(f(u)-\Pi f(U),\vartheta)_{\mathcal{H}}\,\mathrm{d}t+\int_0^{t_n}(p,\vartheta')_{\mathcal{H}}\,\mathrm{d}t-(p(t_n),\vartheta_n^-)_{\mathcal{H}}\\
&\quad-\sum_{j=1}^{n-1}([p]_j,\vartheta_j^+)_{\mathcal{H}}-\sum_{j=1}^{n-1}(p(t_j^-),\vartheta_j^-)_{\mathcal{H}}+\sum_{j=1}^{n-1}(p(t_j^+),\vartheta_j^+)_{\mathcal{H}}\\
&=\int_0^{t_n}(f(u)-\Pi f(U),\vartheta)_{\mathcal{H}}\,\mathrm{d}t+\int_0^{t_n}(p,\vartheta')_{\mathcal{H}}\,\mathrm{d}t-(p(t_n),\vartheta_n^-)_{\mathcal{H}}\\
&\quad+\sum_{j=1}^{n-1}(p(t_j^-),[\vartheta]_j)_{\mathcal{H}},
\end{aligned}\tag{4.8}$$

by integration by parts with respect to the time variable and by noting that $p(t_j^{\pm})=u(t_j)-\mathrm{P}u(t_j^{\pm})$.

Also, we have

$$a(u-U,\vartheta)=a(u-P_hu,\vartheta)+a((\mathrm{I}-\pi^n)\otimes P_hu,\vartheta)+a(\vartheta,\vartheta),\tag{4.9}$$

with I denoting the identity operator with respect to the t-variable in this particular instance. Upon invoking the defining property (3.6) of the elliptic projection, the first term on the right–hand side of (4.9) vanishes and, thus, after integration with respect to the time variable, we have

$$\tilde{\lambda}\int_0^{t_n}a(u-U,\vartheta)\,\mathrm{d}t=\int_0^{t_n}a((\mathrm{I}-\pi^n)\otimes P_hu,\vartheta)\,\mathrm{d}t+\int_0^{t_n}a(\vartheta,\vartheta)\,\mathrm{d}t.\tag{4.10}$$

Again, the first term on the right-hand side of (4.10) vanishes from the orthogonality of the piecewise L_2-projection operator π^n with respect to the time variable

and the simplifying assumption (4.4); hence, (4.8) yields

$$\begin{aligned}
&\frac{1}{2}\|\vartheta_n^-\|_{\mathcal{H}}^2+\frac{1}{2}\sum_{j=2}^{n}\|[\vartheta]_{j-1}\|_{\mathcal{H}}^2+\frac{1}{2}\|\vartheta_0^+\|_{\mathcal{H}}^2+C_{\mathrm{coer}}\int_0^{t_n}\|\vartheta\|_V^2\,\mathrm{d}t\\
\leq&\int_0^{t_n}(f(u)-\Pi f(U),\vartheta)_{\mathcal{H}}\,\mathrm{d}t+\int_0^{t_n}(p,\vartheta')_{\mathcal{H}}\,\mathrm{d}t-(p(t_n),\vartheta_n^-)_{\mathcal{H}}\\
&+\sum_{j=1}^{n-1}(p(t_j^-),[\vartheta]_j)_{\mathcal{H}}.
\end{aligned}\tag{4.11}$$

Using the coercivity of the elliptic operator. Standard arguments such as Cauchy-Schwarz and Young inequalities now yield

$$\begin{aligned}
&\frac{1}{2}\|\vartheta_n^-\|_{\mathcal{H}}^2+\frac{1}{2}\sum_{j=2}^{n}\|[\vartheta]_{j-1}\|_{\mathcal{H}}^2+\frac{1}{2}\|\vartheta_0^+\|_{\mathcal{H}}^2+C_{\mathrm{coer}}\int_0^{t_n}\|\vartheta\|_V^2\,\mathrm{d}t\\
\leq&\frac{2}{C_{\mathrm{coer}}}\int_0^{t_n}\|f(u)-\Pi f(U)\|_{\mathcal{V}^*}^2\,\mathrm{d}t+\frac{C_{\mathrm{coer}}}{8}\int_0^{t_n}\|\vartheta\|_V^2\,\mathrm{d}t\\
&+\int_0^{t_n}\tilde{\lambda}^{-1}\|p\|_{\mathcal{H}}^2\,\mathrm{d}t+\frac{1}{4}\int_0^{t_n}\tilde{\lambda}\|\vartheta'\|_{\mathcal{H}}^2\,\mathrm{d}t+\|p(t_n)\|_{\mathcal{H}}^2+\frac{1}{4}\|\vartheta_n^-\|_{\mathcal{H}}^2\\
&+2\sum_{j=1}^{n-1}\|p(t_j^-)\|_{\mathcal{H}}^2+\frac{1}{8}\sum_{j=1}^{n-1}\|[\vartheta]_j\|_{\mathcal{H}}^2.
\end{aligned}\tag{4.12}$$

For some $\tilde{\lambda}>0$ constant on each subinterval $\mathcal{I}_j$ to be defined precisely below, giving

$$\begin{aligned}
&\frac{1}{4}\|\vartheta_n^-\|_{\mathcal{H}}^2+\frac{1}{4}\sum_{j=2}^{n}\|[\vartheta]_{j-1}\|_{\mathcal{H}}^2+\frac{1}{2}\|\vartheta_0^+\|_{\mathcal{H}}^2+\frac{C_{\mathrm{coer}}}{4}\int_0^{t_n}\|\vartheta\|_V^2\,\mathrm{d}t\\
\hat{\lambda}\leq&\frac{2}{C_{\mathrm{coer}}}\int_0^{t_n}\|f(u)-\Pi f(U)\|_{\mathcal{V}^*}^2\,\mathrm{d}t+\int_0^{t_n}\tilde{\lambda}^{-1}\|p\|_{\mathcal{H}}^2\,\mathrm{d}t\\
&+\frac{1}{4}\int_0^{t_n}\tilde{\lambda}\|\vartheta'\|_{\mathcal{H}}^2\,\mathrm{d}t+2\sum_{j=1}^{n}\|p(t_j^-)\|_{\mathcal{H}}^2.
\end{aligned}\tag{4.13}$$

We observe that the right–hand side of (4.13) includes ϑ' which is not present on the left–hand side. To deal with this term we employ the ideas from [27, 26], in that we seek to strengthen the norm on the left–hand side of (4.12) via an inf-sup condition argument. To that end, in line with the proof of [26, Theorem 4.5] (cf. also, [82]), we set

$$\mathtt{v}=\tilde{\lambda}\vartheta',\quad \text{where } \tilde{\lambda}|_{\mathcal{I}_n}:=\tilde{\gamma}\frac{k_n}{r_n^2}\quad n=1,\ldots,N,$$

for some $\tilde{\gamma} > 0$ constant (to be defined precisely below) in (4.6), to arrive at

$$\begin{aligned}
&\int_0^{t_n} \tilde{\lambda}\|\vartheta'\|_{\mathcal{H}}^2 + \tilde{\lambda}a(\vartheta,\vartheta')\,\mathrm{d}t - \sum_{j=2}^{n} \tilde{\lambda}([U]_{j-1},(\vartheta')_{j-1}^{+})_{\mathcal{H}} + \tilde{\lambda}(\vartheta_0^{+},(\vartheta')_0^{+})_{\mathcal{H}} \\
&= \int_0^{t_n} \tilde{\lambda}(f(u)-\Pi f(U),\vartheta')_{\mathcal{H}}\,\mathrm{d}t - \int_0^{t_n} \tilde{\lambda}\Big((p',\vartheta')_{\mathcal{H}} + a(p,\vartheta')\Big)\,\mathrm{d}t \\
&\quad - \tilde{\lambda}(p(0),(\vartheta')_0^{+})_{\mathcal{H}}.
\end{aligned} \tag{4.14}$$

For $t \in \mathcal{I}_j$, standard inverse estimates with respect to the time variable imply, respectively,

$$\tilde{\lambda}a(\vartheta,\vartheta') \le \tilde{\lambda}C_{\mathrm{cont}}\|\vartheta\|_{\mathcal{V}}\|\vartheta'\|_{\mathcal{V}} \le \tilde{\gamma}CC_{\mathrm{cont}}\|\vartheta\|_{\mathcal{V}}^2,$$

and

$$\begin{aligned}
\tilde{\lambda}([U]_{j-1},(\vartheta')_{j-1}^{+})_{\mathcal{H}} &\le \tilde{\lambda}\|[U]_{j-1}\|_{\mathcal{H}}\|(\vartheta')_{j-1}^{+}\|_{\mathcal{H}} \\
&\le C\tilde{\lambda}\frac{r_j}{\sqrt{k_j}}\|[U]_{j-1}\|_{\mathcal{H}}\Big(\int_{\mathcal{I}_j}\|\vartheta'\|_{\mathcal{H}}^2\,\mathrm{d}t\Big)^{\frac{1}{2}} \\
&\le C\tilde{\gamma}\|[U]_{j-1}\|_{\mathcal{H}}^2 + \frac{1}{4}\int_{\mathcal{I}_j}\tilde{\lambda}\|\vartheta'\|_{\mathcal{H}}^2\,\mathrm{d}t,
\end{aligned}$$

which, upon summation for $j = 2,\dots,n$ gives

$$\begin{aligned}
\sum_{j=2}^{n}\tilde{\lambda}([U]_{j-1},(\vartheta')_{j-1}^{+})_{\mathcal{H}} &\le \tilde{\lambda}\|[U]_{j-1}\|_{\mathcal{H}}\|(\vartheta')_{j-1}^{+}\|_{\mathcal{H}} \\
&\le C\tilde{\lambda}\frac{r_j}{\sqrt{k_j}}\|[U]_{j-1}\|_{\mathcal{H}}\Big(\int_{\mathcal{I}_j}\|\vartheta'\|_{\mathcal{H}}^2\,\mathrm{d}t\Big)^{\frac{1}{2}} \\
&\le C\tilde{\gamma}\sum_{j=2}^{n}\|[U]_{j-1}\|_{\mathcal{H}}^2 + \frac{1}{4}\int_0^{t_n}\tilde{\lambda}\|\vartheta'\|_{\mathcal{H}}^2\,\mathrm{d}t.
\end{aligned}$$

Similarly, for $w \in \{p(0),\vartheta_0^{+}\}$,we also have

$$\tilde{\lambda}(w,(\vartheta')_0^{+})_{\mathcal{H}} \le C\tilde{\lambda}\frac{r_1}{\sqrt{k_1}}\|w\|_{\mathcal{H}}\Big(\int_{I_1}\|\vartheta'\|_{\mathcal{H}}^2\,\mathrm{d}t\Big)^{\frac{1}{2}} \le C\tilde{\gamma}\|w\|_{\mathcal{H}}^2 + \frac{1}{8}\int_{I_1}\tilde{\lambda}\|\vartheta'\|_{\mathcal{H}}^2\,\mathrm{d}t.$$

Also, from (4.9) with ϑ replaced by $\vartheta' \in \mathcal{X}(\mathcal{V}_h)$, we have

$$\int_0^{t_n}\tilde{\lambda}a(p,\vartheta')\,\mathrm{d}t = 0,$$

since $\tilde{\lambda}$ is constant on each $\mathcal{I}_j$.

Using the above estimates, along with standard arguments such as Cauchy-Schwarz and Young inequalities into (4.14), we arrive at the bound

$$\begin{aligned}\frac{1}{4}\int_0^{t_n}\tilde{\lambda}\|\vartheta'\|_{\mathcal{H}}^2\,\mathrm{d}t \leq C\tilde{\gamma}\sum_{j=2}^{n}\|[U]_{j-1}\|_{\mathcal{H}}^2 + C\tilde{\gamma}\|\vartheta_0^+\|_{\mathcal{H}}^2 + C\tilde{\gamma}\|p(0)\|_{\mathcal{H}}^2 \\ + CC_{\mathrm{cont}}\tilde{\gamma}\int_0^{t_n}\|\vartheta\|_{\mathcal{V}}^2\,\mathrm{d}t \\ + \int_0^{t_n}2\tilde{\lambda}\Big(\|f(u)-\Pi f(U)\|_{\mathcal{H}}^2 + \|p'\|_{\mathcal{H}}^2\Big)\,\mathrm{d}t.\end{aligned} \tag{4.15}$$

Using (4.15) to bound the third term on the right-hand side of (4.13), along with the bound

$$\sum_{j=2}^{n}\|[U]_{j-1}\|_{\mathcal{H}}^2 \leq \sum_{j=2}^{n}\|[\vartheta]_{j-1}\|_{\mathcal{H}}^2 + \sum_{j=2}^{n}\|[\mathrm{P}u]_{j-1}\|_{\mathcal{H}}^2,$$

(arising from the identity $-[U]_{j-1} = [\vartheta]_{j-1} - [\mathrm{P}u]_{j-1}$,) results in (4.13) giving

$$\begin{aligned}&\frac{1}{4}\|\vartheta_n^-\|_{\mathcal{H}}^2 + \frac{1}{8}\sum_{j=2}^{n}\|[U]_{j-1}\|_{\mathcal{H}}^2 + \frac{1}{2}\|\vartheta_0^+\|_{\mathcal{H}}^2 + \frac{C_{\mathrm{coer}}}{4}\int_0^{t_n}\|\vartheta\|_{\mathcal{V}}^2\,\mathrm{d}t \\ &\leq \frac{2}{C_{\mathrm{coer}}}\int_0^{t_n}\|f(u)-\Pi f(U)\|_{\mathcal{V}^*}^2\,\mathrm{d}t + \int_0^{t_n}\tilde{\lambda}^{-1}\|p\|_{\mathcal{H}}^2\,\mathrm{d}t \\ &\quad + 2\sum_{j=1}^{n}\|p(t_j^-)\|_{\mathcal{H}}^2 + C\tilde{\gamma}\sum_{j=2}^{n}\|[U]_{j-1}\|_{\mathcal{H}}^2 + C\tilde{\gamma}\|\vartheta_0^+\|_{\mathcal{H}}^2 + C\tilde{\gamma}\|p(0)\|_{\mathcal{H}}^2 \\ &\quad + CC_{\mathrm{cont}}\tilde{\gamma}\int_0^{t_n}\|\vartheta\|_{\mathcal{V}}^2\,\mathrm{d}t + \frac{1}{4}\sum_{j=2}^{n}\|[\mathrm{P}u]_{j-1}\|_{\mathcal{H}}^2 \\ &\quad + \int_0^{t_n}2\tilde{\lambda}\Big(\|f(u)-\Pi f(U)\|_{\mathcal{H}}^2 + \|p'\|_{\mathcal{H}}^2\Big)\,\mathrm{d}t.\end{aligned} \tag{4.16}$$

Upon selecting now $\tilde{\gamma} > 0$ small enough so that $C\tilde{\gamma} \leq 1/32$ and $CC_{\mathrm{cont}}\tilde{\gamma} \leq C_{\mathrm{coer}}/16$, (4.16) finally implies

$$\begin{aligned}&\frac{1}{4}\|\vartheta_n^-\|_{\mathcal{H}}^2 + \frac{1}{16}\sum_{j=2}^{n}\|[U]_{j-1}\|_{\mathcal{H}}^2 + \frac{1}{16}\|\vartheta_0^+\|_{\mathcal{H}}^2 + \frac{C_{\mathrm{coer}}}{8}\int_0^{t_n}\|\vartheta\|_{\mathcal{V}}^2\,\mathrm{d}t \\ &\leq \frac{2}{C_{\mathrm{coer}}}\int_0^{t_n}\|f(u)-\Pi f(U)\|_{\mathcal{V}^*}^2\,\mathrm{d}t + \int_0^{t_n}\tilde{\lambda}^{-1}\|p\|_{\mathcal{H}}^2\,\mathrm{d}t \\ &\quad + 2\sum_{j=1}^{n}\|p(t_j^-)\|_{\mathcal{H}}^2 + C\tilde{\gamma}\|p(0)\|_{\mathcal{H}}^2 + \frac{1}{4}\sum_{j=2}^{n}\|[\mathrm{P}u]_{j-1}\|_{\mathcal{H}}^2 \\ &\quad + \int_0^{t_n}2\tilde{\lambda}\Big(\|f(u)-\Pi f(U)\|_{\mathcal{H}}^2 + \|p'\|_{\mathcal{H}}^2\Big)\,\mathrm{d}t.\end{aligned} \tag{4.17}$$

To simplify matters, we postulate the validity of a Poincaré–Friedrichs inequality between $\mathcal{H}$ and $\mathcal{V}$; this is, of course, the case in the canonical pairs we have in

mind, such at $\mathcal{H} = L_2(\Omega)$ and $\mathcal{V} = H_0^1(\Omega)$.

Assumption 4.3. There exists positive constant C_{PF}, such that $\|v\|_{\mathcal{H}}^2 \leq C_{PF}\|v\|_{\mathcal{V}}^2$ for all $v \in \mathcal{V}$.

Hence, the above assumption leads to the inequality $\|v\|_{\mathcal{V}^*}^2 \leq C_{PF}\|v\|_{\mathcal{H}}^2$.

Using the last estimate, (4.17) then implies

$$\begin{aligned} &\|\vartheta_n^-\|_{\mathcal{H}}^2 + \sum_{j=2}^{n} \|[U]_{j-1}\|_{\mathcal{H}}^2 + \|\vartheta_0^+\|_{\mathcal{H}}^2 + C_{\text{coer}} \int_0^{t_n} \|\vartheta\|_{\mathcal{V}}^2 \,\mathrm{d}t \\ &\leq C \int_0^{t_n} \|f(u) - \Pi f(U)\|_{\mathcal{H}}^2 \,\mathrm{d}t + \frac{1}{2}\mathcal{E}_n(u) \\ &\leq C \int_0^{t_n} \|\Pi(f(u) - f(U))\|_{\mathcal{H}}^2 \,\mathrm{d}t + \mathcal{E}_n(u), \end{aligned} \tag{4.18}$$

where

$$\begin{aligned} \mathcal{E}_n(u) := C \int_0^{t_n} \|f(u) - \Pi f(u)\|_{\mathcal{H}}^2 \,\mathrm{d}t + \int_0^{t_n} 2\tilde{\lambda}^{-1}\|p\|_{\mathcal{H}}^2 + 4\tilde{\lambda}\|p'\|_{\mathcal{H}}^2 \,\mathrm{d}t \\ + 4\sum_{j=1}^{n} \|p(t_j^-)\|_{\mathcal{H}}^2 + C\tilde{\gamma}\|p(0)\|_{\mathcal{H}}^2 + \frac{1}{2}\sum_{j=2}^{n} \|[\mathrm{P}u]_{j-1}\|_{\mathcal{H}}^2. \end{aligned}$$

Adding now four times (4.15) to (4.24) aiming to include the left–hand side of (4.15) into the estimation and recalling that $\tilde{\gamma}$ is chosen small enough, we arrive at

$$\begin{aligned} &\|\vartheta_n^-\|_{\mathcal{H}}^2 + \frac{1}{4}\sum_{j=2}^{n} \|[U]_{j-1}\|_{\mathcal{H}}^2 + \frac{1}{4}\|\vartheta_0^+\|_{\mathcal{H}}^2 + \frac{C_{\text{coer}}}{4} \int_0^{t_n} \|\vartheta\|_{\mathcal{V}}^2 \,\mathrm{d}t + \int_0^{t_n} \tilde{\lambda}\|\vartheta'\|_{\mathcal{H}}^2 \,\mathrm{d}t \\ &\leq C \int_0^{t_n} \|\Pi(f(u) - f(U))\|_{\mathcal{H}}^2 \,\mathrm{d}t + 2\mathcal{E}_n(u), \end{aligned} \tag{4.19}$$

or, dropping the constants

$$\begin{aligned} &\|\vartheta_n^-\|_{\mathcal{H}}^2 + \sum_{j=2}^{n} \|[U]_{j-1}\|_{\mathcal{H}}^2 + \|\vartheta_0^+\|_{\mathcal{H}}^2 + C_{\text{coer}} \int_0^{t_n} \|\vartheta\|_{\mathcal{V}}^2 \,\mathrm{d}t + \int_0^{t_n} \tilde{\lambda}\|\vartheta'\|_{\mathcal{H}}^2 \,\mathrm{d}t \\ &\leq C \int_0^{t_n} \|\Pi(f(u) - f(U))\|_{\mathcal{H}}^2 \,\mathrm{d}t + 8\mathcal{E}_n(u). \end{aligned} \tag{4.20}$$

4.2.2 Completing the bound

Now, [52, Lemma 4.3] ensures us that

$$\|f(u)-\Pi f(u)\|_{L_\infty(\mathcal{I}_n;\mathcal{H})} \leq C \max_{n-\jmath-\mu\leq\ell\leq n-\jmath} \min_{s\leq r_n+1} k_\ell^s \|D^{(s)} f(u)\|_{L_\infty(\mathcal{I}_n;\mathcal{H})}, \tag{4.21}$$

i.e., we have optimal convergence with respect to the maximum timestep locally. Also, recalling the uniform stability of the Lagrangian interpolation basis functions used in the construction of Π from the proof of [52, Lemma 4.1], viz.,

$$|\xi_\eta(t)| \leq C,$$

for C independent of the local timestep (the validity of this estimate can be shown upon observing that the support of $\xi_\eta(t)$ grows proportionally with the polynomial degree), we deduce

$$\int_0^{t_n} \|\Pi(f(u)-f(U))\|_{\mathcal{H}}^2 \,\mathrm{d}t \leq C \sum_{m=1}^{n} \sum_{\eta=m-\jmath-\mu}^{m-\jmath} \max_{n-\jmath-\mu\leq\eta\leq n-\jmath} k_\eta \|f(u(t_\eta))-f(U_\eta)\|_{\mathcal{H}}^2. \tag{4.22}$$

Remark 4.4. Despite our effort in being explicit with respect to the local polynomial degree in the time variable in this *a priori* error analysis, we are not aware of the mode of dependence of the constants C in (4.21) and (4.22). We do expect, however, that they decrease as the local polynomial degree increases.

Now, upon identifying $f:\mathbb{R}\to\mathbb{R}$ with a function $f:\mathcal{H}\to\mathcal{H}$ by $f(v(t,x)) := (f(v(t)))(x)$ with x being the spatial variable, we also consider $f^L:\mathcal{H}\to\mathcal{H}$ satisfying

$$\|f^L(w)-f^L(v)\|_{\mathcal{H}} \leq C_L \|w-v\|_{\mathcal{H}}, \tag{4.23}$$

i.e., a globally Lipschitz function, such that we have $f(v)=f^L(v)$, for all $v\in\mathcal{H}$ with $\|v\|_{\mathcal{H}} \leq L := 2\max_{0\leq t\leq T}\|u(t)\|_{\mathcal{H}}$. This implies, in particular, that $f^L(u)=f(u)$. Upon replacing f by f^L on the numerical method (2.23), we denote the resulting numerical solution by $U^L\in\mathcal{X}_{\mathbf{r}}(\mathcal{V}_h)$. Therefore, (4.24) and (4.22) hold

with U replaced by U^L and $f(U)$ replaced by $f^L(U^L)$, giving

$$\begin{aligned}&\|(\vartheta^L)_n^-\|_{\mathcal{H}}^2+\sum_{j=2}^n\|[U^L]_{j-1}\|_{\mathcal{H}}^2+\|(\vartheta^L)_0^+\|_{\mathcal{H}}^2+\int_0^{t_n}C_{\mathrm{coer}}\|\vartheta^L\|_{\mathcal{V}}^2+\tilde{\lambda}\|(\vartheta^L)'\|_{\mathcal{H}}^2\,\mathrm{d}t\\&\leq C\sum_{m=1}^n\tilde{k}_m\|f(u(t_m))-f^L(U_m^L)\|_{\mathcal{H}}^2+8\mathcal{E}_n(u),\end{aligned}\tag{4.24}$$

where we have introduced the notation $\tilde{k}_m := \mu\max_{n-\jmath-\mu\leq\eta\leq n-\jmath}k_\eta$ and $\vartheta^L := \mathrm{P}u-U^L$. Due to (4.23), the first term on the right–hand side of (4.24) can, therefore, be further estimated as follows:

$$\|f(u(t_m))-f^L(U_m^L)\|_{\mathcal{H}}\leq C_L\|u(t_m)-U_m^L\|_{\mathcal{H}}\leq C_L\|p(t_m)\|_{\mathcal{H}}+C_L\|\vartheta_m^L\|_{\mathcal{H}},$$

which, in conjunction with (4.24) yields

$$\begin{aligned}&\|(\vartheta^L)_n^-\|_{\mathcal{H}}^2+\sum_{j=2}^n\|[U^L]_{j-1}\|_{\mathcal{H}}^2+\|(\vartheta^L)_0^+\|_{\mathcal{H}}^2+\int_0^{t_n}C_{\mathrm{coer}}\|\vartheta^L\|_{\mathcal{V}}^2+\tilde{\lambda}\|(\vartheta^L)'\|_{\mathcal{H}}^2\,\mathrm{d}t\\&\leq CC_L\sum_{m=1}^n\tilde{k}_m\|\vartheta_m^L\|_{\mathcal{H}}^2,+2C_L\sum_{m=1}^n\|p(t_m)\|_{\mathcal{H}}^2+8\mathcal{E}_n(u).\end{aligned}\tag{4.25}$$

This, upon further assuming that there exists a constant $c_{\mathrm{quas}}>0$ such that

$$\tilde{k}_m\leq c_{\mathrm{quas}}\min\{r_m,m\}k_m,\qquad\text{for all } m\in\{1,\ldots,N\},\tag{4.26}$$

uniformly, in conjunction with the discrete version of the Grönwall inequality, gives

$$\begin{aligned}&\|(\vartheta^L)_n^-\|_{\mathcal{H}}^2+\sum_{j=2}^n\|[U^L]_{j-1}\|_{\mathcal{H}}^2+\|(\vartheta^L)_0^+\|_{\mathcal{H}}^2+\int_0^{t_n}C_{\mathrm{coer}}\|\vartheta^L\|_{\mathcal{V}}^2+\tilde{\lambda}\|(\vartheta^L)'\|_{\mathcal{H}}^2\,\mathrm{d}t\\&\leq\ \exp(CC_Lr_{\max})\Big(2C_L\sum_{m=1}^n\|p(t_m)\|_{\mathcal{H}}^2+8\mathcal{E}_n(u)\Big)=:\mathcal{E}_n^{\max}(u),\end{aligned}\tag{4.27}$$

with $r_{\max}:=\max\{\max_{1\leq n\leq N}r_n,N\}$.

Now, using standard approximation estimates (*hp*–version approximation estimates) we can see that the right-hand side of (4.27) decays to zero, as the maximum timestep and the maximum diameter of the spatial elements converge to zero and/or as the respective temporal and spatial polynomial degrees in the space-time method increase. Assuming, however, for the moment that this is, indeed, the case,

we aim to prove that $U^L = U$. Hence, we want to show that

$$\max_{0\leq t\leq T} \|U^L(t)\|_{\mathcal{H}} \leq L, \tag{4.28}$$

because this would mean that $f^L(U^L) = f(U^L)$ and, thus (4.22) is valid with f (as per original method), which necessarily implies that $U^L = U$, since they are solutions to the same method. Implicitly, the last statement assumes the uniqueness of the solution of the numerical method (4.22), which we shall assume in the final theorem.

To this end, we have

$$\max_{0\leq t\leq T} \|U^L(t)\|_{\mathcal{H}} \leq \max_{0\leq t\leq T} \|u - U^L(t)\|_{\mathcal{H}} + \max_{0\leq t\leq T} \|u\|_{\mathcal{H}} = \max_{0\leq t\leq T} \|u - U^L(t)\|_{\mathcal{H}} + \frac{L}{2}.$$

Therefore, it is enough to prove that $\max_{0\leq t\leq T} \|u - U^L(t)\|_{\mathcal{H}} \leq L/2$ also. To do so, we employ the triangle inequality and Lemma 4.1 as follows:

$$\begin{aligned}
\max_{0\leq t\leq T} \|u - U^L(t)\|_{\mathcal{H}} \leq & \max_{0\leq t\leq T} \|u - \mathrm{P}u\|_{\mathcal{H}} + \max_{0\leq t\leq T} \|\vartheta^L(t)\|_{\mathcal{H}} \\
\leq & \max_{0\leq t\leq T} \|u - \mathrm{P}u\|_{\mathcal{H}} + \max_{t\in\mathcal{I}_{j^*}} \|\vartheta^L(t)\|_{\mathcal{H}} \\
\leq & \max_{0\leq t\leq T} \|u - \mathrm{P}u\|_{\mathcal{H}} + C\Big(k_{j^*} \int_{\mathcal{I}_{j^*}} \|(\vartheta^L)'\|_{\mathcal{H}}^2 \,\mathrm{d}t \\
& + \|\vartheta_{j^*}^-\|_{\mathcal{H}}^2\Big)^{\frac{1}{2}},
\end{aligned} \tag{4.29}$$

for j^* the index of an interval $\mathcal{I}_{j^*}$ on which the maximum is attained. Therefore, Assumption 4.3 and (4.27) finally give

$$\max_{0\leq t\leq T} \|u - U^L(t)\|_{\mathcal{H}} \leq \max_{0\leq t\leq T} \|u - \mathrm{P}u\|_{\mathcal{H}} + r_{\max}\Big(\mathcal{E}_N^{\max}(u)\Big)^{\frac{1}{2}}, \tag{4.30}$$

with $t_N = T$, i.e., the final time. Since the right–hand side of (4.30) can be chosen arbitrarily small by selecting sufficiently small maximum time–steps and spatial meshsizes and/or sufficiently large polynomial degrees with respect to the time and the space discretisations, we can conclude that, for such discretisation parameters the right–hand side of (4.30) is less than or equal to $L/2$. This, as discussed above, in turn yields that (4.28) holds and, therefore, $U^L = U$. Hence, (4.27) holds with

$U^L = U$ and, thus, with $\vartheta^L = \vartheta$, viz.,

$$\|\vartheta_n^-\|_{\mathcal{H}}^2 + \sum_{j=2}^{n} \|[U]_{j-1}\|_{\mathcal{H}}^2 + \|\vartheta_0^+\|_{\mathcal{H}}^2 + \int_0^{t_n} C_{\mathrm{coer}}\|\vartheta\|_{\mathcal{V}}^2 + \tilde{\lambda}\|\vartheta'\|_{\mathcal{H}}^2 \,\mathrm{d}t \leq \mathcal{E}_n^{\max}(u). \quad (4.31)$$

Therefore, we have already proven the following result.

Theorem 4.5. *With the above assumptions, for sufficiently small spatial and temporal meshsizes and/or sufficiently large polynomial degrees so that*

$$\max_{0\leq t\leq T} \|u - \mathrm{P}u\|_{\mathcal{H}} + r_{\max}\Big(\mathcal{E}_n^{\max}(u)\Big)^{\frac{1}{2}} \leq \|u\|_{L_\infty(0,t_n;\mathcal{H})},$$

the following bounds hold

$$\begin{aligned} &\|u(t_n) - U_n^-\|_{\mathcal{H}}^2 + \sum_{j=2}^{n} \|[U]_{j-1}\|_{\mathcal{H}}^2 + \|u(0) - U_0^+\|_{\mathcal{H}}^2 \\ &\quad + C_{\mathrm{coer}} \int_0^{t_n} \|u - U\|_{\mathcal{V}}^2 \,\mathrm{d}t + \tilde{\lambda}\|(u-U)'\|_{\mathcal{H}}^2 \,\mathrm{d}t \\ &\leq \mathcal{E}_n^{\max}(u) + C_{\mathrm{coer}} \int_0^{t_n} \|u - \mathrm{P}u\|_{\mathcal{V}}^2 \,\mathrm{d}t, \end{aligned} \quad (4.32)$$

and

$$\|u(t_n) - U_n^-\|_{\mathcal{H}}^2 + \sum_{j=2}^{n} \|[U]_{j-1}\|_{\mathcal{H}}^2 + \|u(0) - U_0^+\|_{\mathcal{H}}^2 + \tilde{\lambda}\|(u-U)'\|_{\mathcal{H}}^2 \,\mathrm{d}t \leq \mathcal{E}_n^{\max}(u). \quad (4.33)$$

Proof. The proof follows immediately by the triangle inequality. □

Going back to the growth assumption (2.14) for the nonlinear reaction f, upon assuming that both u and U are bounded in $L_\infty(\mathcal{I};\mathcal{V})$, with the latter independent from the mesh parameters, we can conclude that f satisfies a local Lipschitz condition of the form

$$\|f(u) - f(U)\|_{\mathcal{H}} \leq C(u,U)\|u - U\|_{\mathcal{H}},$$

for which we can conclude (4.23) needed for the proof of the above *a priori* bounds.

We finally remark on the optimality of the above *a priori* error bounds. The use of the elliptic projection in conjunction with the L_2-projection in the time variable

will lead to optimal *a priori* error bounds in the $L_2(H^1)$-norm. As we shall see, however, the respective *a priori* bounds in the $L_\infty(L_2)$–norm error are slightly suboptimal by half an order of k_n, due to the presence of the term

$$\sum_{j=1}^{n} \|p(t_j^-)\|_{\mathcal{H}}^2$$

in $\mathcal{E}_n^{\max}(u)$. We shall comment further on this point further below.

We are now in a position to finalise the *a priori* error analysis.

4.2.3 *A priori* error bounds

We are now ready to complete the *a priori* error analysis.

Theorem 4.6 ($L_\infty(\mathcal{I};\mathcal{H})$–norm estimate)**.** *Assuming the validity of estimate* (4.22) *and of Assumption 4.2, (or, in the special case of $\mathcal{H} = L_2(\Omega)$, assuming the hypotheses of Theorem 4.5 and Lemma 4.1, respectively) and assuming the regularity $u^{(\eta)}|_{\mathcal{I}_n} \in L_2(\mathcal{I}_n;\mathcal{H})$ and $u|_{\mathcal{I}_n} \in H^{\kappa_n}(\mathcal{I}_n;\mathcal{H})$ for some $\eta \geq 2$ and $\kappa_n \geq 2$, for each $n = 1, \ldots, N$. Then, for $n = 1, ..., N$, we have the* a priori *error bound*

$$\|u-U\|_{L_\infty(0,t_n;\mathcal{H})}^2 \leq C \sum_{j=1}^{n} \Big(\frac{k_j^{2s_j+1}}{r_j^{2s_j}} \|u^{(s_j)}\|_{L_2(\mathcal{I}_j;\mathcal{H})}^2 + \frac{r_j^2}{k_j} h^{2t+2} \|\nabla^{(t)} u\|_{L_2(\mathcal{I}_j;\mathcal{H})}^2 \Big), \tag{4.34}$$

for every $1 \leq s_j \leq \min\{r_j, \kappa_j\}$ and $1 \leq t \leq \min\{r_s, \eta\}$, where r_s denotes the polynomial degree of the space discretisation.

Proof. In view of Assumption 4.2 (or of Lemma 4.1), along with (4.33), we have

$$\begin{aligned} \|u-U\|_{L_\infty(\mathcal{I}_n;\mathcal{H})}^2 &\leq C\Big(k_n \int_{\mathcal{I}_n} \|(u-U)'(t)\|_{\mathcal{H}}^2 \,\mathrm{d}t + \|(u-U)(t_n^-)\|_{\mathcal{H}}^2 \Big) \\ &\leq C r_{\max} \mathcal{E}_n^{\max}(u). \end{aligned} \tag{4.35}$$

We now estimate the right–hand side of the last bound via the use of standard *hp*–version approximation results. From *hp*-version approximation estimates for

the L_2-projection π^n, see, e.g., [**?**], we have on each $\mathcal{I}_n$:

$$\begin{aligned}\int_{\mathcal{I}_n} \tilde{\lambda}^{-1}\|p\|_{\mathcal{H}}^2 \,\mathrm{d}t &\leq 2\int_{\mathcal{I}_n} \tilde{\lambda}^{-1}\|u-\pi^n u\|_{\mathcal{H}}^2 \,\mathrm{d}t + \int_{\mathcal{I}_n} \tilde{\lambda}^{-1}\|\pi^n(u-P_h u)\|_{\mathcal{H}}^2 \,\mathrm{d}t \\ &\leq C\frac{k_n^{2s+1}}{r_n^{2s}}\|u^{(s)}\|_{L_2(\mathcal{I}_n;\mathcal{H})}^2 + C\frac{r_n^2}{k_n}h^{2t+2}\|\nabla^{(t)}u\|_{L_2(\mathcal{I}_n;\mathcal{H})}^2,\end{aligned}$$

for some $0 \leq s \leq \min\{r_n, \kappa\}$ and $0 \leq t \leq \min\{r_s, \eta\}$, where r_s denotes the polynomial degree of the space discretisation. Working analogously and using a standard inverse estimate, we also have

$$\begin{aligned}\int_{\mathcal{I}_n} \tilde{\lambda}\|p'\|_{\mathcal{H}}^2 \,\mathrm{d}t &\leq 2\int_{\mathcal{I}_n} \tilde{\lambda}\|(u-\pi^n u)'\|_{\mathcal{H}}^2 \,\mathrm{d}t + 2\int_{\mathcal{I}_n} \tilde{\lambda}\|(\pi^n(u-P_h u))'\|_{\mathcal{H}}^2 \,\mathrm{d}t \\ &\leq 2\int_{\mathcal{I}_n} \tilde{\lambda}\|(u-\pi^n u)'\|_{\mathcal{H}}^2 \,\mathrm{d}t + C\int_{\mathcal{I}_n} \|\pi^n(u-P_h u)\|_{\mathcal{H}}^2 \,\mathrm{d}t \\ &\leq C\frac{k_n^{2s+1}}{r_n^{2s+2}}\|u^{(s)}\|_{L_2(\mathcal{I}_n;\mathcal{H})}^2 + Ch^{2t+2}\|\nabla^{(t)}u\|_{L_2(\mathcal{I}_n;\mathcal{H})}^2,\end{aligned}$$

for $1 \leq s \leq \min\{r_n, \kappa\}$ and $0 \leq t \leq \min\{r_s, \eta\}$. Further, using the trace–inverse estimate, and approximation estimates from the boundary to $\mathcal{I}_n$, see, e.g., [56], we have

$$\begin{aligned}\|p(t_n^-)\|_{\mathcal{H}}^2 &\leq 2\|u(t_n)-\pi^n u(t_n^-)\|_{\mathcal{H}}^2 + 2\|\pi^n(u-P_h u)(t_n^-))\|_{\mathcal{H}}^2 \\ &\leq 2\|u(t_n)-\pi^n u(t_n^-)\|_{\mathcal{H}}^2 + C\frac{r_n^2}{k_n}\int_{\mathcal{I}_n} \|\pi^n(u-P_h u))\|_{\mathcal{H}}^2 \,\mathrm{d}t \\ &\leq 2\|u(t_n)-\pi^n u(t_n^-)\|_{\mathcal{H}}^2 + C\frac{r_n^2}{k_n}\int_{\mathcal{I}_n} \|u-P_h u\|_{\mathcal{H}}^2 \,\mathrm{d}t \\ &\leq C\frac{k_n^{2s+1}}{r_n^{2s}}\|u^{(s)}\|_{L_2(\mathcal{I}_n;\mathcal{H})}^2 + C\frac{r_n^2}{k_n}h^{2t+2}\|\nabla^{(t)}u\|_{L_2(\mathcal{I}_n;\mathcal{H})}^2,\end{aligned}$$

and, completely analogously for $\|p(0)\|_{\mathcal{H}}^2$, giving

$$\|p(0)\|_{\mathcal{H}}^2 \leq C\frac{k_1^{2s+1}}{r_1^{2s}}\|u^{(s)}\|_{L_2(\mathcal{I}_1;\mathcal{H})}^2 + C\frac{r_1^2}{k_n}h^{2t+2}\|\nabla^{(t)}u\|_{L_2(\mathcal{I}_1;\mathcal{H})}^2.$$

Finally, the trace inequality and working as above implies

$$\begin{aligned}\sum_{j=2}^{n}\|[\mathrm{P}u]_{j-1}\|_{\mathcal{H}}^2 &= \|[u-\mathrm{P}u]_{j-1}\|_{\mathcal{H}}^2\\ &\le 2\sum_{j=2}^{n}\Big(\|(u-\mathrm{P}u)(t_{j-1}^-)\|_{\mathcal{H}}^2+\|(u-\mathrm{P}u)(t_{j-1}^+)\|_{\mathcal{H}}^2\Big)\\ &= 2\sum_{j=2}^{n}\Big(\|p(t_{j-1}^-)\|_{\mathcal{H}}^2+\|p(t_{j-1}^+)\|_{\mathcal{H}}^2\Big)\\ &\le C\sum_{j=1}^{n}\Big(\frac{k_j^{2s+1}}{r_j^{2s}}\|u^{(s)}\|_{L_2(\mathcal{I}_j;\mathcal{H})}^2+\frac{r_j^2}{k_j}h^{2t+2}\|\nabla^{(t)}u\|_{L_2(\mathcal{I}_j;\mathcal{H})}^2\Big).\end{aligned}$$

Combining the above, the result already follows. □

Similarly, we have an *a priori* bound in the $L_2(\mathcal{I},\mathcal{V})$–norm.

Theorem 4.7 ($L_2(\mathcal{I};\mathcal{V})$–norm estimate)**.** *Assuming the validity of estimate* (4.22)*, (or, in the special case of* $\mathcal{H}=L_2(\Omega)$*, assuming the hypotheses of Theorem 4.5), and assuming the regularity* $\nabla^{(\eta)}u|_{\mathcal{I}_n}\in L_2(\mathcal{I}_n;\mathcal{H})$*,* $\nabla^{(\eta-1)}u|_{\mathcal{I}_n}\in L_2(\mathcal{I}_n;\mathcal{V})$*,* $u|_{\mathcal{I}_n}\in H^{\kappa_n}(\mathcal{I}_n;\mathcal{H})$*, and* $u|_{\mathcal{I}_n}\in H^{\kappa_n-1}(\mathcal{I}_n;\mathcal{V})$*, for some* $\eta\ge 2$ *and* $\kappa_n\ge 2$*, for each* $n=1,\dots,N$*. Then, for* $n=1,...,N$*, we have the* a priori *error bound*

$$\|u-U\|_{L_2(0,t_n;\mathcal{V})}^2\le C\sum_{j=1}^{n}\Big(\frac{k_j^{2s_j+1}}{r_j^{2s_j}}\|u^{(s_j)}\|_{L_2(\mathcal{I}_j;\mathcal{H})}^2+\frac{r_j^2}{k_j}h^{2t+2}\|\nabla^{(t)}u\|_{L_2(\mathcal{I}_j;\mathcal{H})}^2\Big),\tag{4.36}$$

for every $1\le s_j\le\min\{r_j,\kappa_j\}$ *and* $1\le t\le\min\{r_s,\eta\}$*.*

Proof. The proof follows as the respective one in the previous theorem with the addition of estimating the term

$$\begin{aligned}\int_{\mathcal{I}_n}\|u-\mathrm{P}u\|_{\mathcal{V}}^2\,\mathrm{d}t &\le 2\int_{\mathcal{I}_n}\|u-\pi^n u\|_{\mathcal{V}}^2\,\mathrm{d}t+2\int_{\mathcal{I}_n}\|\pi^n(u-P_hu)\|_{\mathcal{V}}^2\,\mathrm{d}t\\ &\le \frac{k_n^{2s_n}}{r_n^{2s_n}}\|u^{(s_n-1)}\|_{L_2(\mathcal{I}_n;\mathcal{V})}^2+2\int_{\mathcal{I}_n}\|\pi^n(u-P_hu)\|_{\mathcal{V}}^2\,\mathrm{d}t\\ &\le \frac{k_n^{2s_n}}{r_n^{2s_n}}\|u^{(s_n-1)}\|_{L_2(\mathcal{I}_n;\mathcal{V})}^2+Ch^{2t}\|\nabla^{(t-1)}u\|_{L_2(\mathcal{I}_n;\mathcal{V})}^2,\end{aligned}$$

and the proof already follows. □

We remark that the bound in Theorem 4.6 is slightly suboptimal by half an order of k_n with respect to the time discretisation. It is possible to use duality arguments

to recover optimal rate for the case of linear problems [109]. However, this has not been possible to extend in the current nonlinear setting of only locally Lipschitz continuous nonlinearities. Instead, we opted for the "inf-sup"–type argument from [26, 27] which is more general but delivers this slightly suboptimal rate.

4.3 Numerical examples

We present a series of numerical experiments to study the asymptotic convergence behaviour of the dG time–stepping methods with continuous finite elements in space i.e. dG(r)–cG(p). We report the experimental order of convergence (EOC) relative to the last computed quantities in all figures as an indication of the asymptotic rate of convergence. In all cases, $\mathcal{A} = \Delta$, i.e., the Dirichlet Laplacian, yielding the heat equation with linear source term and $\mathcal{H} = L_2(\Omega)$, $\mathcal{V} = H_0^1(\Omega)$, giving $\mathcal{H}^* = H^{-1}(\Omega)$. The numerical implementation is based on the `deal.II` finite element library [16] and the tests run in the high performance computing facility ALICE at the University of Leicester.

4.3.1 Example 1

We consider the heat equation as a standard example of the linear parabolic problems, where the initial condition and the right hand side function are chosen such that the exact solution is

$$u(x, y, t) = e^{-t}x(1 - x)y(1 - y).$$

We solve the problem on the space–time cylinder $\mathcal{I} \times \Omega := [0, 1] \times [0, 1]^2$, on a fixed uniform rectangular mesh consisting of 1024 uniform biquadratic elements in space ($p = 2$), with elements of orders $r = 0, 1, 2, 3, 4$ in time. We study the asymptotic behaviour of the error e in $L_2(H^1)$-, $L_2(L_2)$-, $L_\infty(L_2)$-, $L_\infty(L_\infty)$-, and $L_\infty(H^1)$-error norms and also we examine the superconvergence of the $\ell_\infty(L_2)$-error norm at the endpoints of the time intervals by monitoring the evolution of

the experimental order of convergence (EOC) over time on a sequence of uniformly refined meshes in time. In each instance, we fix a constant mesh step size $h = 1/32$ and we also use fixed polynomial degree in space with various polynomial degrees in time (dG(r)-cG(2)), $r = 0, 1, 2, 3, 4$. The resulting errors are plotted against the corresponding time step size k_n. In the Figure 4.1 (a)–(e) below, we notice the optimal order of convergence of the $L_2(H^1)$-, $L_2(L_2)$-, $L_\infty(L_2)$-, $L_\infty(L_\infty)$-, and $L_\infty(H^1)$-error norms, respectively, which is $r + 1$ of the polynomial degrees $r = 0, 1, 2, 3, 4$. Figure 4.1 (f) shows the superconvergence of the $\ell_\infty(L_2)$-error norm at the endpoints of the time intervals. The superconvergence is investigated to show that the method has better convergence properties at the time interval endpoints than within the time interval. The results confirm the theoretical results of Theorems 4.6 and 4.7.

4.3.2 Example 2

We solve in this example the same problem as in Example 4.3.1 on the space–time cylinder $\mathcal{I} \times \Omega := [0, 0.1] \times [0, 1]^2$, on a fixed uniform rectangular mesh consisting of 1024 uniform quartic elements in space ($p = 4$), with elements of orders $r = 0, 1, 2, 3, 4$ in time. We study the asymptotic behaviour of the error e in $L_2(H^1)$-, $L_2(L_2)$-, $L_\infty(L_2)$-, $L_\infty(L_\infty)$-, and $L_\infty(H^1)$-error norms and, also, we examine the superconvergence of the $\ell_\infty(L_2)$-error norm at the endpoints of the time intervals by monitoring the evolution of the experimental order of convergence (EOC) over time on a sequence of uniformly refined meshes in time.

In each instance, we fix a constant mesh step size $h = 1/32$ and we also use fixed polynomial degree in space with various polynomial degrees in time (dG(r)-cG(4)), $r = 0, 1, 2, 3, 4$. The resulting errors are plotted against the corresponding time step size k_n. In the figure (a) below, we notice that all the error norms mentioned above have linear convergence (dG(0)-cG(4), also, we observe that there is no superconvergence in this case (where SCon stands for superconvergence) since dG(0) is equivalent to the backward Euler method. The Figure 4.2 (b)-(e) for the cases dG(r)-cG(4), $r = 1, 2, 3, 4$, respectively, show that the error norms mentioned

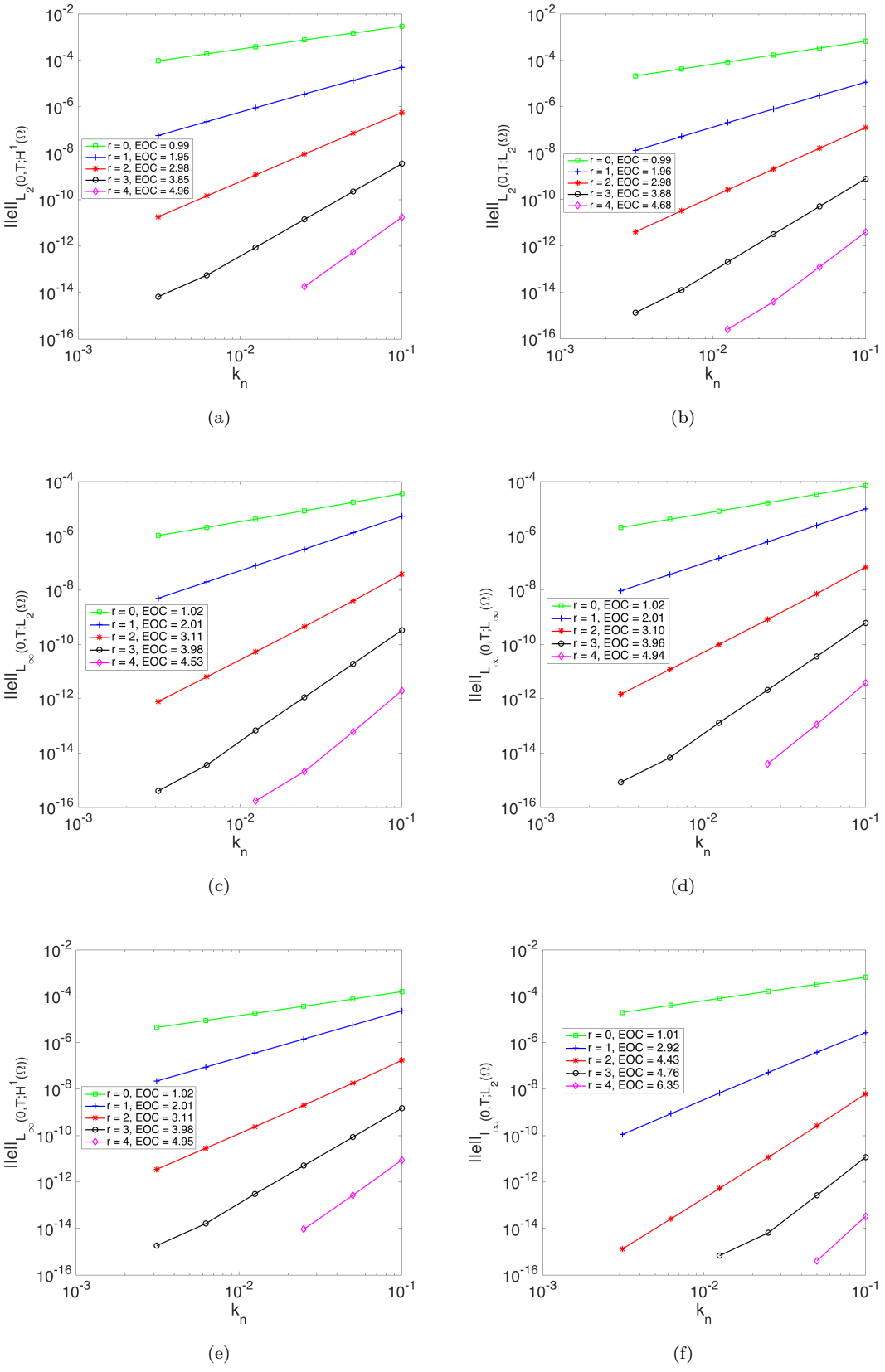

FIGURE 4.1: Example 1: h–version IMEX dG(r)–cG(2) scheme, $r = 0, 1, 2, 3, 4$, for different error norms vs the time steps k_n.

above have optimal order of convergence EOC $\approx r+1$ and superconvergence of the $\ell_\infty(L_2)$-error norm with EOC $\approx r+2$. The results are in agreement with the theoretical results of Theorems 4.6 and 4.7.

4.3.3 Example 3

We solve the same problem as in Example 4.3.1. We consider in this example the p–version IMEX dG time–advancing schemes. We solve the problem on $\mathcal{I}\times\Omega := [0,1]\times[0,1]^2$ on a fixed uniform rectangular mesh consisting of 1024 uniform quartic elements in space ($p=4$), and different time elements of orders $r=0,1,2,3,4$ with fixed time step size $k_n = 0.01$ and space mesh $h = 1/16$.

For the p–version, Figure 4.3 shows the error for the numerical method in the $L_2(H^1)$-, $L_2(L_2)$-, $L_\infty(L_2)$-, and $L_\infty(L_\infty)$-error norms for fixed space–time mesh size under p–refinement. We observe exponential convergence in these error norms since the solution is analytic over the computational domain.

4.3.4 Example 4

We implement in this Example the h–version IMEX dG time—marching schemes of the heat equation with the initial condition and source function are chosen such that the exact solution is

$$u(x,y,t) = e^{-t}\sin(\pi x)\sin(\pi y),$$

on the space–time cylinder $\mathcal{I}\times\Omega := [0,0.1]\times[0,1]^2$, on a fixed uniform rectangular mesh consisting of 1024 uniform quintic elements in space ($p=5$), with uniform quadratic elements in time $r=2$. We study the asymptotic behaviour of the error e in $L_2(H^1)$-, $L_2(L_2)$-, $L_\infty(L_2)$-, $L_\infty(L_\infty)$-, and $L_\infty(H^1)$-error norms and also we we examine the superconvergence of the $\ell_\infty(L_2)$-error norm at the endpoints of the time intervals by monitoring the evolution of the experimental order of convergence (EOC) over time on a sequence of uniformly refined meshes in time.

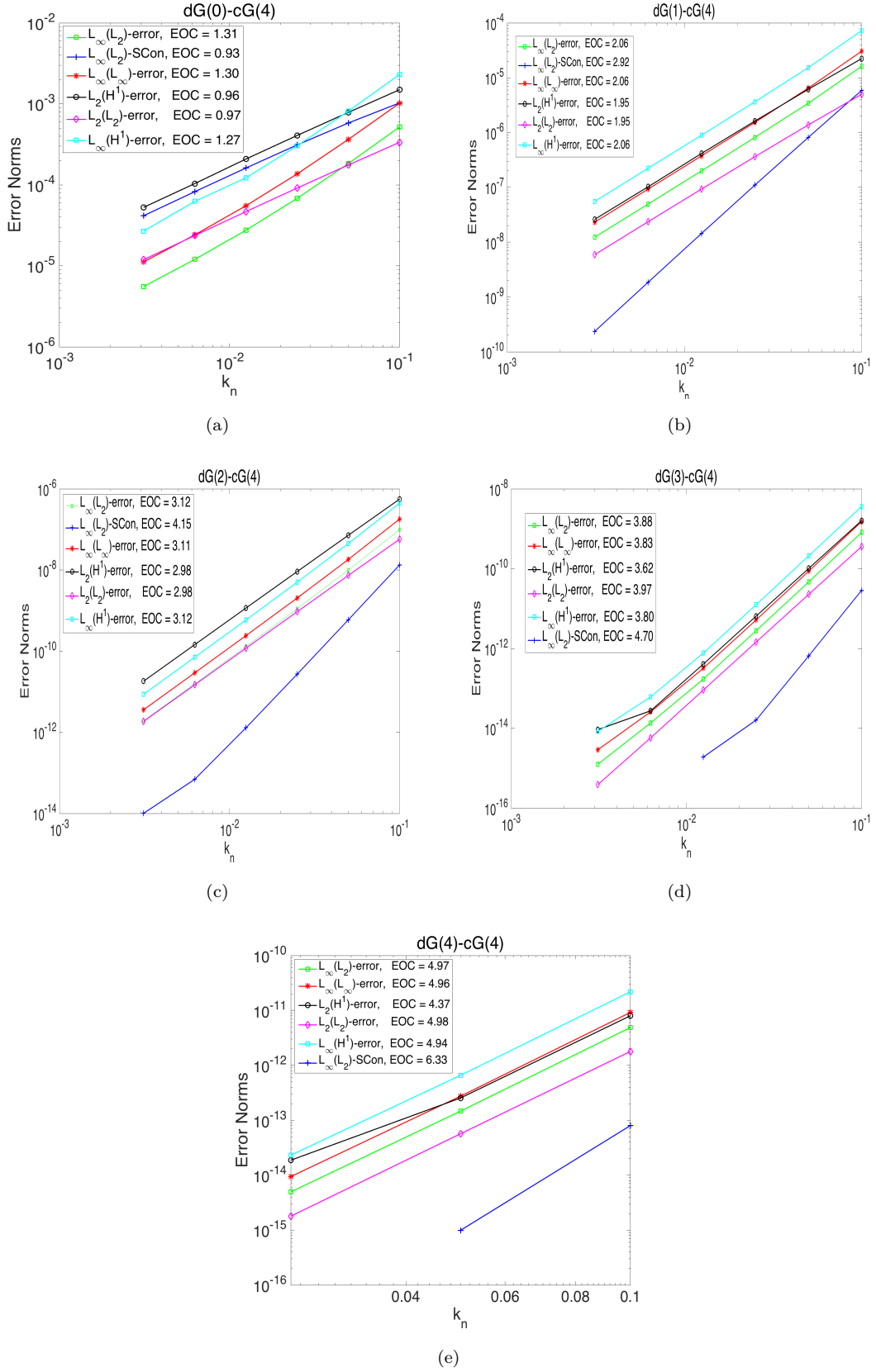

FIGURE 4.2: Example 2: h–version IMEX dG(r)–cG(4), $r = 0, 1, 2, 3, 4$ for different error norms vs the time steps k_n.

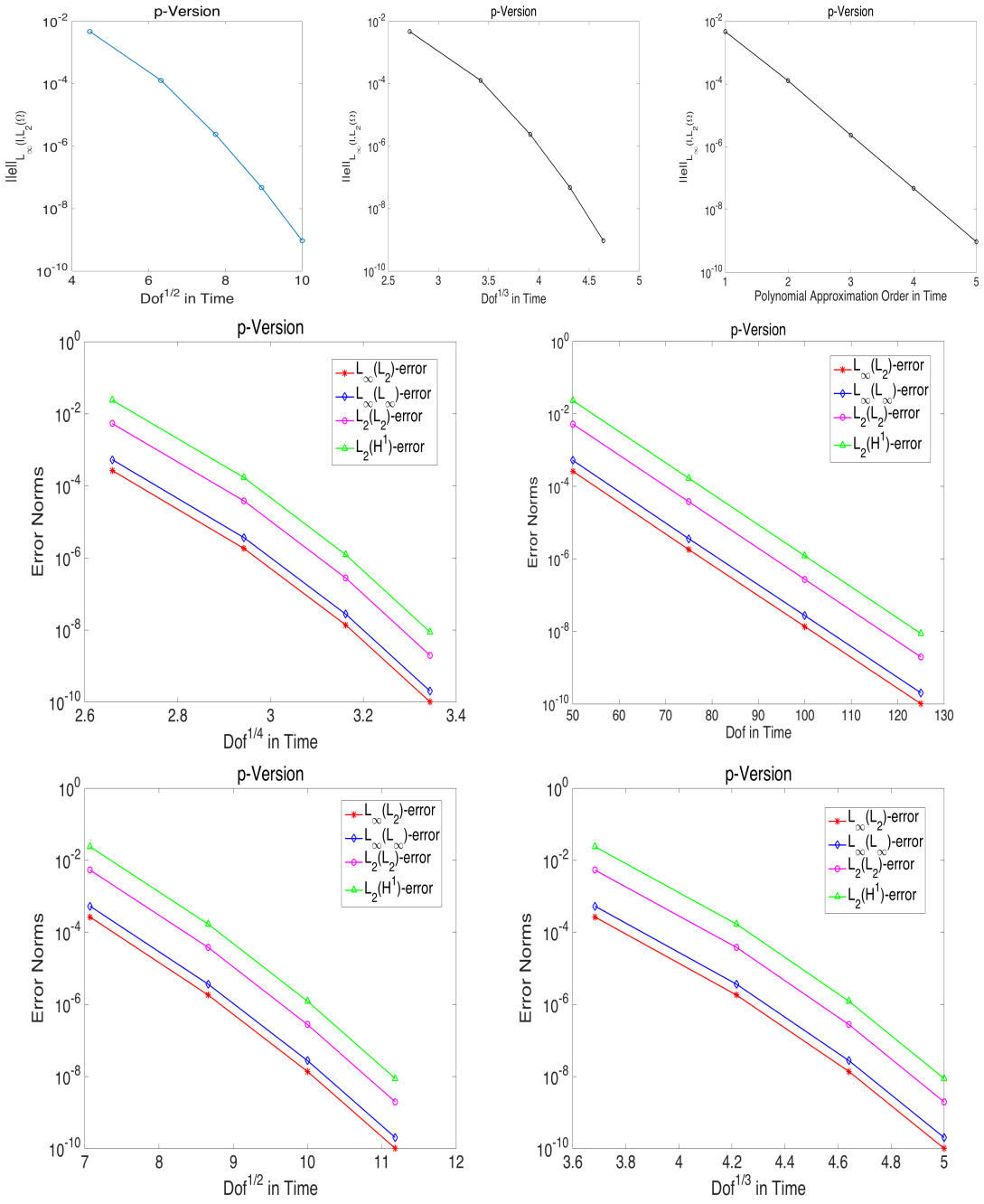

FIGURE 4.3: Example 3: p–version IMEX dG timestepping scheme for $r = 2$ and time step $k_n = 0.01$, for different error norms.

In each instance, we fix a constant mesh step size $h = 1/32$ and we also use fixed polynomial degrees in both space and time (dG(2)-cG(5)). In the Fig. 4.4 below, we notice that all the error norms mentioned above have cubic convergence, also, we observe the superconvergence in the $\ell_\infty(L_2)$-error norm EOC ≈ 4. Note that N.SDof it means the total number of space degrees of freedom. The numerical results coincide with the theoretical results of Theorems 4.6 and 4.7.

4.3.5 Example 5

We implement in this Example the h–version IMEX dG time—marching scheme with the initial condition and source function are chosen such that the exact solution is

$$u(x, y, t) = t^\alpha x(1 - x)y(1 - y).$$

We solve the problem over the computational domain $\mathcal{I} \times \Omega := [0, 0.1] \times [0, 1]^2$, on a fixed uniform rectangular mesh consisting of 1024 uniform quintic elements in space $p = 5$ and uniform quadratic elements in time $r = 2$, with fixed mesh size $h = 1/32$, over a sequence of algebraically graded meshes in time with grading factor $\alpha = 0.75$.

This solution has initial layer and low regularity at $t = 0$ but it is analytic over the spatial domain Ω. We use temporal meshes, geometrically graded towards $t = 0$, to achieve exponential rates of convergence. For this reason, we consider a short time interval with $T = 0.1$. Let $0 < \tilde{\lambda} < 1$ be the mesh grading factor which defines a class of temporal meshes $t_n = \tilde{\lambda}^{N-n},\ n = 1, ..., N$. In this example, we set $\tilde{\lambda} = 0.5$. The Fig. 4.5 shows that the convergence rates are recovered by using algebraically graded meshes in the $L_2(H^1)$-, $L_2(L_2)$-, $L_\infty(L_2)$-, $L_\infty(L_\infty)$-, and $L_\infty(H^1)$-error norms with the expected EOC ≈ 2, and also the nodal superconvergence in the $\ell_\infty(L_2)$ norm with EOC ≈ 3.

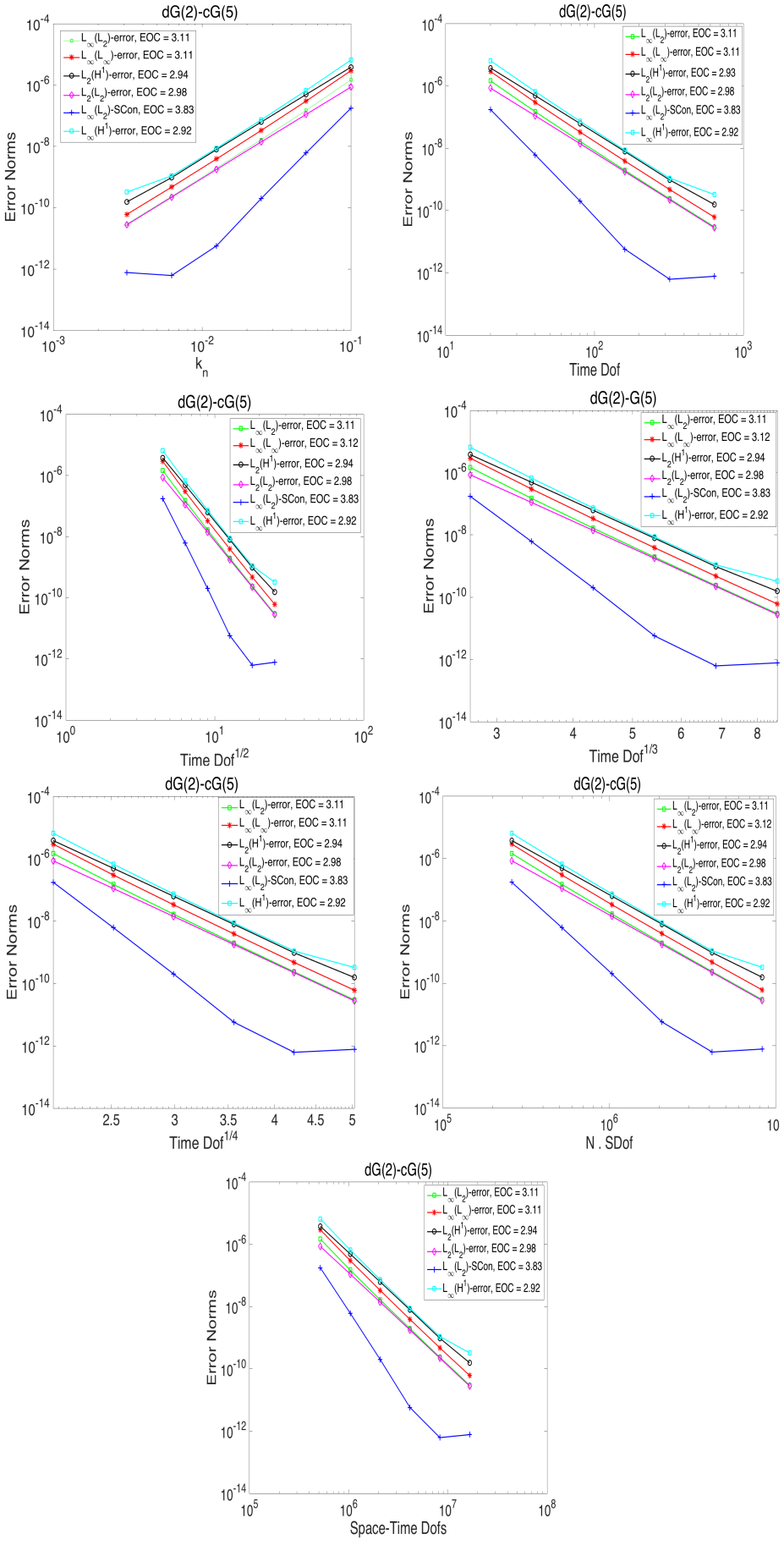

FIGURE 4.4: Example 4: h–version IMEX dG timestepping dG(2)–cG(5) scheme for different error norms.

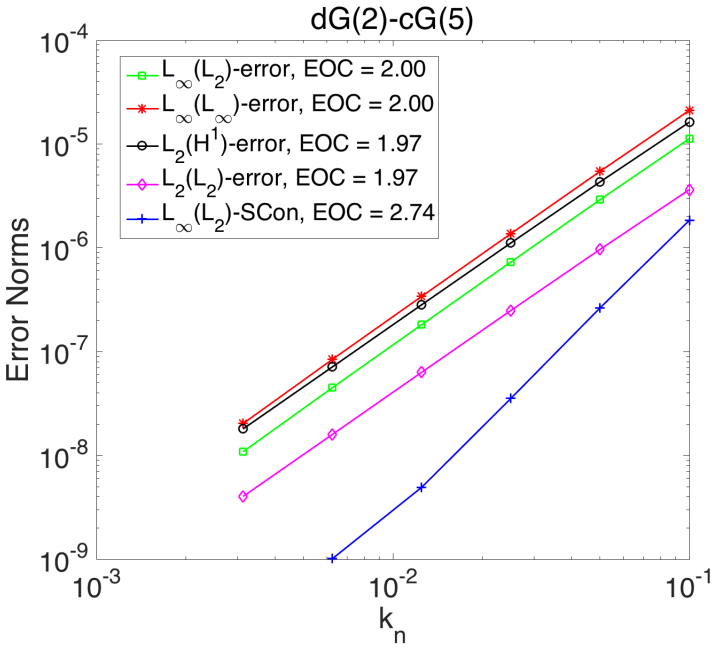

FIGURE 4.5: Example 5: h–version on algebraically graded meshes dG(2)–cG(5) for different error norms.

Chapter 5

Conclusions

5.1 Conclusions

In this work we studied discontinuous Galerkin timestepping for semilinear parabolic problems. In particular, we considered fully discrete implicit–explicit (IMEX) variational discretisations using the discontinuous Galerkin (dG) method in time combined with standard (continuous) Galerkin (cG) finite element methods in space. The time discretisation consists of a *hp*–version discontinuous Galerkin method treating implicitly the diffusion spatial operator and using an explicit multistep method for the nonlinear reaction term. We analysed general dG(r)–cG(p) combinations, where r is the polynomial degree in time and p is the polynomial degree in space. These methods were first proposed and analysed in the *a priori* setting by Estep and Larsson [52] under the assumption of globally Lipschitz nonlinearities.

We derived optimal $L_\infty(L_2)$ and $L_2(H^1)$ *a posteriori* error bounds under the more general assumption of locally Lipschitz continuous nonlinearities satisfying a certain growth condition dictated by suitable Sobolev imbedding results. The analysis builds on new *a posteriori* error estimates for linear parabolic problems presented in [60], using the elliptic reconstruction technique of Makridakis and Nochetto [83]. The performance of the error estimators are highlighted by a set of numerical examples, confirming that the *a posteriori* error estimators are optimal, reliable, and efficient.

We also consider the challenging problem of extending the *a priori* error analysis of discontinuous Galerkin timestepping methods to semilinear problems with merely locally-Lipschitz continuous nonlinear reaction terms. In this setting, we derived *a priori* error bounds in the $L_\infty(L_2)$ and $L_2(H^1)$ norms. The analysis is based on the classical elliptic projection technique and discrete stability estimates combined with an inf-sup argument in time. A fixed-point argument combined with a discrete version of the Grönwall inequality is used to control the nonlinear terms in the spirit of [4, 29]. The treatment of general nonlinearities comes at the expense of certain assumptions, such as local quasi-uniformity of the timestep and boundedness of the exact and approximate solutions. By using *hp*-version approximation estimates we were able to derive the analysis keeping the dependence on the polynomial degree as much as possible explicit. Furthermore, we tested the *a priori* error estimates by implementing a series of numerical examples. The results of the numerical experiments are in agreement with the theoretical results and, in the particular case of the $L_\infty(L_2)$–error norm, the observed behaviour is better than what is proven by about half an order.

An interesting aspect of the *a posteriori* analysis concerning implicit–explicit time stepping methods, is that no *a priori* CFL type conditions are required for the validity of the conditional *a posteriori* error bounds. Hence, the *a posteriori* estimators remain reliable even for unstable combinations of local spatial and temporal mesh sizes. In future work, we will consider using this property to estimate CFL constants in a rigorous, *a posteriori* fashion.

The study of nonlinear time–dependent PDE problems necessitates further investigation, as a number of important issues are yet to be addressed. One of these issues-, is the derivation of a posteriori error estimates for explicit and implicit–explicit timestepping methods for evolution PDEs, especially treating fully–discrete numerical schemes. There is a very limited number of works discussing a posteriori error bounds for explicit timestepping methods for linear evolution problems [58, 57]. The challenge of studying the explicit (or implicit–explicit) timestepping schemes in the context of rigorous a posteriori error control is the careful construction of an implicit perturbation of the explicit scheme for which

we can construct suitable, optimal order, reconstructions that, in turn, can be naturally inserted into the original PDE to construct residuals.

Regarding the *a priori* analysis, the study of semilinear evolution problems is still a challenge, since the classical timestepping typically are defined only on time–nodes. In the discontinuous Galerkin timestepping schemes however, the approximate solution is available on the whole time interval but it is discontinuous at the time–nodes and a careful analysis is needed in this case. In the future, we aim to apply the techniques we used in the *a posteriori* error analysis, namely, the dG reconstruction technique [84] combined with the continuous version of the Grönwall inequality, to derive optimal *a priori* error estimates for the semilinear parabolic problems.

Appendix A

Numerical computations of Chapter 2

A.1 Matrix form of the dG–timestepping schemes for semilinear parabolic problems

The matrix form representation of the fully space–time discrete scheme in (2.46) for the problem in (2.10) is given by

$$\begin{bmatrix} \epsilon_{0,0}M + k_n\beta_{0,0}S & \cdots & \epsilon_{0,r}M + k_n\beta_{0,r}S \\ \epsilon_{1,0}M + k_n\beta_{1,0}S & \cdots & \epsilon_{1,r}M + k_n\beta_{1,r}S \\ \vdots & \vdots & \vdots \\ \epsilon_{r-1,0}M + k_n\beta_{r-1,0}S & \cdots & \epsilon_{r-1,r}M + k_n\beta_{r-1,r}S \\ \epsilon_{r,0}M + k_n\beta_{r,0}S & \cdots & \epsilon_{r,r}M + k_n\beta_{r,r}S \end{bmatrix} \begin{bmatrix} \underline{\mathbf{U}}_n^0 \\ \underline{\mathbf{U}}_n^1 \\ \vdots \\ \underline{\mathbf{U}}_n^{r-1} \\ \underline{\mathbf{U}}_n^r \end{bmatrix} = \begin{bmatrix} \sigma_0 M\underline{\mathbf{U}}_{n-1}^{(0)} \\ \sigma_1 M\underline{\mathbf{U}}_{n-1}^{(0)} \\ \vdots \\ \sigma_{r-1} M\underline{\mathbf{U}}_{n-1}^{(0)} \\ \sigma_r M\underline{\mathbf{U}}_{n-1}^{(0)} \end{bmatrix} + \tag{A.1}$$

$$\begin{bmatrix} k_n\varrho_{0,n-\jmath-\mu}M & k_n\varrho_{0,n-\jmath-(\mu-1)}M & \cdots & k_n\varrho_{0,n-\jmath-(\mu-(\mu-1))}M & k_n\varrho_{0,n-\jmath}M \\ k_n\varrho_{1,n-\jmath-\mu}M & k_n\varrho_{1,n-\jmath-(\mu-1)}M & \cdots & k_n\varrho_{1,n-\jmath-(\mu-(\mu-1))}M & k_n\varrho_{1,n-\jmath}M \\ \vdots & \vdots & \vdots & \vdots & \vdots \\ k_n\varrho_{r-1,n-\jmath-\mu}M & k_n\varrho_{r-1,n-\jmath-(\mu-1)}M & \cdots & k_n\varrho_{r-1,n-\jmath-(\mu-(\mu-1))}M & k_n\varrho_{r-1,n-\jmath}M \\ k_n\varrho_{r,n-\jmath-\mu}M & k_n\varrho_{r,n-\jmath-(\mu-1)}M & \cdots & k_n\varrho_{r,n-\jmath-(\mu-(\mu-1))}M & k_n\varrho_{r,n-\jmath}M \end{bmatrix}$$

$$\begin{bmatrix} f(\underline{\mathbf{U}}_{n-\jmath-\mu}^-) \\ f(\underline{\mathbf{U}}_{n-\jmath-(\mu-1)}^-) \\ \vdots \\ f(\underline{\mathbf{U}}_{n-\jmath-(\mu-(\mu-1))}^-) \\ f(\underline{\mathbf{U}}_{n-\jmath}^-) \end{bmatrix}.$$

When $\jmath = 0$ we have the fully implicit timestepping scheme and when $\jmath = 1$ we obtain the implicit–explicit (IMEX) timestepping scheme.

Similarly, the matrix form representation for the fully space–time discrete scheme of the system of semilinear parabolic equations in (2.48) is given by

$$\begin{bmatrix} \epsilon_{0,0}M + l_1k_n\beta_{0,0}S & \epsilon_{0,1}M + l_1k_n\beta_{0,1}S & \cdots & \epsilon_{0,r}M + l_1k_n\beta_{0,r}S \\ \epsilon_{1,0}M + l_1k_n\beta_{1,0}S & \epsilon_{1,1}M + l_1k_n\beta_{1,1}S & \cdots & \epsilon_{1,r}M + l_1k_n\beta_{1,r}S \\ \vdots & \vdots & \ddots & \vdots \\ \epsilon_{r,0}M + l_1k_n\beta_{r,0}S & \epsilon_{r,1}M + l_1k_n\beta_{r,1}S & \cdots & \epsilon_{r,r}M + l_1k_n\beta_{r,r}S \\ \epsilon_{0,0}M + l_2k_n\beta_{0,0}S & \epsilon_{0,1}M + l_2k_n\beta_{0,1}S & \cdots & \epsilon_{0,r}M + l_2k_n\beta_{0,r}S \\ \epsilon_{1,0}M + l_2k_n\beta_{1,0}S & \epsilon_{1,1}M + l_2k_n\beta_{1,1}S & \cdots & \epsilon_{1,r}M + l_2k_n\beta_{1,r}S \\ \vdots & \vdots & \ddots & \vdots \\ \epsilon_{r,0}M + l_2k_n\beta_{r,0}S & \epsilon_{r,1}M + l_2k_n\beta_{r,1}S & \cdots & \epsilon_{r,r}M + l_2k_n\beta_{r,r}S \end{bmatrix} \begin{bmatrix} \underline{\mathbf{U}}_n^0 \\ \underline{\mathbf{U}}_n^1 \\ \vdots \\ \underline{\mathbf{U}}_n^r \\ \underline{\mathbf{V}}_n^0 \\ \underline{\mathbf{V}}_n^1 \\ \vdots \\ \underline{\mathbf{V}}_n^r \end{bmatrix} = \begin{bmatrix} \sigma_0 M\underline{\mathbf{U}}_{n-1}^{(0)} \\ \sigma_1 M\underline{\mathbf{U}}_{n-1}^{(0)} \\ \vdots \\ \sigma_r M\underline{\mathbf{U}}_{n-1}^{(0)} \\ \sigma_0 M\underline{\mathbf{V}}_{n-1}^{(0)} \\ \sigma_1 M\underline{\mathbf{V}}_{n-1}^{(0)} \\ \vdots \\ \sigma_r M\underline{\mathbf{V}}_{n-1}^{(0)} \end{bmatrix} \tag{A.2}$$

$$+ \begin{bmatrix} k_n\varrho_{0,n-\jmath-\mu}M & k_n\varrho_{0,n-\jmath-(\mu-1)}M & \cdots & k_n\varrho_{0,n-\jmath}M \\ k_n\varrho_{1,n-\jmath-\mu}M & k_n\varrho_{1,n-\jmath-(\mu-1)}M & \cdots & k_n\varrho_{1,n-\jmath}M \\ \vdots & & & \\ k_n\varrho_{r,n-\jmath-\mu}M & k_n\varrho_{r,n-\jmath-(\mu-1)}M & \cdots & k_n\varrho_{r,n-\jmath}M \\ k_n\varrho_{0,n-\jmath-\mu}M & k_n\varrho_{0,n-\jmath-(\mu-1)}M & \cdots & k_n\varrho_{0,n-\jmath}M \\ k_n\varrho_{1,n-\jmath-\mu}M & k_n\varrho_{1,n-\jmath-(\mu-1)}M & \cdots & k_n\varrho_{1,n-\jmath}M \\ \vdots & & & \\ k_n\varrho_{r,n-\jmath-\mu}M & k_n\varrho_{r,n-\jmath-(\mu-1)}M & \cdots & k_n\varrho_{r,n-\jmath}M \end{bmatrix} \begin{bmatrix} f(\underline{\mathbf{U}}_{n-\jmath-\mu}^-, \underline{\mathbf{V}}_{n-\jmath-\mu}^-) \\ f(\underline{\mathbf{U}}_{n-\jmath-\mu-1}^-, \underline{\mathbf{V}}_{n-\jmath-\mu-1}^-) \\ \vdots \\ f(\underline{\mathbf{U}}_{n-\jmath}^-, \underline{\mathbf{V}}_{n-\jmath}^-) \\ g(\underline{\mathbf{U}}_{n-\jmath-\mu}^-, \underline{\mathbf{V}}_{n-\jmath-\mu}^-) \\ g(\underline{\mathbf{U}}_{n-\jmath-\mu-1}^-, \underline{\mathbf{V}}_{n-\jmath-\mu-1}^-) \\ \vdots \\ g(\underline{\mathbf{U}}_{n-\jmath}^-, \underline{\mathbf{V}}_{n-\jmath}^-) \end{bmatrix}.$$

Also, when $\jmath = 0$ we have the fully implicit timestepping scheme and when $\jmath = 1$ we obtain the implicit–explicit (IMEX) timestepping scheme.

A.2 Starting process on the previous time intervals

As we mentioned in Chapter 2, we use a multistep interpolation process to approximate the nonlinear term on the right–hand side of our semilinear problems, whether it is a single equation or a system. Hence, to evaluate the method on the current time interval $\mathcal{I}_n$ we need the solution values on previous time intervals

and/or the current time interval. We will give below a detailed explanation of how to start and proceed with our time marching schemes.

A.2.1 Starting process when $\jmath = 0$ (The implicit case)

Assume that the order of the method in time is r. Ideally, the interpolant of the nonlinear source term $\Pi f(U)$ should be taken of order $\mu = 2r$. In the solution process, in order to be able to solve the nonlinear problem on the time interval $\mathcal{I}_\mu$, the interpolant values on the previous time intervals $\mathcal{I}_1$, $\mathcal{I}_2$, ..., $\mathcal{I}_{\mu-1}$ are required, and also on the current time interval $\mathcal{I}_\mu$ i.e. we need $\Pi f(U_n^-),\ n = 1, ..., \mu$. Since the interpolant $\Pi f(U)$ on the time interval $\mathcal{I}_\mu$ is of order μ then we need $\mu+1$ time nodes t_μ, $t_{\mu-1}$, $t_{\mu-2}, ..., t_1$, t_0 to construct this interpolating polynomial and then we need the solution values at these support time points U_μ^-, $U_{\mu-1}^-$, $U_{\mu-2}^-, ..., U_1^-$, U_0^-. We can compute the interpolant values at these time points and solutions values, via computing the source term values at these time nodes and solution values i.e. $f(U_\mu^-)$, $f(U_{\mu-1}^-)$, $f(U_{\mu-2}^-), ..., f(U_1^-)$, $f(U_0^-)$. Hence in this case we need the first μth time intervals to construct this polynomial interpolant of order μ.

However, this is not possible on the first $(\mu - 1)$ time intervals. The interpolant $\Pi f(U)$ is of order μ on the intervals starting from the interval $\mathcal{I}_\mu$ onwards i.e. for the intervals $\mathcal{I}_\mu$, $\mathcal{I}_{\mu+1}$, ..., $\mathcal{I}_N$. For the remaining intervals $\mathcal{I}_1$, $\mathcal{I}_2$, ..., $\mathcal{I}_{\mu-1}$, the interpolant has to be different on each interval. The interpolant on the interval $\mathcal{I}_{\mu-1}$ is of order $\mu - 1$ and on the interval $\mathcal{I}_{\mu-2}$ it is of order $\mu - 2$ and so on until the interval $\mathcal{I}_1$ where the interpolant is linear.

In summary, if the order of time polynomial is r (i.e. when using the dG(r) time stepping scheme) then we need the interpolant of the nonlinear source term $\Pi f(U)$ to be of degree $\mu = 2r$. To determine the degree of the source term interpolant $\Pi f(U)$ on any time interval $\mathcal{I}_n$ we have to cases:

(1) For the first μ time intervals $\mathcal{I}_n,\ n = 1, ..., \mu$ the degree of the source term interpolant $\Pi f(U)$ is the same as the index of the time interval $\mathcal{I}_n$ i.e. $\mu = n$. Then the interpolant on the first time interval $\mathcal{I}_1$ is linear, $\mu = 1$, and on the

second time interval $\mathcal{I}_2$ is quadratic, $\mu = 2$, and so on until the μth time interval $\mathcal{I}_\mu$ where the interpolant degree is μ.

(2) The interpolant degree $\Pi f(U)$ on all the remaining intervals $\mathcal{I}_{\mu+1}$, $\mathcal{I}_{\mu+2}$, ..., $\mathcal{I}_N$ is μ i.e the same degree of interpolant on the interval $\mathcal{I}_\mu$.

(I) The solution on the first time interval $\mathcal{I}_1$ when $n = 1$.

To proceed with the solution process, we start from the first time interval $\mathcal{I}_1$. On this interval we need to construct the linear interpolant $\Pi_1^1 f(U) = f(U_0^-)\xi_0(t) + f(U_1^-)\xi_1(t)$. Hence we need only to compute $f(U_1^-)$, since ($f(U_0^-)$ is known from the initial value) i.e. we need to solve the nonlinear system on this interval to obtain the solution nodal values vector U_1^- at the time node t_1, which we will need for computing the interpolant of the right hand side to solve on the next time interval $\mathcal{I}_2$, and so on. Now we can solve the problem (2.46) to obtain the following nonlinear system

$$\begin{bmatrix} \epsilon_{0,0}M + k_1\beta_{0,0}S & \epsilon_{0,1}M + k_1\beta_{0,1}S & \cdots & \epsilon_{0,r}M + k_1\beta_{0,r}S \\ \epsilon_{1,0}M + k_1\beta_{1,0}S & \epsilon_{1,1}M + k_1\beta_{1,1}S & \cdots & \epsilon_{1,r}M + k_1\beta_{1,r}S \\ \vdots & \vdots & \ddots & \vdots \\ \epsilon_{r,0}M + k_1\beta_{r,0}S & \epsilon_{r,1}M + k_1\beta_{r,1}S & \cdots & \epsilon_{r,r}M + k_1\beta_{r,r}S \end{bmatrix} \begin{bmatrix} \underline{\mathbf{U}}_1^0 \\ \underline{\mathbf{U}}_1^1 \\ \vdots \\ \underline{\mathbf{U}}_1^r \end{bmatrix} =$$

$$\begin{bmatrix} \sigma_0 M\underline{\mathbf{U}}_0^{(0)} \\ \sigma_1 M\underline{\mathbf{U}}_0^{(0)} \\ \vdots \\ \sigma_r M\underline{\mathbf{U}}_0^{(0)} \end{bmatrix} + \begin{bmatrix} k_1\varrho_{0,0}M & k_1\varrho_{0,1}M \\ k_1\varrho_{1,0}M & k_1\varrho_{1,1}M \\ \vdots & \\ k_1\varrho_{r,0}M & k_1\varrho_{r,1}M \end{bmatrix} \begin{bmatrix} f(\underline{\mathbf{U}}_0^-) \\ f(\underline{\mathbf{U}}_1^-) \end{bmatrix}. \qquad \text{(A.3)}$$

Note that, here, $\underline{\mathbf{U}}_0^{(0)}$ and $\underline{\mathbf{U}}_0^-$ actually represent the same function, that is, the known solution at $t = 0$ while $\underline{\mathbf{U}}_1^- = [\underline{\mathbf{U}}_1^0, \underline{\mathbf{U}}_1^1, \ldots, \underline{\mathbf{U}}_1^r]$ is the unknown solution at $t = t_1$.

(II) The Solution on the second time interval $\mathcal{I}_2$ when $n = 2$.

We proceed now to the second interval $\mathcal{I}_2$ and the interpolant is taken to be a

quadratic polynomial

$$(\Pi f(U), v)_{\mathcal{H}} = (\Pi_2^2 f(U), v)_{\mathcal{H}} \text{ on } \mathcal{I}_2,$$

where

$$\Pi_2^2 f(U) = f(\underline{\mathbf{U}}_0^-)\xi_0(t) + f(\underline{\mathbf{U}}_1^-)\xi_1(t) + f(\underline{\mathbf{U}}_2^-)\xi_2(t),$$

by solving the following problem

$$\int_{\mathcal{I}_2} ((U', v)_{\mathcal{H}} + a(U, v))\ dt + ([U]_1, v_1^+)_{\mathcal{H}} = \int_{\mathcal{I}_2} (\Pi_2^2 f(U), v)_{\mathcal{H}}\, dt,\ \forall v \in \mathcal{V}_2. \quad \text{(A.4)}$$

we get the following linear system

$$\begin{bmatrix} \epsilon_{0,0}M + k_2\beta_{0,0}S & \epsilon_{0,1}M + k_2\beta_{0,1}S & \cdots & \epsilon_{0,r}M + k_2\beta_{0,r}S \\ \epsilon_{1,0}M + k_2\beta_{1,0}S & \epsilon_{1,1}M + k_2\beta_{1,1}S & \cdots & \epsilon_{1,r}M + k_2\beta_{1,r}S \\ \vdots & \vdots & \ddots & \vdots \\ \epsilon_{r,0}M + k_2\beta_{r,0}S & \epsilon_{r,1}M + k_2\beta_{r,1}S & \cdots & \epsilon_{r,r}M + k_2\beta_{r,r}S \end{bmatrix} \begin{bmatrix} \underline{\mathbf{U}}_2^0 \\ \underline{\mathbf{U}}_2^1 \\ \vdots \\ \underline{\mathbf{U}}_2^r \end{bmatrix} =$$

$$\begin{bmatrix} \sigma_0 M \underline{\mathbf{U}}_1^{(0)} \\ \sigma_1 M \underline{\mathbf{U}}_1^{(0)} \\ \vdots \\ \sigma_r M \underline{\mathbf{U}}_1^{(0)} \end{bmatrix} + \begin{bmatrix} k_2\varrho_{0,0}M & k_2\varrho_{0,1}M & k_2\varrho_{0,2}M \\ k_2\varrho_{1,0}M & k_2\varrho_{1,1}M & k_2\varrho_{1,2}M \\ \vdots & \vdots & \vdots \\ k_2\varrho_{r,0}M & k_2\varrho_{r,1}M & k_2\varrho_{r,2}M \end{bmatrix} \begin{bmatrix} f(\underline{\mathbf{U}}_0^-) \\ f(\underline{\mathbf{U}}_1^-) \\ f(\underline{\mathbf{U}}_2^-) \end{bmatrix}. \quad \text{(A.5)}$$

(III) The solution on the μth time interval $\mathcal{I}_\mu$ when $n = \mu$.

Now, we can solve on the μth interval $\mathcal{I}_\mu$ by using the μth degree interpolant

$$(\Pi f(U), v)_{\mathcal{H}} = (\Pi_\mu^\mu f(U), v)_{\mathcal{H}} \text{ on } \mathcal{I}_\mu,$$

where

$$\Pi_\mu^\mu f(U) = f(\underline{\mathbf{U}}_0^-)\xi_0(t) + f(\underline{\mathbf{U}}_1^-)\xi_1(t) + ... + f(\underline{\mathbf{U}}_\mu^-)\xi_\mu(t),$$

we solve now the following problem on the interval μ

$$\int_{\mathcal{I}_\mu} ((U', v)_{\mathcal{H}} + a(U, v))\ dt + ([U]_{\mu-1}, v^+_{\mu-1})_{\mathcal{H}} = \int_{\mathcal{I}_\mu} (\Pi^\mu_\mu f(U), \nu)_{\mathcal{H}}\, dt,\ \forall v \in \mathcal{V}_\mu. \tag{A.6}$$

Finally, we have the following linear system

$$\begin{bmatrix} \epsilon_{0,0}M + k_n\beta_{0,0}S & \cdots & \epsilon_{0,r}M + k_n\beta_{0,r}S \\ \epsilon_{1,0}M + k_n\beta_{1,0}S & \cdots & \epsilon_{1,r}M + k_n\beta_{1,r}S \\ \vdots & \vdots & \vdots \\ \epsilon_{r-1,0}M + k_n\beta_{r-1,0}S & \cdots & \epsilon_{r-1,r}M + k_n\beta_{r-1,r}S \\ \epsilon_{r,0}M + k_n\beta_{r,0}S & \cdots & \epsilon_{r,r}M + k_n\beta_{r,r}S \end{bmatrix} \begin{bmatrix} \underline{\mathbf{U}}^0_n \\ \underline{\mathbf{U}}^1_n \\ \vdots \\ \underline{\mathbf{U}}^{r-1}_n \\ \underline{\mathbf{U}}^r_n \end{bmatrix} = \begin{bmatrix} \sigma_0 M\underline{\mathbf{U}}^{(0)}_{n-1} \\ \sigma_1 M\underline{\mathbf{U}}^{(0)}_{n-1} \\ \vdots \\ \sigma_{r-1} M\underline{\mathbf{U}}^{(0)}_{n-1} \\ \sigma_r M\underline{\mathbf{U}}^{(0)}_{n-1} \end{bmatrix} +$$

$$\begin{bmatrix} k_n\varrho_{0,n-\mu}M & k_n\varrho_{0,n-(\mu-1)}M & \cdots & k_n\varrho_{0,n-(\mu-(\mu-1))}M & k_n\varrho_{0,n}M \\ k_n\varrho_{1,n-\mu}M & k_n\varrho_{1,n-(\mu-1)}M & \cdots & k_n\varrho_{1,n-(\mu-(\mu-1))}M & k_n\varrho_{1,n}M \\ \vdots & \vdots & \vdots & \vdots & \vdots \\ k_n\varrho_{r-1,n-\mu}M & k_n\varrho_{r-1,n-(\mu-1)}M & \cdots & k_n\varrho_{r-1,n-(\mu-(\mu-1))}M & k_n\varrho_{r-1,n}M \\ k_n\varrho_{r,n-\mu}M & k_n\varrho_{r,n-(\mu-1)}M & \cdots & k_n\varrho_{r,n-(\mu-(\mu-1))}M & k_n\varrho_{r,n}M \end{bmatrix} \begin{bmatrix} f(\underline{\mathbf{U}}^-_{n-\mu}) \\ f(\underline{\mathbf{U}}^-_{n-(\mu-1)}) \\ \vdots \\ f(\underline{\mathbf{U}}^-_{n-(\mu-(\mu-1))}) \\ f(\underline{\mathbf{U}}^-_n) \end{bmatrix} \tag{A.7}$$

A.2.2 Starting process when $\jmath = 1$ (The implicit–explicit case)

As we mentioned before, the interpolant of the nonlinear source term $\Pi f(U)$ on the first μth intervals is different from the interpolant on the interval $\mathcal{I}_{\mu+1}$ onwards. The interpolant $\Pi f(U)$ is of order μ on the intervals starting from the interval $\mathcal{I}_{\mu+1}$ onwards i.e. for the intervals $\mathcal{I}_{\mu+1}$, $\mathcal{I}_{\mu+2}$, ..., $\mathcal{I}_N$. For the remaining intervals $\mathcal{I}_1$, $\mathcal{I}_2$, ..., $\mathcal{I}_{\mu-1}$, $\mathcal{I}_\mu$, the interpolant will be different and its order on each interval is $1, 2, \cdots, \mu-1, \mu$, except for the first interval where a predictor-corrector procedure based on a constant and linear interpolant is used. For brevity, we will not repeat the same details since most of them are similar to the implicit case. To determine the degree of the source term interpolant $\Pi f(U)$ on any time interval $\mathcal{I}_n$ we have two cases:

(1) For the first μth time intervals $\mathcal{I}_n$, $n = 1, ..., \mu$ the degree of the source term interpolant $\Pi f(U)$ is the index of the time interval $\mathcal{I}_n$ minus one i.e. $\mu = n - 1$

except for the first interval $\mathcal{I}_1$ where, in order to obtain a linear algorithm, we need to use a constant interpolant for the predicted values and then use it in the linear interpolant for the corrected values. Then the interpolants on the first time interval $\mathcal{I}_1$ are constant and linear $\mu = 0$ and $\mu = 1$ respectively, and on the second time interval $\mathcal{I}_2$ is linear $\mu = 1$ and so on until the μth time interval $\mathcal{I}_\mu$ where the interpolant degree will be $\mu - 1$.

(2) The interpolant degree $\Pi f(U)$ on all the remaining intervals $\mathcal{I}_{\mu+1}$, $\mathcal{I}_{\mu+2}$, ..., $\mathcal{I}_N$ is μ.

(I) The solution on the first time interval $\mathcal{I}_1$ when $n = 1$.

To proceed with solution process we start from the first time interval $\mathcal{I}_1$. On this interval we need to construct the linear interpolant $\Pi_1^1 f(U) = f(U_0^-)\xi_0(t) + f(U_1^-)\xi_1(t)$. We will face the problem that we do not have the solution values vector U_1^-, hence using this would result into a nonlinear system. To overcome this difficulty we will use the prediction–correction procedure to attain the required correct accuracy. We define the time polynomial solution function $\bar{U}|_{\mathcal{I}_1} \in \mathcal{X}_1$ of order 1 such that $\bar{U} = \sum_{j=0}^{1} \xi_j(t) f(\bar{U}_j^-)$ and $\bar{U}_0^- = u_0$.

Now, we need to solve the following problem to obtain the value $\bar{U}_1^-$: Indeed,

$$\int_{\mathcal{I}_1} \left((\bar{U}', v)_{\mathcal{H}} + a(\bar{U}, v) \right) dt + ([\bar{U}]_0, v_0^+)_{\mathcal{H}} = \int_{\mathcal{I}_1} (\Pi_0^0 f(\bar{U}), v)_{\mathcal{H}}\, dt, \ \forall v \in \mathcal{V}_1, \quad \text{(A.8)}$$

here we approximate $f(\bar{U})$ by the constant interpolant $\Pi_0^0 f(\bar{U}) = f(., 0, u_0)$ i.e. $\mu = 0$, which implies that

$$\int_{\mathcal{I}_1} \left((\bar{U}', v)_{\mathcal{H}} + a(\bar{U}, v) \right) dt + ([\bar{U}]_0, v_0^+)_{\mathcal{H}} = \int_{\mathcal{I}_1} (f(\bar{U}_0^-), v)_{\mathcal{H}}\, dt, \ \forall v \in \mathcal{V}_1. \quad \text{(A.9)}$$

In matrix form, this predictive step yields the following linear system:

$$\begin{bmatrix} \epsilon_{0,0}M + k_1\beta_{0,0}S & \epsilon_{0,1}M + k_1\beta_{0,1}S & \cdots & \epsilon_{0,r}M + k_1\beta_{0,r}S \\ \epsilon_{1,0}M + k_1\beta_{1,0}S & \epsilon_{1,1}M + k_1\beta_{1,1}S & \cdots & \epsilon_{1,r}M + k_1\beta_{1,r}S \\ \vdots & \vdots & \ddots & \vdots \\ \epsilon_{r,0}M + k_1\beta_{r,0}S & \epsilon_{r,1}M + k_1\beta_{r,1}S & \cdots & \epsilon_{r,r}M + k_1\beta_{r,r}S \end{bmatrix} \begin{bmatrix} \bar{\underline{\mathbf{U}}}_1^0 \\ \bar{\underline{\mathbf{U}}}_1^1 \\ \vdots \\ \bar{\underline{\mathbf{U}}}_1^r \end{bmatrix} =$$

$$\begin{bmatrix} \sigma_0 M \underline{\mathbf{U}}_0^{(0)} \\ \sigma_1 M \underline{\mathbf{U}}_0^{(0)} \\ \vdots \\ \sigma_r M \underline{\mathbf{U}}_0^{(0)} \end{bmatrix} + \begin{bmatrix} 0 & k_1\varrho_{0,0}M \\ 0 & k_1\varrho_{1,0}M \\ \vdots & \\ 0 & k_1\varrho_{r,0}M \end{bmatrix} \begin{bmatrix} 0 \\ f(\underline{\mathbf{U}}_0^-) \end{bmatrix}. \quad \text{(A.10)}$$

Actually, we just need the predictive value of $\bar{U}_1^-$ to use it in the next step to solve for the value U_1^-, the value of $\bar{U}_0^-$ will not be used. We then use these predictive solution values to solve the following problem for the corrected solutions values $\underline{\mathbf{U}}_1^0$ and $\underline{\mathbf{U}}_1^1$ i.e. solving for $U|_{\mathcal{I}_1} \in \mathcal{X}_1$ such that $U_0^- = u_0$:

$$\int_{\mathcal{I}_1} ((U', \nu)_{\mathcal{H}} + a(U,)) \, dt + ([U]_0, v_0^+)_{\mathcal{H}} = \int_{\mathcal{I}_1} (\Pi_1^1 f(\bar{U}), v)_{\mathcal{H}} \, dt, \ \forall v \in \mathcal{V}_1. \quad \text{(A.11)}$$

Here, we also choose the interpolant as a linear polynomial $\Pi_1^1 f(\bar{U}) = f(\bar{\underline{\mathbf{U}}}_0^-)\xi_0(t) + f(\bar{\underline{\mathbf{U}}}_1^-)\xi_1(t)$ and now the equation (A.11) implies to the following linear system

$$\begin{bmatrix} \epsilon_{0,0}M + k_1\beta_{0,0}S & \epsilon_{0,1}M + k_1\beta_{0,1}S & \cdots & \epsilon_{0,r}M + k_1\beta_{0,r}S \\ \epsilon_{1,0}M + k_1\beta_{1,0}S & \epsilon_{1,1}M + k_1\beta_{1,1}S & \cdots & \epsilon_{1,r}M + k_1\beta_{1,r}S \\ \vdots & \vdots & \ddots & \vdots \\ \epsilon_{r,0}M + k_1\beta_{r,0}S & \epsilon_{r,1}M + k_1\beta_{r,1}S & \cdots & \epsilon_{r,r}M + k_1\beta_{r,r}S \end{bmatrix} \begin{bmatrix} \underline{\mathbf{U}}_1^0 \\ \underline{\mathbf{U}}_1^1 \\ \vdots \\ \underline{\mathbf{U}}_1^r \end{bmatrix} =$$

$$\begin{bmatrix} \sigma_0 M \underline{\mathbf{U}}_0^{(0)} \\ \sigma_1 M \underline{\mathbf{U}}_0^{(0)} \\ \vdots \\ \sigma_r M \underline{\mathbf{U}}_0^{(0)} \end{bmatrix} + \begin{bmatrix} k_1\varrho_{0,0}M & k_1\varrho_{0,1}M \\ k_1\varrho_{1,0}M & k_1\varrho_{1,1}M \\ \vdots & \\ k_1\varrho_{r,0}M & k_1\varrho_{r,1}M \end{bmatrix} \begin{bmatrix} f(\underline{\mathbf{U}}_0^-) \\ f(\bar{\underline{\mathbf{U}}}_1^-) \end{bmatrix}. \quad \text{(A.12)}$$

(II) The solution on the second time interval $\mathcal{I}_2$ when $n = 2$.

We proceed now to the second interval $\mathcal{I}_2$ and the interpolant is also taken as a linear polynomial

$$(\Pi f(U), v)_{\mathcal{H}} = (\Pi_1^1 f(U), v)_{\mathcal{H}} \text{ on } \mathcal{I}_2,$$

where

$$\Pi_1^1 f(U) = f(\underline{\mathbf{U}}_0^-)\xi_0(t) + f(\underline{\mathbf{U}}_1^-)\xi_1(t),$$

by solving the following problem

$$\int_{\mathcal{I}_2} ((U', v)_{\mathcal{H}} + a(U, v))\, dt + ([U]_1, v_1^+)_{\mathcal{H}} = \int_{I_2} (\Pi_1^1 f(U), v)_{\mathcal{H}}\, dt,\ \forall v \in \mathcal{V}_2, \quad \text{(A.13)}$$

we get the following linear system

$$\begin{bmatrix} \epsilon_{0,0}M + k_2\beta_{0,0}S & \epsilon_{0,1}M + k_2\beta_{0,1}S & \cdots & \epsilon_{0,r}M + k_2\beta_{0,r}S \\ \epsilon_{1,0}M + k_2\beta_{1,0}S & \epsilon_{1,1}M + k_2\beta_{1,1}S & \cdots & \epsilon_{1,r}M + k_2\beta_{1,r}S \\ \vdots & \vdots & \ddots & \vdots \\ \epsilon_{r,0}M + k_2\beta_{r,0}S & \epsilon_{r,1}M + k_2\beta_{r,1}S & \cdots & \epsilon_{r,r}M + k_2\beta_{r,r}S \end{bmatrix} \begin{bmatrix} \underline{\mathbf{U}}_2^0 \\ \underline{\mathbf{U}}_2^1 \\ \vdots \\ \underline{\mathbf{U}}_2^r \end{bmatrix} =$$

$$\begin{bmatrix} \sigma_0 M\underline{\mathbf{U}}_1^{(0)} \\ \sigma_1 M\underline{\mathbf{U}}_1^{(0)} \\ \vdots \\ \sigma_r M\underline{\mathbf{U}}_1^{(0)} \end{bmatrix} + \begin{bmatrix} k_2\varrho_{0,0}M & k_2\varrho_{0,1}M \\ k_2\varrho_{1,0}M & k_2\varrho_{1,1}M \\ \vdots & \\ k_2\varrho_{r,0}M & k_2\varrho_{r,1}M \end{bmatrix} \begin{bmatrix} f(\underline{\mathbf{U}}_0^-) \\ f(\underline{\mathbf{U}}_1^-) \end{bmatrix}. \quad \text{(A.14)}$$

(III) The solution on the $(\mu+1)$th time interval $\mathcal{I}_{\mu+1}$ when $n = \mu + 1$.
Now, we can solve on the time interval $\mathcal{I}_{\mu+1}$ by using the μth degree interpolant

$$(\Pi f(U), v)_{\mathcal{H}} = (\Pi_\mu^\mu f(U), v)_{\mathcal{H}} \text{ on } \mathcal{I}_{\mu+1},$$

where

$$\Pi_\mu^\mu f(U) = f(\underline{\mathbf{U}}_0^-)\xi_0(t) + f(\underline{\mathbf{U}}_1^-)\xi_1(t) + ... + f(\underline{\mathbf{U}}_\mu^-)\xi_\mu(t),$$

we solve now the following problem on the interval $I_{\mu+1}$

$$\int_{I_{\mu+1}} ((U', v)_{\mathcal{H}} + a(U, v))\, dt + ([U]_\mu, v_\mu^+)_{\mathcal{H}} = \int_{I_{\mu+1}} (\Pi_\mu^\mu f(U), v)_{\mathcal{H}}\, dt,\ \forall v \in \mathcal{V}_{\mu+1}, \quad \text{(A.15)}$$

which results to the linear system given in (A.1) for $\jmath = 1$.

We now conclude with a few relevant examples of the general scheme detailed above.

Example 1: dG(0) with two–point Gauss–Lobatto quadrature rule (dG(0)-QGL(2)).

The two–point Gauss–Lobatto quadrature rule on the reference interval $\hat{\mathcal{I}} = [0, 1]$ is:

$$QGL(2) = \begin{cases} \hat{t}_0 = 0, & \hat{t}_1 = 1, \\ \hat{w}_0 = \frac{1}{2}, & \hat{w}_1 = \frac{1}{2}. \end{cases}$$

When $r = 0$, we have

$$(U_n^-, v)_{\mathcal{H}} + k_n a(U_n^-, v) = (U_{n-1}^-, v)_{\mathcal{H}} + k_n (f(., t_{n-\jmath}, U_{n-\jmath}^-), v)_{\mathcal{H}}, \\ \forall v \in \mathcal{V}, t \in (0, T], \tag{A.16}$$

which implies that

$$(M + k_n S)U_n^- = MU_{n-1}^- + k_n F_{n-\jmath}, t \in (0, T]. \tag{A.17}$$

When $\jmath = 0$ we have

$$\frac{1}{k_n}(U_n^- - U_{n-1}^-, v)_{\mathcal{H}} + a(U_n^-, v) = (f(., t_n, U_n^-), v)_{\mathcal{H}}, \ \forall v \in X_n^0, t \in (0, T], \tag{A.18}$$

which is equivalent to the backward (implicit) Euler method and here we need to solve the nonlinear term by using Newton method or by any other suitable method.

When $\jmath = 1$ then we have

$$\frac{1}{k_n}(U_n^- - U_{n-1}^-, v)_{\mathcal{H}} + a(U_n^-, v) = (f(., t_{n-1}, U_{n-1}^-), v)_{\mathcal{H}}, \ \forall v \in X_n^0, t \in (0, T] \tag{A.19}$$

which is equivalent to the forward (explicit) Euler method which can be solved directly.

Example 2: dG(1) with three-point Gauss–Lobatto quadrature rule (dG(1)-QGL(3)) We will give below some details about the basis and reference functions.

The Lagrange basis functions corresponding the the time points t_{n-3}, t_{n-2}, t_{n-1} are

$$\xi_{n-1}(t) = \tfrac{t^2-(t_{n-3}+t_{n-2})t+t_{n-3}t_{n-2}}{k_{n-1}(k_{n-2}+k_{n-1})}, \quad \xi'_{n-1}(t) = \tfrac{2t-(t_{n-3}+t_{n-2})}{k_{n-1}(k_{n-2}+k_{n-1})},$$

$$\xi_{n-2}(t) = \tfrac{t^2-(t_{n-3}+t_{n-1})t+t_{n-3}t_{n-1}}{k_{n-2}k_{n-1}}, \quad \xi'_{n-2}(t) = \tfrac{2t-(t_{n-3}+t_{n-1})}{k_{n-2}k_{n-1}},$$

$$\xi_{n-3}(t) = \tfrac{t^2-(t_{n-2}+t_{n-1})t+t_{n-2}t_{n-1}}{k_{n-2}(k_{n-2}+k_{n-1})}, \quad \xi'_{n-3}(t) = \tfrac{2t-(t_{n-2}+t_{n-1})}{k_{n-2}(k_{n-2}+k_{n-1})}.$$

The mapped functions to the reference interval $\hat{\mathcal{I}} = [0, 1]$ are

$$\hat{\xi}_0(\hat{t}) = \tfrac{k_n^2\hat{t}^2-(2k_{n-1}+k_{n-2})k_n\hat{t}+k_{n-1}(k_{n-1}+k_{n-2})}{k_{n-1}(k_{n-2}+k_{n-1})}, \quad \hat{\xi}'_0(\hat{t}) = \tfrac{2k_n^2\hat{t}-(2k_{n-1}+k_{n-2})k_n}{k_{n-1}(k_{n-2}+k_{n-1})},$$

$$\hat{\xi}_1(\hat{t}) = \tfrac{-(k_n^2\hat{t}^2-(k_{n-1}+k_{n-2})k_n\hat{t})}{k_{n-2}k_{n-1}}, \quad \hat{\xi}'_1(\hat{t}) = \tfrac{-(2k_n^2\hat{t}-(k_{n-1}+k_{n-2})k_n)}{k_{n-2}k_{n-1}},$$

$$\hat{\xi}_2(\hat{t}) = \tfrac{k_n^2\hat{t}^2+k_{n-1}k_n\hat{t}}{k_{n-2}(k_{n-2}+k_{n-1})}, \quad \hat{\xi}'_2(\hat{t}) = \tfrac{2k_n^2\hat{t}+k_{n-1}k_n}{k_{n-2}(k_{n-2}+k_{n-1})}.$$

In the case of linear function i.e. when $r = 1$, we have

$$QGL(3) = \begin{cases} \hat{t}_0 = 0, & \hat{t}_1 = \frac{1}{2}, \quad \hat{t}_2 = 1, \\ \hat{w}_0 = \frac{1}{6}, & \hat{w}_1 = \frac{4}{6}, \quad \hat{w}_2 = \frac{1}{6}. \end{cases}$$

Therefore, the reference trial and test functions are linear polynomials in $\hat{t}$ as follows:

$$\hat{\phi}_0(\hat{t}) = (1-\hat{t}), \quad \hat{\phi}'_0(\hat{t}) = -1,$$

$$\hat{\phi}_1(\hat{t}) = \hat{t}, \quad \hat{\phi}'_1(\hat{t}) = 1,$$

and by following the same steps mentioned in the previous section, we end with the following linear system

$$\begin{bmatrix} \frac{1}{2}M + \frac{k_n}{3}S & \frac{1}{2}M + \frac{k_n}{6}S \\ -\frac{1}{2}M + \frac{k_n}{6}S & \frac{1}{2}M + \frac{k_n}{3}S \end{bmatrix} \begin{bmatrix} \underline{\mathbf{U}}_n^0 \\ \underline{\mathbf{U}}_n^1 \end{bmatrix} = \begin{bmatrix} M\underline{\mathbf{U}}_{n-1}^0 \\ 0 \end{bmatrix}$$

$$+ \begin{bmatrix} \varrho_{1,n-3}M & \varrho_{1,n-2}M & \varrho_{1,n-1}M \\ \varrho_{2,n-3}M & \varrho_{2,n-2}M & \varrho_{2,n-1}M \end{bmatrix} \begin{bmatrix} f(\underline{\mathbf{U}}_{n-3}^0) \\ f(\underline{\mathbf{U}}_{n-2}^0) \\ f(\underline{\mathbf{U}}_{n-1}^0) \end{bmatrix}, n \geq 3. \tag{A.20}$$

(a) The nonlinear implicit case.

When $i = 0$ the quadratic interpolant can not be used on the first interval $\mathcal{I}_1$. On $\mathcal{I}_1$ we will use a linear interpolant while on the other intervals we will proceed with the quadratic interpolant.

(1) The solution process on the first time interval $\mathcal{I}_1$.

We proceed as described above, and we arrive at the following linear system

$$\begin{bmatrix} \epsilon_{0,0}M + k_1\beta_{0,0}S & \epsilon_{0,1}M + k_1\beta_{0,1}S \\ \epsilon_{1,0}M + k_1\beta_{1,0}S & \epsilon_{1,1}M + k_1\beta_{1,1}S \end{bmatrix} \begin{bmatrix} \bar{\underline{\mathbf{U}}}_1^0 \\ \bar{\underline{\mathbf{U}}}_1^1 \end{bmatrix} =$$

$$\begin{bmatrix} \sigma_0 M\underline{\mathbf{U}}_0^- \\ \sigma_1 M\underline{\mathbf{U}}_0^- \end{bmatrix} + \begin{bmatrix} 0 & k_1\xi_0 M \\ 0 & k_1\xi_1 M \end{bmatrix} \begin{bmatrix} 0 \\ f(\underline{\mathbf{U}}_0^-) \end{bmatrix}. \tag{A.21}$$

By solving this linear system for $\bar{\underline{\mathbf{U}}}_1^1$ ($\bar{\underline{\mathbf{U}}}_1^0$ is known), we obtain

$$\begin{bmatrix} \frac{1}{2}M + \frac{k_1}{3}S & \frac{1}{2}M + \frac{k_1}{6}S \\ -\frac{1}{2}M + \frac{k_1}{6}S & \frac{1}{2}M + \frac{k_1}{3}S \end{bmatrix} \begin{bmatrix} \bar{\underline{\mathbf{U}}}_1^0 \\ \bar{\underline{\mathbf{U}}}_1^1 \end{bmatrix} =$$

$$\begin{bmatrix} M\underline{\mathbf{U}}_0^- \\ 0 \end{bmatrix} + \begin{bmatrix} 0 & \frac{k_1}{2}M \\ 0 & \frac{k_1}{2}M \end{bmatrix} \begin{bmatrix} 0 \\ f(\underline{\mathbf{U}}_0^-) \end{bmatrix}. \tag{A.22}$$

Now, we can solve for U_1^0 and U_1^1 on $\mathcal{I}_1$ to have

$$\begin{bmatrix} \frac{1}{2}M + \frac{k_1}{3}S & \frac{1}{2}M + \frac{k_1}{6}S \\ -\frac{1}{2}M + \frac{k_1}{6}S & \frac{1}{2}M + \frac{k_1}{3}S \end{bmatrix} \begin{bmatrix} \underline{\mathbf{U}}_1^0 \\ \underline{\mathbf{U}}_1^1 \end{bmatrix} = \begin{bmatrix} M\underline{\mathbf{U}}_0^- \\ 0 \end{bmatrix} + \begin{bmatrix} \frac{k_1}{3}M & \frac{k_1}{6}M \\ \frac{k_1}{6}M & \frac{k_1}{3}M \end{bmatrix} \begin{bmatrix} f(\underline{\mathbf{U}}_0^-) \\ f(\bar{\underline{\mathbf{U}}}_1^1) \end{bmatrix}. \tag{A.23}$$

(b) The semi-implicit case.

When $i = 1$ the quadratic interpolant can not be used on the first two intervals $\mathcal{I}_1$ and $\mathcal{I}_2$ respectively. So we need to construct special interpolants for these intervals.

(1) The solution process on the first time interval $\mathcal{I}_1$.

Continuing as explained in the previous sections, we end with the required linear system for $\underline{\mathbf{U}}_1^0$ and $\underline{\mathbf{U}}_1^1$,

$$\begin{bmatrix} \frac{1}{2}M + \frac{k_1}{3}S & \frac{1}{2}M + \frac{k_1}{6}S \\ -\frac{1}{2}M + \frac{k_1}{6}S & \frac{1}{2}M + \frac{k_1}{3}S \end{bmatrix} \begin{bmatrix} \underline{\mathbf{U}}_1^0 \\ \underline{\mathbf{U}}_1^1 \end{bmatrix} = \begin{bmatrix} M\underline{\mathbf{U}}_0^- \\ 0 \end{bmatrix} + \begin{bmatrix} \frac{k_1}{3}M & \frac{k_1}{6}M \\ \frac{k_1}{6}M & \frac{k_1}{3}M \end{bmatrix} \begin{bmatrix} f(\underline{\mathbf{U}}_0^-) \\ f(\bar{\underline{\mathbf{U}}}_1^1) \end{bmatrix}. \tag{A.24}$$

(2) The solution process on the second time interval $\mathcal{I}_2$.

Now, after getting the required nodal solution values on the time interval $\mathcal{I}_1$, then we can construct our linear interpolant in the second time interval $\mathcal{I}_2$, to obtain the following linear system

$$\begin{bmatrix} \frac{1}{2}M + \frac{k_2}{3}S & \frac{1}{2}M + \frac{k_2}{6}S \\ -\frac{1}{2}M + \frac{k_2}{6}S & \frac{1}{2}M + \frac{k_2}{3}S \end{bmatrix} \begin{bmatrix} \underline{\mathbf{U}}_2^0 \\ \underline{\mathbf{U}}_2^1 \end{bmatrix} = \begin{bmatrix} M\underline{\mathbf{U}}_1^1 \\ 0 \end{bmatrix} + \begin{bmatrix} -\frac{k_2^2}{6k_1}M & \frac{k_2}{k_1}(\frac{k_2}{6} + \frac{k_1}{2})M \\ -\frac{k_2^2}{3k_1}M & \frac{k_2}{k_1}(\frac{k_2}{3} + \frac{k_1}{2})M \end{bmatrix} \begin{bmatrix} f(\underline{\mathbf{U}}_0^-) \\ f(\underline{\mathbf{U}}_1^1) \end{bmatrix}. \tag{A.25}$$

Bibliography

[1] M. Adamson and A. Morozov. Revising the role of species mobility in maintaining biodiversity in communities with cyclic competition. *Bull. Math. Biol.*, 74(9):2004–2031, 2012.

[2] N. Ahmed, G. Matthies, L. Tobiska, and H. Xie. Discontinuous Galerkin time stepping with local projection stabilization for transient convection–diffusion–reaction problems. *Comput. Meth. Appl. Mech. Engrg.*, 200(21):1747–1756, 2011.

[3] M. Ainsworth and J. Oden. *A Posteriori Error Estimation in Finite Element Analysis*. Wiley–Interscience (John Wiley & Sons), New York, 2000.

[4] G. Akrivis, M. Crouzeix, and C. Makridakis. Implicit–explicit multistep methods for quasilinear parabolic equations. *Numer. Math.*, 82(4):521–541, 1999.

[5] G. Akrivis and C. Makridakis. Convergence of a time discrete Galerkin method for semilinear parabolic equations. 2002.

[6] G. Akrivis and C. Makridakis. Galerkin time–stepping methods for nonlinear parabolic equations. *ESAIM: M2AN Math. Model. Numer. Anal.*, 38(2):261–289, 2004.

[7] G. Akrivis, C. Makridakis, and R. Nochetto. Optimal order a posteriori error estimates for a class of Runge–Kutta and Galerkin methods. *Numer. Math.*, 114(1):133–160, 2009.

[8] G. Akrivis, C. Makridakis, and R. Nochetto. Galerkin and Runge–Kutta methods: Unified formulation, a posteriori error estimates and nodal superconvergence. *Numer. Math.*, 118(3):429–456, 2011.

[9] A. Ambrosetti and A. Malchiodi. *Perturbation Methods and Semilinear Elliptic Problems on* $\mathbb{R}^n$. Second Edition, Springer, 2006.

[10] M. Amrein, J. Melenk, and T. Wihler. An *hp*- adaptive Newton–Galerkin finite element procedure for semilinear boundary value problems. *Math. Meth. Appl. Sci.*, 40(6):1973–1985, 2017.

[11] M. Amrein and T. Wihler. Fully adaptive Newton–Galerkin methods for semilinear elliptic partial differential equations. *SIAM J. Sci. Comput.*, 37(4):1637–1657, 2015.

[12] J. Argyris and D. Scharpf. Finite elements in time and space. *Nuclear Engineering and Design*, 10(4):456–464, 1969.

[13] A. Aziz and P. Monk. Continuous finite elements in space and time for the heat equation. *Math. Comput.*, 52(186):255–274, 1989.

[14] I. Babŭska and M. Suri. The *p*– and *hp*–versions of the finite element method: An overview. *Comput. Meth. Appl. Mech. Engrg.*, 80:5–26, 1990.

[15] I. Babŭska and M. Suri. The *p*– and *hp*–versions of the finite element method, basic principles and properties. *Comput. Meth. Appl. Mech. Engrg.*, 36(4):578–632, 1994.

[16] W. Bangerth, R. Hartmann, and G. Kanschat. deal.II-A general-purpose object-oriented finite element library. *ACM Transactions on Mathematical Software (TOMS)*, 33(4):24–es, 2007.

[17] L. Banjai, E. Georgoulis, and O. Lijoka. A Trefftz polynomial space–time discontinuous Galerkin method for the second order wave equation. *SIAM J. Numer. Anal.*, 55(1):63–86, 2017.

[18] E. Bänsch, F. Karakatsani, and C. Makridakis. A posteriori error control for fully discrete Crank-Nicolson schemes. *SIAM J. Numer. Anal.*, 50(6):2845–2872, 2012.

[19] S. Bartels. A posteriori error analysis for time–dependent Ginzburg–Landau type equations. *Numer. Math.*, 99(4):557–583, 2005.

[20] S. Bartels, R. Müller, and C. Ortner. Robust a priori and a posteriori error analysis for the approximation of Allen-Cahn and Ginzburg-Landau equations past topological changes. *SIAM J. Numer. Anal.*, 49(1):110–134, 2011.

[21] M. Bause, F. Radu, and U. Köcher. Error analysis for discretizations of parabolic problems using continuous finite elements in time and mixed finite elements in space. *Numer. Math.*, 137(4):773–818, 2017.

[22] A. Bonito, I. Kyza, and R. Nochetto. Error analysis of time–discrete higher order ALE formulations: A posteriori error analysis. *Preprint*, 2013.

[23] A. Bonito, I. Kyza, and R. Nochetto. Time discrete higher order ALE formulations: A priori error analysis. *Numer. Math.*, 125(2):225–257, 2013.

[24] A. Bonito, I. Kyza, and R. Nochetto. Time discrete higher order ALE formulations: Stability. *SIAM J. Numer. Anal.*, 51(1):577–604, 2013.

[25] A. Bonito, I. Kyza, and R. Nochetto. A DG approach to higher order ALE formulations in time. *IMA Volumes in Mathematics and Its Applications, Chapter in Recent Developments in Discontinuous Galerkin Finite Element Methods for Partial Differential Equations, 2012 Barrett Lectures*, 157:223–258, 2014.

[26] A. Cangiani, Z. Dong, and E. Georgoulis. *hp*–version space–time discontinuous Galerkin methods for parabolic problems on prismatic meshes. *SIAM J. Sci. Comput.*, 39(4):1251–1279, 2017.

[27] A. Cangiani, Z. Dong, E. Georgoulis, and P. Houston. *hp*-version discontinuous Galerkin methods for advection–diffusion–reaction problems on polytopic meshes. *ESAIM: M2AN Math. Model. Numer. Anal.*, 50(3):699–725, 2016.

[28] A. Cangiani, E. Georgoulis, and M. Jensen. Discontinuous Galerkin methods for mass transfer through semipermeable membranes. *SIAM J. Numer. Anal.*, 51(5):2911–2934, 2013.

[29] A. Cangiani, E. Georgoulis, and M. Jensen. Discontinuous Galerkin methods for fast reactive mass transfer through semi-permeable membranes. *Appl. Numer. Math.*, 104:3–14, 2016.

[30] A. Cangiani, E. Georgoulis, I. Kyza, and S. Metcalfe. Adaptivity and blow–up detection for nonlinear evolution problems. *SIAM J. Sci. Comput.*, 38(6):3833–3856, 2016.

[31] A. Cangiani, E. Georgoulis, A. Morozov, and O. Sutton. Revealing new dynamical patterns in a reaction-diffusion model with cyclic competition via a novel computational framework. *arXiv:1709.10043*, 2017.

[32] K. Chrysafinos. Convergence of discontinuous Galerkin approximations of an optimal control problem associated to semilinear parabolic PDE's. *ESAIM: M2AN Math. Model. Numer. Anal.*, 44(1):189–206, 2010.

[33] K. Chrysafinos, S. Filopoulos, and T. Papathanasiou. Error estimates for a FitzHugh–Nagumo parameter–dependent reaction– diffusion system. *ESAIM: M2AN Math. Model. Numer. Anal.*, 47(1):281–304, 2013.

[34] K. Chrysafinos and E. Karatzas. Symmetric error estimates for a discontinuous Galerkin approximations for optimal control problem associated to semilinear parabolic PDE's. *Discr. Cont. Dynam. Syst., Ser. B*, 17(5):1473–1506, 2012.

[35] K. Chrysafinos and E. Karatzas. Symmetric error estimates for a discontinuous Galerkin time–stepping schemes for optimal control problems constrained to evolutionary Stokes equations. *Computational Optimization and Applications*, 60(3):719–751, 2015.

[36] K. Chrysafinos and N. Walkington. Error estimates for the discontinuous Galerkin methods for parabolic equations. *SIAM J. Numer. Anal.*, 44(1):349–366, 2006.

[37] M. Delfour, W. Hager, and F. Trochu. Discontinuous Galerkin methods for ordinary differential equations. *Math. Comp.*, 36(4):455–473, 1981.

[38] A. Demlow, O. Lakkis, and C. Makridakis. A posteriori error estimates in the maximum norm for parabolic problems. *SIAM J. Numer. Anal.*, 47(3):2157–2176, 2009.

[39] T. Dupont. Mesh modification for evolution equations. *Math. Comp.*, 39:85–107, 1982.

[40] K. Eriksson, D. Estep, P. Hansbo, and C. Johnson. Introduction to adaptive methods for differential equations. *Acta Numer.*, 4:105–158, 1995.

[41] K. Eriksson, D. Estep, P. Hansbo, and C. Johnson. *Computational Differential Equations*. Cambridge University Press, 1996.

[42] K. Eriksson and C. Johnson. Error estimates and automatic time step control for nonlinear parabolic problems, I. *SIAM J. Numer. Anal.*, 24(1):12–23, 1987.

[43] K. Eriksson and C. Johnson. Adaptive finite element methods for parabolic problem I: A linear model problems. *SIAM J. Numer. Anal.*, 28(1):43–77, 1991.

[44] K. Eriksson and C. Johnson. Adaptive finite element methods for parabolic problems II: Optimal error estimates in $L_\infty L_2$ and $L_\infty L_\infty$. *SIAM J. Numer. Anal.*, 32(3):706–740, 1995.

[45] K. Eriksson and C. Johnson. Adaptive finite element methods for parabolic problems IV: Nonlinear problems. *SIAM J. Numer. Anal.*, 32(6):1729–1749, 1995.

[46] K. Eriksson, C. Johnson, and S. Larsson. Adaptive finite element methods for parabolic problems. VI Analytical semigroup. *SAIM J. Numer. Anal.*, 35(4):1315–1325, 1998.

[47] K. Eriksson, C. Johnson, and V. Thomée. Time discretization of parabolic problems by the discontinuous Galerkin method. *ESAIM: M2AN Math. Model. Numer. Anal.*, 19(4):611–643, 1985.

[48] A. Ern, I. Smears, and M. Vohralík. Guaranteed, locally space-time efficient, and polynomial-degree robust a posteriori error estimates for high-order discretizations of parabolic problems. Technical report, 2016.

[49] A. Ern, I. Smears, and M. Vohralík. Equilibrated flux a posteriori error estimates in $L^2(H^1)$-norms for high-order discretizations of parabolic problems. Technical report, 2017.

[50] A. Ern and M. Vohralík. A posteriori error estimation based on potential and flux reconstruction for the heat equation. *SIAM J. Numer. Anal.*, 48:198–223, 2010.

[51] D. Estep. A posteriori error bounds and global error control for approximation of ordinary differential equations. *SIAM J. Numer. Anal.*, 32(1):1–48, 1995.

[52] D. Estep and S. Larsson. The discontinuous Galerkin method for semilinear parabolic problems. *ESAIM: M2AN Math. Model. Numer. Anal.*, 27(1):35–54, 1993.

[53] D. Estep and A. Stuart. The dynamical behavior of the discontinuous Galerkin method and related difference schemes. *Math. Comput.*, 71(239):1073–1103, 2002.

[54] X. Feng and H. Wu. A posteriori error estimates and an adaptive finite element method for the Allen– Cahn equation and the mean curvature flow. *Sci. Comput.*, 24(2):121–146, 2005.

[55] F. Gaspoz, C. Kreuzer, K. Siebert, and D. Ziegler. A convergent time-space adaptive DG(s) finite element method for parabolic problems motivated by equal error distribution. *https://arxiv.org/abs/1610.06814*, 2016.

[56] E. Georgoulis. *Discontinuous Galerkin Methods on Shape-Regular and Anisotropic Meshes*. PhD thesis, University of Oxford, 2003.

[57] E. Georgoulis, E. Hall, and C. Makridakis. A posteriori error estimates for Runge–Kutta discontinuous Galerkin methods for hyperbolic problems. *In preparation*.

[58] E. Georgoulis, O. Lakkis, C. Makridakis, and J. Virtanen. A posteriori error estimates for leap–frog and cosine methods for second order evolution problems. *SIAM J. Numer. Anal.*, 54(1):120–136, 2016.

[59] E. Georgoulis, O. Lakkis, and J. Virtanen. A posteriori error control for discontinuous Galerkin methods for parabolic problems. *SIAM J. Numer. Anal.*, 49(1/2):427–458, 2011.

[60] E. Georgoulis, O. Lakkis, and T. Wihler. A posteriori error bounds for fully–discrete *hp*-discontinuous Galerkin timestepping methods for parabolic problems. *arXiv:1708.05832*.

[61] E. Georgoulis and C. Makridakis. On a posteriori error control for the Allen–Cahn problem. *Math. Meth. Appl. Sci.*, 37(2):173–179, 2014.

[62] S. Gottlieb, G. Wei, and S. Zhao. A unified discontinuous Galerkin framework for time integration. *Preprint*, 2010.

[63] T. Hughes and G. Hulbert. Space–time finite element methods for elastodynamics: Formulations and error estimates. *Comput. Meth. Appl. Mech. Engrg.*, 66(3):339–363, 1988.

[64] G. Hulbert and T. Hughes. Space–time finite element methods for second–order hyperbolic equations. *Comput. Meth. Appl. Mech. Engrg.*, 84(3):327–348, 1990.

[65] B. Hulme. Discrete Galerkin and related one–step methods for ordinary differential equations. *Math. Comput.*, 26(120):881–891, 1972.

[66] B. Hulme. One–step piecewise polynomial Galerkin methods for initial value problems. *Math. Comput.*, 26(120):415–426, 1972.

[67] S. Hussain, F. Schieweck, and S. Turek. Higher order Galerkin time discretizations and fast multigrid solvers for the heat equation. *J. Numer. Math.*, 19(1):41–61, 2011.

[68] P. Jamet. Galerkin–type approximations which are discontinuous in time for parabolic equations in a variable domain. *SIAM J. Numer. Anal.*, 15(5):912–928, 1978.

[69] B. Janssen and T. Wihler. Existence results for the continuous and discontinuous Galerkin time stepping methods for nonlinear initial value problems. *arXiv:1407.5520v1*, 2014.

[70] B. Janssen and T. Wihler. Continuous and discontinuous Galerkin time stepping methods for nonlinear initial value problems with applications to finite time blow–up. *arXiv:1407.5520v4*, 2016.

[71] O. Karakashian and C. Makridakis. A space-time finite element method for the nonlinear Schrödinger equation: the discontinuous Galerkin method. *Maths. Comput.*, 67(222):479–499, 1998.

[72] D. Kessler, R. Nochetto, and A. Schmidt. A posteriori error control for the Allen–Cahn problem: Circumventing Grönwall's inequality. *ESIAM: M2AN Math. Model. Numer. Anal.*, 38(1):129–142, 2004.

[73] U. Köcher. *Variational Space-Time Methods for the Elastic Wave Equation and the Diffusion Equation.* PhD thesis, Helmut–Schmidt University, Hamburg, University of the German Federal Armed Forces Hamburg, 2015.

[74] N. Kopteva and T. Linss. Maximum norm a posteriori error estimation for parabolic problems using elliptic reconstructions. *SIAM J. Numer. Anal.*, 51(3):1494–1524, 2013.

[75] I. Kyza and C. Makridakis. Analysis for time discrete approximations of blow–up solutions of semilinear parabolic equations. *SIAM J. Numer. Anal.*, 49(1/2):405–426, 2011.

[76] I. Kyza, S. Metcalfe, and T. Wihler. *hp*–adaptive Galerkin time stepping methods for nonlinear initial value problems. *arXiv:1612.06612*, 2017.

[77] O. Lakkis and C. Makridakis. Elliptic reconstruction and a posteriori error estimates for fully discrete linear parabolic problems. *Math. Comp.*, 75(256):1627–1658, 2006.

[78] O. Lakkis, C. Makridakis, and T. Pryer. A comparison of duality and energy a posteriori estimates for $\mathrm{L}_\infty(0,T;\mathrm{L}_2(\omega))$ in parabolic problems. *Math. Comp.*, 84(294):1537–1569, 2015.

[79] S. Larsson, V. Thomée, and L. Wahlbin. Numerical solution of parabolic integro-differential equations by the discontinuous Galerkin method. *Math. Comput.*, 64(221):45–71, 1998.

[80] P. Lesaint and P. Raviart. On a finite element method for solving the neutron transport equation. *Publication*, (33):89–123, 1974.

[81] C. Makridakis. Space and time reconstructions in a posteriori analysis of evolution problems. *ESIAM: Procedings*, 21:31–44, 2007.

[82] C. Makridakis and I. Babuška. On the stability of the discontinuous Galerkin method for the heat equation. *SIAM J. Numer. Anal.*, 34(1):389–401, 1997.

[83] C. Makridakis and R. Nochetto. Elliptic reconstruction and a posteriori error estimates for parabolic problems. *SIAM J. Numer. Anal.*, 41(4):1585–1594, 2003.

[84] C. Makridakis and R. Nochetto. A posteriori error analysis for higher order dissipative methods for evolution problems. *Numer. Math.*, 104(4):489–514, 2006.

[85] G. Matthies and F. Schieweck. Higher order variational time discretizations for nonlinear systems of ordinary differential equations. *Preprint Otto von Guericke Universität Magdeburg*, (23):130, 2011.

[86] R. May and W. Leonard. Nonlinear aspects of competition between three species. *SIAM J. Appl. Math.*, 29(2):243–253, 1975.

[87] S. Memon, N. Nataraj, and A. Pani. An a posteriori error analysis of mixed finite element Galerkin approximations to second order linear parabolic problems. *SIAM J. Numer. Anal.*, 50(3):1367–1393, 2012.

[88] S. Metcalfe. *Adaptive Discontinuous Galerkin Methods for Nonlinear Parabolic Problems*. PhD thesis, University of Leicester, 2015.

[89] A. Morozov and B. Li. On the importance of dimensionality of space in models of space–mediated population persistence. *Theor. Popul. Biol.*, 71(3):278–289, 2007.

[90] K. Mustapha. Time–stepping discontinuous Galerkin methods for fractional diffusion problems. *Numer. Math.*, 130(3):497–516, 2015.

[91] M. Picasso. Adaptive finite elements for a linear parabolic problem. *Comput. Methods Appl. Mech. Engrg.*, 167:223–237, 1998.

[92] G. Reddy and R. Sinha. Ritz–Volterra reconstructions and a posteriori error analysis of finite element method for parabolic integro–differential equations. *IMA J. of Numer. Anal.*, 35(1):341–371, 2015.

[93] W. Reed and T. Hill. Triangular mesh methods for the neutron transport equation. Tech. Report LA-UR-73-479, Los Alamos Scientific Laboratory, 1973.

[94] T. Richter, A. Springer, and B. Vexler. Efficient numerical realization of discontinuous Galerkin methods for temporal discretization of parabolic problems. *Numer. Math.*, 124(1):151–182, 2013.

[95] B. Riviére. *Discontinuous Galerkin Methods for Solving Elliptic and Parabolic Equations: Theory and Implementation.* SIAM, 2008.

[96] J. Ryan. Exploiting superconvergence through smoothness-increasing accuracy-conserving (SIAC) filtering. In *Spectral and high order methods for partial differential equations—ICOSAHOM 2014*, volume 106 of *Lect. Notes Comput. Sci. Eng.*, pages 87–102. Springer, Cham, 2015.

[97] F. Schieweck. A stable discontinuous Galerkin–Petrov time discretization of higher order. *J. Numer. Math.*, 18(1):429–456, 2010.

[98] D. Schötazu and T. Wihler. A posteriori error estimation for *hp*–version time–stepping methods for parabolic partial differential equations. *Numer. Math.*, 115(3):475–509, 2010.

[99] D. Schötzau. *Discontinuous Galerkin Finite Approximation of Nonlinear Parabolic Problems.* PhD thesis, ETH, Zürich, 1999.

[100] D. Schötzau and C. Schwab. Time discretization of parabolic problems by the *hp*–version of the discontinuous Galerkin finite element method. Research Reports in Mathematics 99–04, Research Report, Seminar für Angewandte Mathematik, Eidgenössische Technische Hochschule, Zürich, Switzerland, 1999.

[101] D. Schötzau and C. Schwab. An *hp* a priori error analysis of the DG time–stepping method for initial value problems. *Calcolo*, 37(4):207–232, 2000.

[102] D. Schötzau and C. Schwab. *hp*–discontinuous Galerkin time–stepping for parabolic problems. *C. R. Acad. Sci. Paris,*, t. 333,(Série 1):1121–1126, 2001.

[103] D. Schötzau and C. Schwab. Time discretization of parabolic problems by the *hp*–version of the discontinuous Galerkin finite element method. *SIAM J. Numer. Anal.*, 38(3):837–875, 2001.

[104] C. Schwab. *p- and hp-finite element methods: Theory and applications in solid and fluid mechanics*. Numerical Mathematics and Scientific Computation. Oxford : Clarendon Press, 1998.

[105] I. Smears. Nonoverlapping domain decomposition preconditioners for discontinuous Galerkin finite element methods in H^2–type norms. *J. Sci. Comput., doi:10.1007/s10915-017-0428-5*, 2017.

[106] I. Smears. Robust and efficient preconditioners for the discontinuous Galerkin time–stepping method. *IMA J. Numer. Anal.*, 37(4):1961–1985, 2017.

[107] I. Smears and E. Süli. Discontinuous Galerkin finite element methods for time-dependent Hamilton- Jacobi-Bellman equations with Cordès coefficients. *Numer. Math.*, 133(1):141–176, 2016.

[108] J. Sudirham, J. Vegt, and R. Damme. Space–time discontinuous Galerkin method for advection–diffusion problems on time–dependent domains. *Appl. Numer. Math.*, 56(12):1491–1518, 2006.

[109] V. Thomée. *Galerkin Finite Element Methods for Parabolic Problems*. Second Edition, Springer, 2006.

[110] V. Thomée and L. Wahlbin. On Galerkin methods in semilinear parabolic problems. *SIAM J. Numer. Anal.*, 12(3):378–389, 1975.

[111] R. Verfürth. A posteriori error estimates for finite element discretizations of the heat equations. *Calcolo*, 40(3):195–212, 2003.

[112] R. Verfürth. *A posteriori error estimation techniques for finite element methods*. Oxford Science Publications, 2013.

[113] M. Vlasák, V. Dolejši, and J. Hájek. A priori error estimates of an extrapolated space–time discontinuous Galerkin method for nonlinear convection–diffusion problems. *Numer. Meth. for Part. Diff. Eqs*, 27(6):1456–1482, 2011.

[114] S. Weller and S. Basting. Efficient preconditioning of variational time discretization methods for parabolic partial differential equations. *ESAIM: M2AN Math. Model. Numer. Anal.*, 49(2):331–347, 2015.

[115] T. Werder, K. Gerdes, D. Schötzau, and C. Schwab. *hp*-discontinuous Galerkin time stepping for parabolic problems. *Comput. Meth. Appl. Mech. Engrg.*, 190(49):6685–6708, 2001.

[116] M. Wheeler. A priori L_2 error estimates for Galerkin approximations to parabolic partial differential equations. *SIAM J. Numer. Anal.*, 10(4):723–759, 1973.

[117] T. Wihler. An priori error analysis of the *hp*–version of the continuous Galerkin FEM for nonlinear initial value problems. *J. Sci. Comput.*, 25(3):523–549, 2005.

[118] S. Zhao and G. Wei. A unified discontinuous Galerkin framework for time integration. *Math. Meth. Appl. Sci.*, 37(7):1042–1071, 2014.